

**Antal Kerpely Doctoral School of Materials
Science & Technology**



**Surface Quality Improvement of 42CrMo4 Hard-
Turned Steel by Two-Step Slide Diamond Burnishing**

Ph.D. Dissertation

By: Jawad Zaghal
(M.Sc. in Metallurgical Engineering)

Supervisor
Prof. Dr. Márton Benke
(Ph.D.)

Head of the Doctoral School
Prof. Dr. Valéria Mertinger
(D.Sc.)

Miskolc, 2024

SUPERVISOR'S EVALUATION

about

Jawad Zaghal

Jawad Zaghal conducted his MSc studies at the University of Miskolc. During his M.Sc. studies, he showed to have the skills to perform and evaluate experiments and measurements on his own. In 2017, he was one of the first foreign students who participated at the institution's TDK conference, on which he obtained the best presenter's award.

Jawad started his Ph.D. studies in 2020/2021 2nd semester in the topic "Characterization the Effect of Different Machining Parameters on Surface Residual Stresses in Steels". He did a comprehensive literature review and found that applying two-step slide diamond burnishing on hard-turned steels - instead of the practiced, combined grinding and a single slide diamond burnishing treatment - may result improved surface quality. This treatment idea of his own, is a knowledge gap, which came to be the backbone of his research. From his early results, Jawad published a paper in a Q2-ranked and from later results another one in a Q1-ranked journal. From his results, one or two additional Q1/Q2-ranked publications are expected to be published. He possesses a large experience in education and supervising students, since he worked as a laboratory supervisor at Palestine Polytechnic University for around ten years. In 2021-2022, he utilized his educational skills as co-supervisor (together with Dr. Zsolt Veres) of the M.Sc. student, Jawhara Marwani. For four years now, he has an educational YouTube channel about the experiments he teaches with 2.24K subscribers.

Jawad Zaghal is a hard-working and pointful researcher who is able to come up with new ideas, design his research, who plans, executes and evaluates experiments and measurements on his own. It was very easy to supervise his PhD activity, since he always had newly found correlations and ideas and he never backed off from the newly formed tasks, no matter the magnitude. Jawad Zaghal is a very respectful, gentle, and kind-hearted person. I am honestly grateful that I could be his supervisor and not a bit sad that I will no longer be that, since we will stay in contact as colleagues, and what is more important, as fiends.

Miskolc, 2024.05.27.

Prof. Dr. Márton Benke
supervisor

ACKNOWLEDGEMENT

First and foremost, I extend my deepest gratitude to the Almighty God (Allah), who endowed me with the perseverance and strength needed for this rigorous journey. His divine guidance and inspiration were the beacons of light illuminating my path throughout this challenging process, as He said: (Allah will raise those who have believed among you and those who were given knowledge, by degrees. And Allah is Acquainted with what you do).

I am also profoundly thankful to my supervisor, Professor Benke Márton, for his boundless patience, invaluable support, and expert guidance. He rigorously reviewed each step of my work, generously offering his assistance whenever sought. His extensive knowledge and insightful feedback were significant in elevating the quality of my research and culminating in a thesis of which I am immensely proud.

Special thanks are due to Dr. Molnár Viktor, whose assistance in preparing the samples and conducting microhardness measurements was indispensable. His readiness to provide support at every turn greatly facilitated my experimental work.

I am also grateful to Prof. Mertinger Valéria, who reviewed my research seminar reports. Her advice not only enhanced the quality of these reports but also steered me towards significant improvements in my overall research.

My appreciation extends to Mr. Süveges Béla, who was responsible for the hard-turning and burnishing tasks, and to Mr. Kovács Árpád, for his thorough work in taking the SEM micrographs.

I also owe a debt of gratitude to Mrs. Márkus Zoltánné for her diligent preparation of the samples for microstructure investigations, and to Mrs. Nyári Bodnárné Napsugár for her patience in conducting the microhardness measurements.

Acknowledgment is also made to Mrs. Solczi Ágnes and Dr. Svéda Mária for their assistance with administrative issues, which ensured the smooth progression of my study.

Lastly, I would like to thank everyone in my department -my academic family- for their solidarity and unwavering support. Each member has contributed in their own way to my personal and professional growth during my doctoral study.

DEDICATION

It is my honor to dedicate this work to:

To my homeland, Palestine, the place of my growth, and in honor of the tens of thousands of its martyrs whose memories and sacrifices permeate my spirit.

To my beloved wife, whose patience and unwavering support have been my anchor. The sacrifices you made managing our home and caring for our children in my absence were immense. Now, it is the time to stand by you as steadfastly as you have stood by me.

To my beloved children, Jawdy, Kinan, Besaan, and Karmil: Being away from you was the hardest part of this journey. Every time you asked, "Dad, when will you come back?" it broke my heart. Everything I've done was to build a brighter future for you. Now, it is time for us to reconnect.

To the soul of my dear mother, who, even from her grave, continues to support and guide me. You hoped to see me achieve this degree; though destiny took you too soon, I am sure you are smiling down on me now, proud of what I have accomplished.

To my father, a pillar of strength and wisdom, who taught me patience, perseverance, independence, and the courage to reach beyond the horizon. Your teachings have been the driving force behind my achievements.

To my siblings, who have always been there to offer support and encouragement, making me feel proud and motivated to reach this milestone.

To Palestine Polytechnic University, from which I graduated and where I am currently working, the time has come for me to contribute back to you, as you have enriched my life immensely.

To the University of Miskolc, where I pursued my master's and Ph.D. degrees, and to its esteemed faculty, you have become a part of my life over these past six years. I am eternally grateful and proud to be one of your alumni.

To my friends in Palestine, your constant concern and readiness to assist fueled my resolve to persevere through my studies.

To the friends I made in Hungary, who became my family away from home. I will never forget the sense of belonging you provided, nor the wonderful times we shared. Your presence ensured I never felt alone.

To every teacher who has guided me from childhood to this moment; your lessons have shaped the person I am today.

And to everyone who has loved, supported, inspired, and wished me well throughout my life, this achievement is also yours.

Jawad Zaghal
Miskolc - Hungary, May 2024

LIST OF APPREVIATIONS AND NOTATIONS

SDB	Slide Diamond Burnishing
HV	Vickers Microhardness
HRC	C-scale of the Rockwell Hardness scale
CNC	Computer Numerical Control
SEM	Scanning Electron Microscopy
CRS	Compressive Residual Stresses
STD	Standard Deviation
F_b	Burnishing force, [N]
f	Burnishing feed, [mm/rev]
v	Burnishing speed, [m/min]
r	Burnishing head radius, [mm]
ω	Workpiece rotational speed, [rpm]
n	Number of burnishing passes
σ_ϕ	Residual stresses in the azimuthal direction in the plane of the surface, [N/m ²]
E	Young's modulus, [N/m ²]
ν	Poisson's ratio
R_a	Arithmetic mean surface roughness, [μm]
d	Interplanar spacings of atoms' planes
L	Evaluation length in roughness measurements
S_{u_i}	The upward surface profile deviations from the mean line
S_{l_j}	The downward surface profile deviations from the mean line
S	Surface profile that deviates both above and below the mean line
R_{ku}	Kurtosis parameter
N	Number of points of the surface profile
R_q	Root mean square roughness parameter
Y_i	The height of the profile at point number i
h	Height of intersection between two burnishing traces, [μm]

$\bar{\sigma}$	Mean contact pressure, [N/m ²]
v_c	Turning cutting speed, [m/min]
r_ϵ	Cutting tool nose radius, [mm]
a_p	Depth of cut
v_T	Grinding wheel speed, [m/sec]
n_W	Grinding workpiece speed, [rpm]
Z	Grinding removed allowance, [mm]
v_r	Polishing speed, [rpm]
F_{in}	Initial (first-step) burnishing force, [N]
F_{fin}	Finishing / second-step burnishing force, [N]
σ_{in}^{axi}	Surface axial residual stresses after turning, grinding, polishing, and the first step of burnishing, [MPa]
σ_{fin}^{axi}	Surface axial residual stresses after the finishing step / second step of burnishing, [MPa]
$\%I\sigma_{axi}$	Percentage of axial residual stress improvement of the two-step SDB process, [%]
$F_{fin-0.0}$	Second-step burnishing force at which $\%I\sigma_{axi} = 0.0$, [N]
R^2	Coefficient of determination, [%]
σ_{in}^{tan}	Surface tangential residual stresses after turning, grinding, polishing, and the first step of burnishing, [MPa]
σ_{fin}^{tan}	Surface tangential residual stresses after the finishing step / second step of burnishing, [MPa]
R_{ku}^{axi}	Kurtosis parameter in the axial direction after the second step of burnishing
R_{ku}^{tan}	Kurtosis parameter in the tangential direction after the second step of burnishing
σ_{axi}	In-depth axial residual stress distribution, [MPa]
σ_{tan}	In-depth tangential residual stress distribution, [MPa]
$R_{a_{in}}$	Surface roughness after turning, grinding, polishing, and the first step of burnishing, [μ m]
$R_{a_{fin}}$	Surface roughness after the finishing step / second step of burnishing, [μ m]
$\%IR_a$	Percentage of surface roughness improvement of the two-step SDB process, [%]

TABLE OF CONTENTS

SUPERVISOR'S EVALUATION	I
ACKNOWLEDGEMENT	II
DEDICATION	III
LIST OF APPREVIATIONS AND NOTATIONS	IV
1. INTRODUCTION	1
1.1. Setting the Knowledge Gap of the Study	2
1.2. Selection of the Steel Grade	3
2. LITERATURE REVIEW	4
2.1. Importance and General Overview of Slide Diamond Burnishing	4
2.2. Influence of Burnishing Parameters on Surface Characteristics	6
2.2.1. Influence of Burnishing Parameters on Residual Stresses	6
2.2.2. Influence of Burnishing Parameters on Surface Roughness	10
2.2.3. Influence of Burnishing Parameters on Microhardness	12
3. OPEN QUESTIONS OF THE STUDY	16
4. EXPERIMENTAL SETUP	18
4.1. Material and Specimens Preparation	18
4.2. Hard-Turning, Grinding, and Polishing Conditions	18
4.3. Burnishing Conditions	19
4.4. Measuring Residual Stresses	22
4.5. Surface Roughness Measurements	23
4.6. Measuring Microhardness (HV 0.2)	24
4.7. SEM Investigations of Surface Morphology and Cross-Sectional Microstructure	24
5. RESULTS AND DISCUSSION	25
5.1. Surface Residual Stresses	25
5.1.1. Surface Axial Residual Stress Component After the Finishing Step of SDB	25
5.1.1.1. Percentage of Axial Residual Stress Improvement of the Two-Step SDB Process	28
5.1.2. Surface Tangential Residual Stress Component After the Finishing Step of SDB	32

5.1.3. Relationship Between Surface Residual Stresses and Kurtosis Parameter (R_{ku})	35
5.2. Residual Stress Depth Distributions	39
5.2.1. Axial Residual Stress Component Depth Distributions	39
5.2.2. Results of Tangential Residual Stress Component Depth Distributions	43
5.3. Results of Surface Roughness	48
5.3.1. Percentage of Surface Roughness Improvement of the Two-Step SDB Process	51
5.4. Results of Surface Microhardness	55
5.5. Analysis of Surface Topography and Morphology	57
5.5.1. 3D Surface Topography After Turning, After Grinding, and After Polishing	57
5.5.2. 3D Surface Topography After Turning and SDB	58
5.5.3. 3D Surface Topography After Grinding and SDB, and After Polishing and SDB	60
5.5.4. 3D Surface Topography After Two-Step SDB	61
5.5.5. Surface Morphology After Grinding and SDB, and After Two-Step SDB	63
5.6. Burnished Cross-Sectional Microstructure	68
5.7. Comprehensive Explanation of the Results	71
6. SUMMARY AND CONCLUSION	74
7. CLAIMS	78
8. UTILIZATION OF THE CLAIMS	80
9. PUBLICATIONS AND PRESENTATIONS	81
REFERENCES	82
APPENDIX	93

1. INTRODUCTION

The surface integrity of machined components plays a critical role in determining their functional performance across a range of properties, including fatigue life, wear resistance, and corrosion resistance. An optimal surface finish is therefore essential for components that will undergo cyclic loading or operation in challenging environments since when the surface quality gets better, there are fewer places where cracks can initiate.

Slide diamond burnishing (SDB) is a surface mechanical finishing operation used after turning to improve surface quality, that is, to further decrease the surface roughness, introduce compressive residual stresses, increase microhardness, and refine the microstructure of the surface and subsurface layers of the workpiece, improving its overall surface integrity components. The main result of improved surface quality is an increase in the fatigue life of the rotating components subjected to cyclic loading.

The initial surface roughness that the workpiece has before applying the burnishing process plays a crucial role in determining the final outcomes of the burnishing process. Commonly, grinding is a pre-burnishing process used to reduce the surface roughness of the turned components by removing the high peaks on the surface, creating a more uniform surface for burnishing. Nevertheless, grinding, while effective in reducing surface roughness, can introduce various challenges and potential defects if not properly controlled. It can introduce tensile residual stresses on the surface of the workpiece, which can be detrimental as they can lead to premature failure of the component, especially under cyclic loading conditions, making the component susceptible to fatigue cracks.

In order to overcome the potential harmful consequences of grinding—in which residual stresses strongly vary depending on parameters, in some cases, even tensile stresses can be formed—prior to SDB, the proposed concept of this doctoral thesis was to split up the SDB process into two steps. The treatment is called two-step SDB, since the force of the first and second treatments differ, unlike during multi-pass SDB, where the same force is applied in the subsequent treatments. The main objective of the first one is to decrease the initial surface roughness of hard-turned samples made of 42CrMo4 steel intended to be burnished with a second finishing step. In addition, given that polishing has the advantage of creating surfaces with lower surface roughness than grinding does, a second option for executing SDB after polishing was included in the workplan as part of the conventional process.

The execution of the experimental work was conducted in two distinct phases. The primary objective of the first phase was to identify the optimal burnishing parameters that would provide the most favorable results in terms of surface roughness. To do so, twenty seven surfaces were burnished with different combinations of speed, feed, and force, using three distinct levels of each.

Consequently, the optimum speed and feed, along with the three levels of force, have been determined.

In the second phase of the study, five bars, each sectioned into eight surfaces, underwent hard turning. These surfaces were then subjected to different finishing processes: one bar was ground, another polished, and the remaining three were initially burnished using distinct forces for each group. Following these treatments, all surfaces underwent a finalizing step of SDB. Considering that each group consisted of eight surfaces, a sequential burnishing force was applied, increasing by increments of 25 N from 25 to 200 N, with each surface receiving a specific force. Throughout the burnishing process, the same optimal feed and speed settings were consistently applied to all surfaces.

After completing the processes of turning, grinding, polishing, and the first step of burnishing, the average values of key parameters such as surface axial and tangential residual stresses, surface roughness (R_a), and microhardness (HV 0.2) were measured for select reference surfaces. Following the finishing SDB step, whether in the first or second phase of the study, these measurements were also taken for all surfaces. Subsequently, the results were analyzed, leading to further evaluations including in-depth residual stress distribution, 3D surface topography, surface morphology, and cross-sectional microstructure for certain selected surfaces.

1.1. Setting the Knowledge Gap of the Study

According to the recent research done on SDB and a very similar technology called ball burnishing, which differs mainly in that the burnishing head is a rotating sphere, similar to a ball pen, results showed that the most important parameters affecting the surface integrity and fatigue life of the burnished components are the initial (input) surface roughness [1–3], [4], [5], and the burnishing force [4–6]. Consequently, reducing the surface roughness of turned parts before burnishing, along with selecting the appropriate finishing burnishing force, significantly impacts the effectiveness of the burnishing process.

Mainly, grinding is the most common process used to decrease the surface roughness of the turned or hard-turned components before burnishing. As an example, Uddin et al. [9], Skoczylas and Kłonica [10], Sai and Lebrun [11], and Shiou and Hsu [12] used grinding to decrease the surface roughness before conducting slide burnishing. Nevertheless, using grinding as a method for reducing surface roughness subsequent to turning may not be the most optimal decision.

Undoubtedly, the process of grinding has several negative consequences for the integrity of the ground surface. The use of this abrasive technique has the potential to induce certain material deteriorations, such as the formation of microcracks both on the surface and inside the subsurface regions [38] and [39], in addition to the scratches and tears on the surface [15]. Moreover, surface

thermal damage to the workpiece might occur at the elevated temperatures generated by grinding [40] and [41]. Furthermore, the process of grinding induces the development of tensile residual stress, both on the surface and in the subsurface region [18]–[20]. Consequently, achieving the desired surface quality standards prior to burnishing proves to be challenging when using the typical grinding process for reducing the surface roughness of the workpiece. Accordingly, this point has formulated the knowledge gap of this study, which shaped the literature review detailed in the next chapter.

1.2. Selection of the Steel Grade

Due to its high hardenability, high strength, and robust toughness, 42CrMo4 steel, also recognized as AISI 4140, finds widespread application in various industrial sectors, including the aerospace, manufacturing, and automotive industries [24], [22]. It is employed in the production of critical components such as gears, shafts, crankshafts, axles, and spindles [23], [24]. These components operate in challenging environments characterized by substantial cyclic loading and rapid rotational speeds, making them susceptible to fatigue failure. Consequently, the finishing surface treatment technology employed, like SDB, significantly impacts their operational lifespan.

In addition, all prior SDB investigations using 42CrMo4 steel had hardness values lower than 33 HRC [5], [15], [21–24]. However, in this study, the burnishing process was accomplished after the hard turning of cylindrical bars of 54 HRC hardness since this steel grade is primarily intended to be hard-turned in some applications [31], [32]. Furthermore, according to Maximov et al. [33], studies processed on slide burnishing processes using hardened steels are much fewer than those done using non-hardened steels (around 33%). Consequently, these reasons and the distinctive properties of 42CrMo4 steel made it an ideal material for investigation in this research study. Chemical composition and mechanical properties 42CrMo4 steel are depicted in Table 1 and Table 2, respectively.

Table 1. Chemical composition of 42CrMo4 steel (wt%) [34]

C	Si	Mn	P	S	Cr	Mo	Ni	V
0.38 – 0.45	0.17 – 0.37	0.5 – 0.8	0.035 max	0.035 max	0.9 – 1.2	0.15 – 0.25	0.3 max	0.06 max

Table 2. Mechanical properties of 42CrMo4 steel [25]

Yield Stress $R_{p0.2}$, [MPa]	Ultimate Tensile Stress R_m , [MPa]	Elongation, [%]	Hardness, [HB]	Toughness [KV, J]
650	900 - 1100	12	265–325	min. 35 at 20 °C

2. LITERATURE REVIEW

2.1. Importance and General Overview of Slide Diamond Burnishing

Mechanical components used in the aerospace, automotive, machinery, and other sectors of industry are subjected to increasingly rigorous demands in terms of high dependability and extended operational lifespan [35]–[37]. The products of these industries contain a lot of rotating parts and components like turbines, gearboxes, shafts, and axles. Fatigue in materials, particularly those used in rotating components, is a significant failure mechanism characterized by the gradual cracking of materials under cyclic or fluctuating stresses [38], [39]. These stresses can be of different types: tensile, compressive, or torsional, but the initiation and propagation of cracks are mainly due to the tensile component [40]–[42]. One of the main factors that improves the fatigue life of the rotating components susceptible to cyclic loading is decreasing the surface roughness as a finishing operation before the usage of the workpiece [43]–[45].

In conventional manufacturing processes, especially when the hardness of the workpiece exceeds 45 HRC or even 60 HRC, the last stage of machine component refinement often involves the use of grinding techniques. Machining processes in this range of high hardness are referred to as "hard" [46]. The other refinement process that is widely used as a hard machining one is turning [47]–[50].

If random surface topography is not required, hard turning is a substitute method that may provide the same level of precision and surface quality as grinding [51]. Moreover, hard turning is often seen as an appropriate alternative to grinding operations owing to its advantages in terms of cost reduction and increased production [52], [53]. Additionally, in comparison to grinding, it is observed that the particular cutting energy in the hard turning case is lower [54].

However, grinding and hard turning may negatively affect the service life of the component, depending on the applied parameters. The process of grinding results in the attainment of the minimum surface micro-hardness [55], and compared to hard turning, a shallower compressive residual stress layer in the cutting direction could be achieved [56]. Furthermore, according to the grinding parameters and other influencing factors, grinding may induce tensile residual stresses at the surface or in-depth of the ground component [57]–[59].

On the other hand, with hard turning, the main problem is the high surface roughness of the machined components [60], [61]. Also, depending on the parameters of the turning and other important factors, hard turning may leave behind tensile stresses in the surface and subsurface layers of the parts that have been turned [62], [63].

It is well known that the outer layers of structural and machine elements experience the highest load while being used [64]. Therefore, the component's durability is directly related to the surface layer's

microstructure, residual stresses, microhardness, and surface roughness, which all comprise the surface integrity elements [65]–[67]. And since hard turning and grinding do not guarantee the fulfilment of these elements, a subsequent finishing process, like slide diamond burnishing, can further enhance the surface properties to meet the specific requirements of surface integrity.

Burnishing is one of the most effective finishing operations [68]–[70]. The main benefits of the burnishing process are decreasing surface roughness, increasing microhardness, inducing compressive residual stress in the surface and subsurface layers, refining the microstructure of grains at the surface, and improving the wear and corrosion resistance of the burnished surface. Consequently, improving the fatigue life of the component [71]–[73].

In SDB, the workpiece is typically mounted on a lathe, either conventional or CNC, and set into rotation at a specified angular velocity, as shown in Figure 1. The process resembles turning kinematically but without chip removal, in which a deforming tool with a spherical end, usually made of natural or synthetic diamond, moves under pressure over the surface of the workpiece, causing plastic deformation and, hence, a minute material flow on the surface and a mirror-like appearance [25], [74].

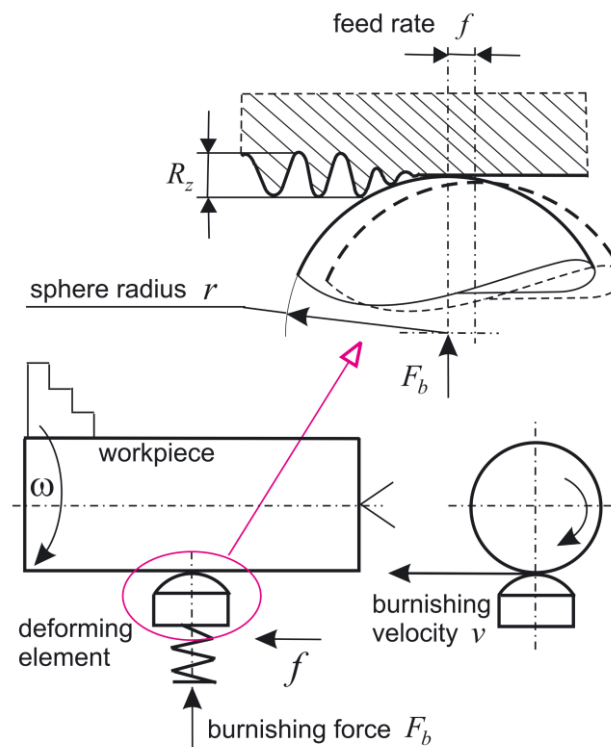


Figure 1. Slide diamond burnishing kinematics and parameters [75]

The process involves several working parameters that are critical for achieving the desired surface finish, microhardness, and residual stresses. These parameters include the burnishing force (F_b , N), which is the radial force applied by the diamond-tipped tool on the workpiece, the burnishing feed (f , mm/rev), which represents the axial feed rate at which the burnishing tool moves along the

workpiece, the rotational speed (ω , rpm), which represents the angular velocity at which the workpiece rotates, the burnishing speed (v , m/min), which stands for the linear speed of the tool relative to the workpiece, the deforming head radius (r , mm) which is the radius of the diamond-tipped tool that comes in contact with the workpiece, and finally, there are some other additional parameters, like the number of passes (n), which represents the number of times the tool passes over the same surface area, lubrication conditions, and the material of the workpiece [25], [76].

2.2. Influence of Burnishing Parameters on Surface Characteristics

So far, many studies have been conducted to investigate the influence of burnishing parameters and their interactions on the outputs of the burnishing process, like surface roughness, surface residual stresses, microhardness, and microstructure. The results of those studies show that the efficacy of the burnishing process highly depends on the range of applied burnishing parameters and their interactions, the type of burnished material and its hardness, and the environment of the burnishing process, like lubrication and wear of the burnishing head. The following studies provide examples of this.

2.2.1. Influence of Burnishing Parameters on Residual Stresses

Residual stresses are those stresses which remain in the solid material after the removal of the external cause or force [77]. X-ray diffraction can be assumed as a non-destructive mean of measuring residual stresses. Simply, it is a strain measurement that will be converted to stress using appropriate elastic relations. The strain can be obtained from measurements of interplanar spacings before and after the application of the stress.

Surface treatment operations often create a biaxial stress state which can be measured using X-ray diffraction techniques. The geometry for the biaxial stress measurement is shown in Figure 2. The sample coordinate system is the X_i ; the stress system is biaxial and lies in the $X_1 - X_2$ plane. The angles ϕ and ψ determine the direction in which the strain is measured. The angle ϕ determines the azimuthal direction in the plane of the surface, while the angle ψ gives the "tilt" around the axis normal to the plane of diffraction. The L_3 direction is the direction of the normal of the planes whose interplanar spacings are being measured.

The residual stress σ_ϕ can be calculated using the following equation [77]:

$$\sigma_\phi = \frac{d_\psi - d_3}{d_3} \frac{E}{(1 + \nu) \sin^2 \psi} \quad (1)$$

Where

E : Young's modulus

ν : Poisson's ratio.

d : Interplanar spacings.

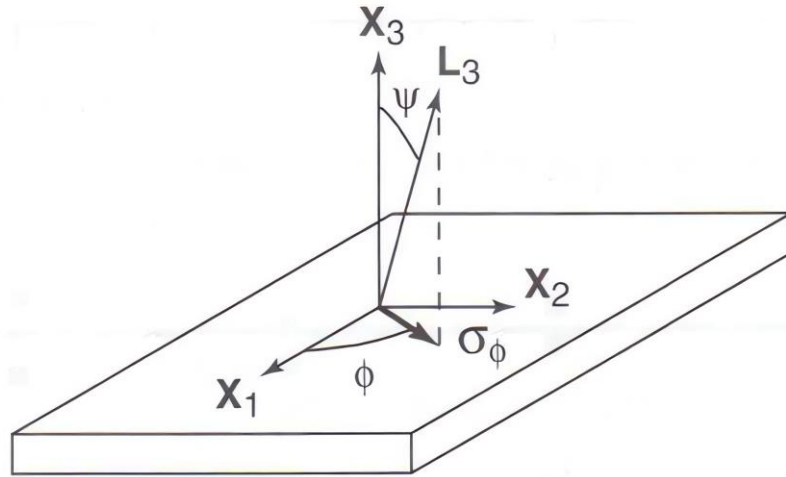


Figure 2. Geometry for biaxial stress measurements [77]

When d_ψ versus $\sin^2\psi$ plot is made, as in Figure 3, the slope will be [77]:

$$\text{slope} = d_{33} \frac{(1 + \nu)}{E} \sigma_\phi \quad (2)$$

Where d_{33} is the interplanar spacing without stress. Therefore, using $\sin^2\psi$ method, the residual stress σ_ϕ can be measured.

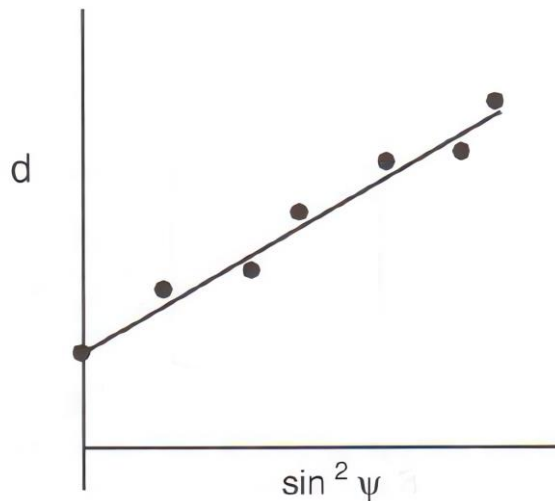


Figure 3. $\sin^2\psi$ method for residual stress measurement [77]

Residual stresses, both tensile and compressive, whether at the surface or subsurface layers of the components, play a pivotal role in influencing the fatigue life of materials, as they directly affect the initiation and propagation of fatigue cracks [78], [79]. Consequently, the introduction of compressive residual stresses by SDB, particularly in terms of their magnitude and influencing depth, is critical for enhancing the fatigue strength of the treated components [80]. Despite the fact that the significant enhancement in fatigue life of axes and shafts undergoing cyclic loading is primarily attributed to the compressive residual stresses in the axial direction introduced in the

surface layer through SDB, the tangential components are also important for that purpose [78], [80]. Therefore, this discussion will cover results from previous studies on the impact of the burnishing process and its parameters on the generation of residual stresses.

The first example is the study conducted by Maximov et al. [79], in which the researchers investigated the effects of slide diamond burnishing on the 2024-T3 Al alloy. The basic burnishing parameters that governed the process were: $r = 4 \text{ mm}$, $F_b = 200 \text{ N}$, $v = 100 \text{ m/min}$, and $f = 0.05 \text{ mm/rev}$. Furthermore, as an additional parameter, the study considered the number of passes to be eight. Samples were divided into five groups. The first two groups were burnished using lubricant (Hocut 795-H), and the other three groups were dry-burnished. The first and fourth groups were burnished with eight passes in one way (forward direction only), while the second and fifth were burnished with eight passes in two ways, and the third was just burnished with one pass.

Findings showed that SDB with lubricant created a zone of residual compressive stresses that is deeper and has a higher absolute value than the zone produced by the dry SDB. The exception was with the multi-pass SDB; in one way, lubrication did nothing. Also, regardless of whether or not a lubricant was used, the depth of the compressive zone dramatically rose as the number of passes increased with the one-way operating scheme. In addition, the two-way technique assured compressive area with much shallower depth than the conventional one-way approach. Also, when comparing dry SDB with SDB treated with lubricant, the biggest variation in residual stress distribution was achieved for the two-way approach. Finally, the highest absolute value of compressive residual stresses was achieved at the superficial layer when SDB was conducted in a single pass and with lubricant, and stress relaxation happened at the surface when the multi-pass scheme was used.

In another study carried out by Varga and Ferencsik [81], the research focused on the effects of burnishing parameters on low-alloyed aluminum shafts. The burnishing parameters were as follows: $r = 3.5 \text{ mm}$, $F_b = 10 \text{ and } 20 \text{ N}$, $f = 0.001 \text{ and } 0.005 \text{ mm/rev}$, $n = 1 \text{ and } 3 \text{ passes}$. Burnishing was done using lubrication oil. The results indicated that, in the tangential direction, the highest improvement ratio of residual stresses was observed when the burnishing parameters were set at a feed of 0.005 mm/rev , a force of 10 N , and a single burnishing pass. Whereas, in the axial direction, the highest percentage of stress improvement ratio was observed at the feed of 0.005 mm/rev , a force of 20 N , and also a single burnishing pass. The overall conclusion of the study was that using a smaller burnishing force with a single pass yielded more positive outcomes, while the feed rate did not have a significant effect on the improvement ratios within the tested parameter ranges.

In another study done by Maximov et al. [64], the main goal was to establish the effect of the process parameters on the surface roughness, micro-hardness, and residual stresses obtained in slide burnishing of D16T aircraft aluminum alloy. The burnishing parameters were as follows: $r = 4$ mm, $F_b = 200$ N, $f = 0.05$ mm/rev, $v = 100$ m/min, $n = 1, 2, 4, 6, 8$ passes. Results showed that the most substantial absolute values of surface stresses measured in the axial direction were observed when a single pass was used. However, as the number of passes increased from one to eight, there was a drastic reduction in the absolute value of the axial residual stresses, attributed to deforming the anisotropy caused by cyclic loading during burnishing, which led to residual stress relaxation. The findings also indicated that stress relaxation was much more significant between the first and second passes, but as the number of passes increased, the relaxation effect was sharply slowing down. While previous results were for a procedure in which lubrication was used, the study indicated that the results of dry burnishing were lower than theirs, even for the single pass of SDB. Also, a two-way scheme in dry slide burnishing resulted in more pronounced residual stress relaxation compared to the one-pass and one-way arrangements' outcomes.

From the previous studies, it can be concluded that lubrication is important for the outcomes of the burnishing process in terms of surface and subsurface residual stresses, and that increasing the number of passes over one will degrade the results at the surface due to stress relaxation, bearing in mind that the burnishing force in those studies was constant while the number of passes was increased.

Another examples of studies done with single pass of burnishing, for instance, in a study accomplished by Okada et al. [82] using AISI 316 stainless steel with a hardness of 200 HV, after the burnishing process, stresses in the axial direction were in the range of 320 to -300 MPa and from 400 to -800 MPa in the tangential direction. In another investigation carried out by Maximov et al. [80] using annealed samples made of 41Cr4 steel, the output axial stress was about -700 MPa, while the tangential stress was around -350 MPa. The third example is of research accomplished by Konefal et al. [83]. The study was carried out on austenitic X6CrNiMoTi17-12-2 alloy steel. After burnishing, the axial stress was -918 MPa and the tangential one was -501 MPa. Lastly, in a study carried out using 42CrMo4 steel with a hardness of 32 HRC carried out by Korzynski et al. [28], only the axial stresses were measured because, according to the author, they play a significant role in improving the fatigue life of the rotating shafts and axles. The results were between -145 and -461 MPa.

2.2.2. Influence of Burnishing Parameters on Surface Roughness

Surface roughness is one of the most important surface integrity components. It provides details of the material's surface topology. Before delving into the literature dealing with surface roughness, two main parameters should be defined, R_a and R_{ku} . One of the most commonly used surface roughness parameters is the arithmetic mean surface roughness ($R_a, \mu\text{m}$), Figure 4. It provides a very good overall description of height variations.

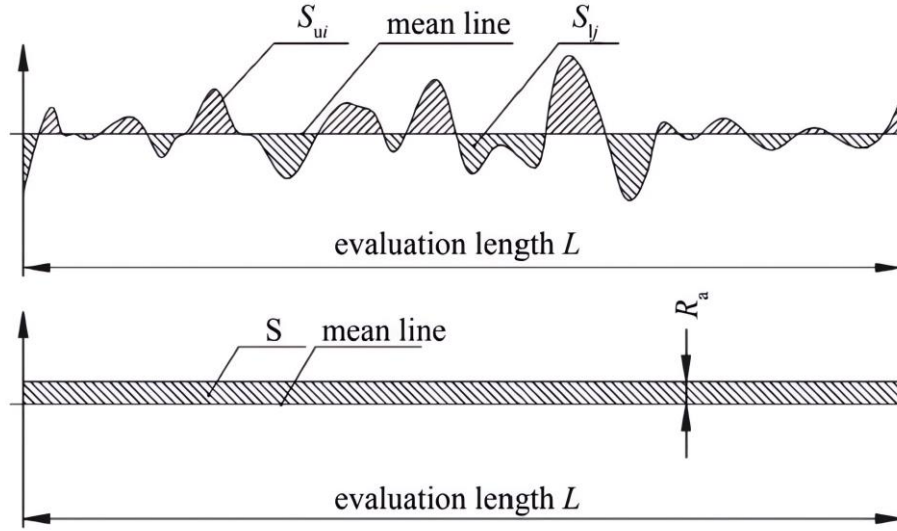


Figure 4. Schematic illustration of surface roughness R_a parameter [84]

R_a surface roughness parameter is defined as [84]:

$$R_a = \frac{1}{L} \left(\sum_{S_{u_i}} + \sum_{S_{l_j}} \right) \quad (3)$$

where:

L : Evaluation length.

S_{u_i} : The upward surface profile deviations from the mean line.

S_{l_j} : The downward surface profile deviations from the mean line.

S : Surface profile that deviates both above and below the mean line.

Another surface roughness parameter that is used to describe the surface profile is the kurtosis of roughness (R_{ku} , dimensionless). R_{ku} describes the probability density sharpness of the profile [85], [86]. As shown in Figure 5, surfaces with $R_{ku} = 3$ (Gaussian profile distribution) indicate a more balanced roughness profile, which means they have surfaces with few peaks. Conversely, high-profile kurtosis factor values with $R_{ku} > 3$ (leptokurtic profile distribution) indicate many high peaks and low valleys. Thus, the irregularities are sharp. On the other hand, $R_{ku} < 3$ (platykurtic profile distribution) indicates surfaces with no sharp parts, few high peaks, and low valleys, leading to a more flattened profile [87].

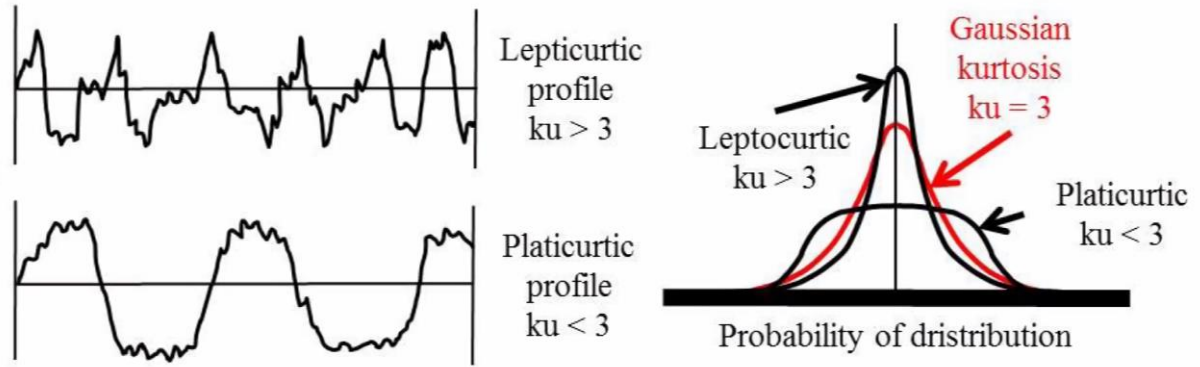


Figure 5. Illustration of roughness kurtosis parameter R_{ku} [88]

The kurtosis parameter can be calculated using the following formula [89]:

$$R_{ku} = \frac{1}{NR_q^4} \left(\sum_{i=1}^N Y_i^4 \right) \quad (4)$$

where:

N : Number of points of the profile.

R_q : Root mean square roughness parameter.

Y_i : The height of the profile at point number i .

Regarding the effect of the single-pass SDB process parameters on the resultant surface roughness (R_a), in research conducted by Liska et al. [90] on 36 surfaces made of 100Cr6 steel with a hardness of 64 HRC, values of R_a changed from 0.291, 0.39, 0.885, and 2.168 μm after hard turning, to 0.118, 0.167, 0.153, and 1.24 μm after burnishing with different burnishing settings, respectively. Kluz et al. [25] performed another recent work on 42CrMo4 steel shafts with a hardness of 22 HRC and a turning surface roughness R_a of 2.6 μm . There were 11 burnished surfaces in all, with R_a values ranging from 0.137 up to 0.225 μm after burnishing.

One of the main outcomes of the previous two studies was that decreasing the burnishing feed would decrease the resulting surface roughness. According to Bouzid et al. [91], the reason behind that is explained by the fact that when the burnishing head has a smaller distance between its traces and a lower height (h) at the intersection of two traces, Figure 6, it has a greater opportunity to smooth out the irregularities.

For relatively modest values of f when compared to the burnishing head radius R , the height h may be found using the formula [91]:

$$h = \frac{125f^2}{R} \quad (5)$$

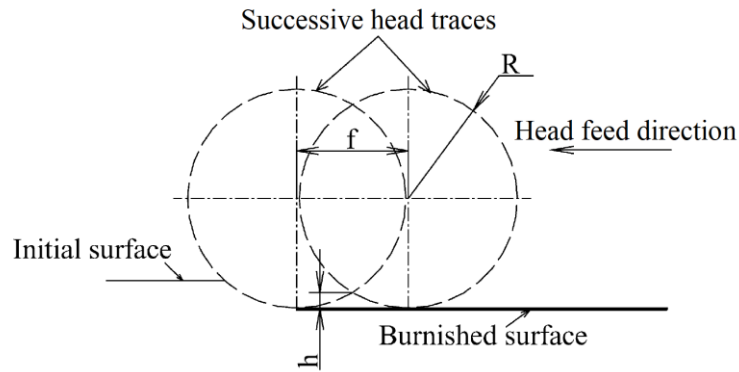


Figure 6. Surface geometry in SDB process [91]

The burnishing feed determines the spacing between burnishing head traces; hence, a larger feed reduces the burnishing head's ability to eliminate all surface irregularities. Therefore, with increasing feed, roughness can increase until it reaches its initial value.

Other examples were done to investigate the effect of changing burnishing parameters on surface roughness; in a third investigation, Tobola et al. [92] found that, on AISI D2 steel of 60 HRC hardness, he was able to lower the turned surface roughness R_a from 0.82 to 0.24 μm after burnishing. In another example, using eight turned surfaces of Vanadis 6 powder metallurgy steel of 61 HRC hardness, Brostow et al. [93] found that the surface roughness R_a was reduced from 0.97 μm after turning to a range of 0.18, 0.26, up to a maximum roughness of 0.41 μm . The last example is the study of Huuki and Laakso [94]. They have succeeded in reducing R_a from 1.78 μm after turning to 0.39 μm after burnishing, carried out on 34CrNiMo6-M steel with a hardness of 30 HRC.

2.2.3. Influence of Burnishing Parameters on Microhardness

The third important result of the burnishing process that was studied by researchers is the improvement of surface microhardness. Raising a surface's hardness primarily serves to increase its resistance to wear [95]. A lot of studies have been done to investigate the effect of the different burnishing parameters and the number of passes on the surface microhardness after the slide burnishing process. For instance, Duncheva et al. [96] investigated the effects of slide diamond burnishing on CuAl8Fe3 single-phase aluminum-bronze alloy cylindrical bars. The primary burnishing parameters that governed the process after turning were: $r = 4$ mm, $F_b = 345$ N, $v = 80$ m/min, $f = 0.07$ mm/rev and $n = 1$ to 6 passes, using a unidirectional working scheme (forward direction only).

Following the turning process, the microhardness (HV 0.05) was approximately 224 HV. It experienced a notable increase to around 298 HV (33% improvement) after the initial burnishing pass. Subsequent to the second and third burnishing passes, the microhardness reached approximately 300 HV and 306 HV (34% and 36.6% improvement), respectively. However, further

increasing the number of passes demonstrated a negligible impact on the microhardness. According to the authors, the slight increase in surface microhardness with each successive burnishing pass, following the initial one, is attributed to the strain hardening effect resulting from the plastic deformation of the dominant alpha Cu-phase in the studied alloy. The overall consequence of this incremental change is a significant improvement in wear resistance after burnishing, particularly in comparison to the turned state.

In another study done by Sachin et al. [35], the study provides a thorough analysis of the surface integrity of 17-4 PH stainless steel cylindrical bars that have been cryogenically diamond-burnished using an innovative diamond burnishing tool. The influence of the different burnishing parameters on the surface integrity components has been examined. The details of the burnishing parameters are shown in Table 3. It can be seen that, each parameter has three levels. Additionally, the number of burnishing passes was two. It is worth noting that the average surface hardness before burnishing was 340 HV. To assess the impact of increasing each of the burnishing parameters, results have been investigated using the three levels of the tool-tip radius with each level of the parameter under investigation while maintaining the other burnishing parameters at their mid-range values, specifically 0.071 mm/rev for feed, 85 m/min for speed, and 120 N for force.

Table 3. Details of burnishing parameters of Sachin et al. study [35]

Burnishing feed, f [mm/rev]	0.048	0.071	0.09
Burnishing speed, v [m/min]	25	85	132
Tool-tip radius, r [mm]	3	4	5
Burnishing force, F_b [N]	65	120	175

Regarding the findings, the primary observation indicates that a rise in the tool-tip radius, while keeping the other burnishing parameters constant, results in a reduction in surface hardness. Furthermore, it has been discovered that, irrespective of the diamond-tip radius, an increase in burnishing speed or feed contributes to a declining trend in surface hardness. Optimal hardness results were attained with the lowest speed or feed in combination with the smallest tool-tip radius. In the examination of burnishing speed's impact, a hardness of 397 HV was attained at the lowest speed, reflecting a 16.7% improvement ratio. Likewise, during the investigation of feed effects, a hardness of 406 HV was reached using the lowest feed, demonstrating a percentage improvement of 19.4%. Finally, it has been observed that the impact of burnishing force contrasts with that of speed and feed. Specifically, an increase in burnishing force leads to an elevation in resulting hardness for all tool-tip radii. Again, the highest surface hardness was achieved by employing the highest force

alongside the smallest tool-tip radius, i.e., 3 mm. Under these conditions, the hardness reached 413 HV, showing an improvement ratio of 21.5%.

Another example is a study conducted by Taamallah et al. [97]. This experimental research was conducted to examine the impact of the slide diamond burnishing technique on the mechanical characteristics of GCr15 steel. The applied burnishing parameters included: $r = 1.25$ mm, $F_b = 100$ N, $v = 560$ rpm, $f = 0.074$ mm/rev and $n = 3$ passes. The process utilized SAE 90 oil, and microhardness measurements were taken with a 3 kg load applied to the indenter.

Results of the study revealed that the microhardness on the outer layer had increased from 300 HV 3 after turning to 538 HV 3 after burnishing, representing an improvement of 79%. Additionally, the improvement was not only on the surface layer but also on the subsurface one. Microhardness measurements beneath the surface indicated the formation of a hardened layer approximately 200 μm deep.

The last example is from a study carried out by Kuznetsov et al. [68]. The study reveals the outcomes of experimental investigations conducted on the surface of discs made of AISI 304 steel to study the effect of the SDB process on their tribological properties. The surface treatments involved finishing turning, electropolishing, and burnishing processes. The burnishing was executed using a natural diamond-tipped tool with a 2 mm radius, and the investigations were performed after both a single pass and five passes of the tool with lubricant. The other burnishing parameters were as follows: $F_b = 200$ N, $v = 50$ m/min, $f = 0.01$ mm/rev.

The study's findings revealed that after five passes of burnishing, the resulting surface layer, reaching a depth of approximately 200 μm , demonstrated elevated microhardness values (HV 0.025) compared to both the initial state (electropolished) and the surface achieved through a single pass of burnishing. Before burnishing, the surface hardness measured 225 HV 0.025. This had increased to 400 and 450 HV 0.025 after one and five passes of burnishing, indicating improvements of 78% and 100%, respectively. Additionally, the results revealed that values of wear intensity (I_h), which is a measure quantifying the degree or rate at which material loss occurs on a surface due to wear, were 4.9 times lower for the one-pass burnished sample compared to the unburnished state. Surprisingly, when employing five passes, the reduction was only 3.3 times less than that of the unburnished one.

An additional examples of studies conducted with single pass of burnishing: in the study of Toboła et al. [98] carried out on Vanadis 6 and D2 steels of hardness ≈ 60 HRC, the increment of microhardness after burnishing was 10%. In another research done by Maximov et al. [64] on D16T aluminum alloy used in the aircraft industry, with a hardness of 110 HB, they improved the

microhardness of the surface by 36% using one SDB pass and 50.4% using seven passes. Another example is an investigation conducted by Łabanowski et al. [99] using UNS S32550 duplex steel with a hardness of 270 HV 0.2. In this work, the highest enhancement of the microhardness was 70.3% with a cold-worked layer of 1020 μm . The final case is about a study in which the goal of using the SDB process was to improve the structure and properties of the surface layer of the detonated coated parts of the gas turbine made of Kh12NMBF-Sh (ÉP-609)

3. OPEN QUESTIONS OF THE STUDY

Identifying the study's knowledge gap and conducting a literature review led to the exploration of the open question: **Is there an alternative method to reduce the initial surface roughness of the workpiece before the final SDB step, other than grinding?** To answer this, the proposed workplan illustrated in Figure 7 was developed.

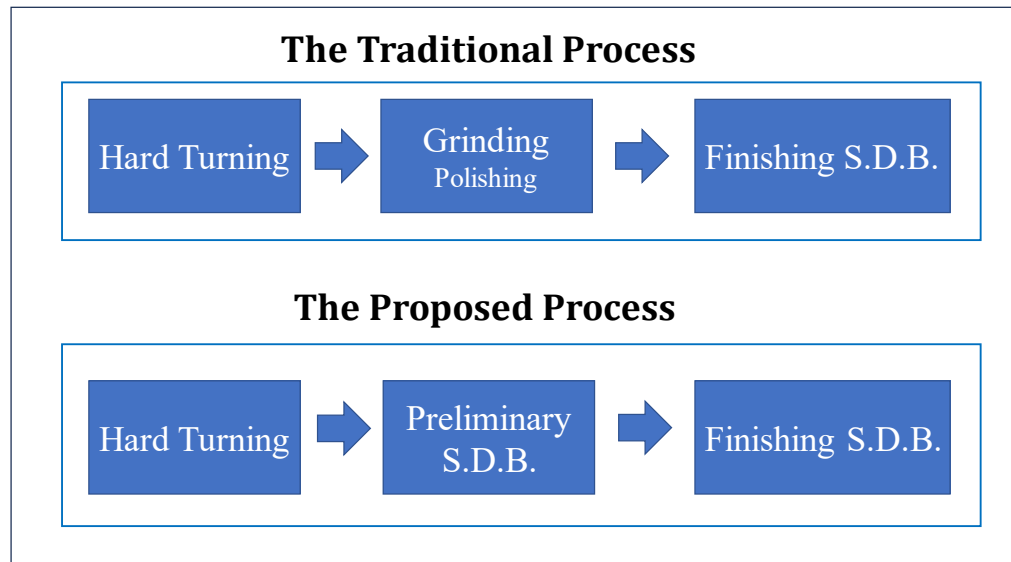


Figure 7. The proposed work plan of the Ph.D. dissertation

Illustrated in the diagram are two distinct processes: the traditional and the proposed. In the conventional approach, a single round of slide diamond burnishing is executed on surfaces that have undergone prior hard turning, followed by grinding or polishing. The results following the concluding SDB in this method, concerning surface integrity components, will be compared with those achieved through the proposed process. In the proposed approach, two consecutive SDB steps will be performed in the same direction immediately after the hard turning.

In the conventional approach, the primary aim of grinding or polishing is to minimize the initial surface roughness before the final burnishing. However, in the proposed method, this objective is accomplished through an initial or first-step SDB. This step not only addresses surface roughness but also introduces compressive residual stresses and increases microhardness to enhance the overall surface integrity before conducting the finishing or second-step SDB. Ultimately, a comprehensive comparison of both approaches will be conducted, evaluating outcomes encompassing surface roughness, residual stresses, microhardness, surface topography and morphology, and the microstructures in the burnished cross-sections. This analysis aims to draw a conclusion regarding which approach proves superiority based on the specified outcomes.

Finally, at the end of this study, the following questions should be answered:

1. What are the optimal parameters (speed, feed, and force) within the examined range that result in the lowest surface roughness for steel rods subjected to hard turning during the initial SDB procedure?
2. When using the optimal burnishing speed and feed, what is the optimum burnishing force to be used in the traditional approach to achieve the best surface quality?
3. What combination of first-step and second-step burnishing forces should be used in the proposed process to achieve the highest surface quality in the finishing SDB process, characterized by low surface roughness, high compressive residual stresses, high hardness, and fine grain structure?
4. Is it possible to achieve superior surface quality (low surface roughness, high compressive residual stresses, high hardness, and improved microstructure) in hard-turned 42CrMo4 steel through a two-step SDB method compared to a single SDB process involving either grinding or polishing?
5. Is the utilization of two-step SDB instead of one-step SDB directly after turning, without subsequent process like grinding or polishing in hard-turned 42CrMo4 steel, more advantageous in terms of surface integrity components?

4. EXPERIMENTAL SETUP

4.1. Material and Specimens Preparation

The specimens were cylindrical in shape, with a diameter of 50 mm and a length of 280 mm. Each bar was partitioned into eight segments, each measuring 25 mm in length, and separated by a 5 mm gap, as shown in Figure 8. The overall number of bars was five. After sectioning, the workpieces underwent austenitization at a temperature of 855°C, followed by oil quenching, and then tempering for a duration of two hours at a temperature of 180°C, resulting in a hardness level of 54 HRC. The processes of hardening and tempering were conducted at the Institute of Physical Metallurgy, Metalforming and Nanotechnology at the University of Miskolc.

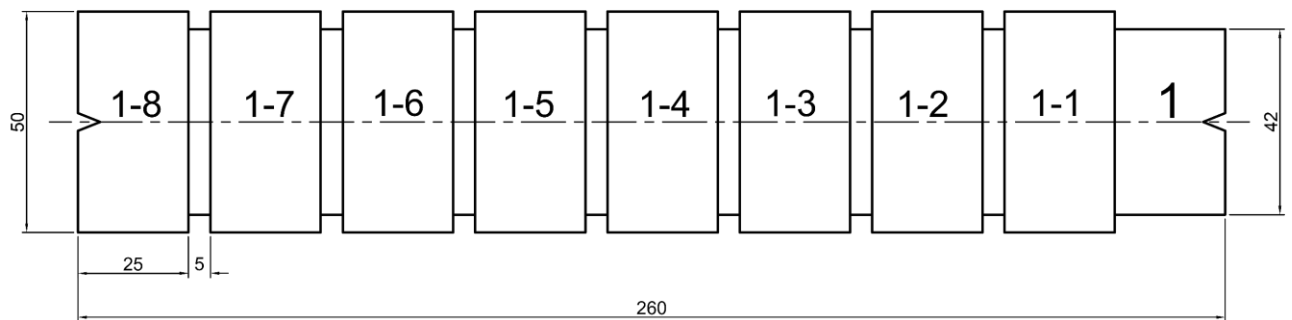


Figure 8. Schematic representation of the samples' outlines

4.2. Hard-Turning, Grinding, and Polishing Conditions

Following the hardening process of the bars, the hard turning was performed on an OPTItorn S 600 CNC lathe using an insert from Mitsubishi Materials Company, model number: CNGA 120408 TA4 MB8025. The cutting speed (v_c) was set at 120 m/min, the cutting feed (f) was 0.1 mm/rev, the tool nose radius (r_ϵ) was 0.8 mm, and the depth of cut (a_p) was 0.2 mm. This turning operation took place at the Institute of Manufacturing Science at the University of Miskolc.

For grinding, a CNC mantle grinder, type Studer S31, was utilized. The grinding wheel speed (v_T) was 25 m/s, the workpiece speed (n_W) was maintained at 600 rpm, the feed rate (f) was set at 700 mm/min, and the removed allowance (Z) was kept at 0.005 mm. The diameter of the corundum wheel was 400 mm, and the grain size was 80 μm .

For the polishing, a manual grinder of the Bernardo DS200-400 type was utilized. The polishing speed (v_T) was set at 2850 rpm, and DIASTAR paste (diamond grit size 5.5-8 μm) was employed. Both the grinding and polishing processes were carried out by Fraisa Hungária Kft, a company specializing in machining and precision engineering.

4.3. Burnishing Conditions

Samples were categorized into three groups: ground-then-burnished (G + SDB), polished-then-burnished (P + SDB), and burnished twice (two-step SDB). Due to the considerable number of surfaces, each surface was assigned a code with two parts for simplicity. The first part denotes the bar's number, and the second part represents the surface's number on that bar. Table 4 and Table 5 outline the burnishing parameters for the surfaces that underwent SDB after grinding and polishing and for those that underwent two-step SDB, respectively. After grinding and polishing, each surface on every bar was subjected to a unique burnishing force, ranging between 25 N and 200 N, in increments of 25 N between the adjacent surfaces. However, for the surfaces that underwent two-step SDB, in the first step of burnishing, the surfaces on bar No. 9 were burnished with 50 N, those on bar No. 10 with 100 N, and those on bar No. 8 with 150 N. Subsequently, each surface on every bar was burnished in the second step with a distinct force from those ranging from 25 to 200 N.

Table 4. Burnishing parameters of the ground and polished surfaces

Surface No.	Surface Code	Pre-Burnishing Process	SDB Parameters		
			v [m/min]	f [mm/rev]	F_{fin} [N]
1	12-1	GRINDING	115 (750 rpm)	0.03	25
2	12-2				50
3	12-3				75
4	12-4				100
5	12-5				125
6	12-6				150
7	12-7				175
8	12-8				200
9	13-1	POLISHING	115 (750 rpm)	0.03	25
10	13-2				50
11	13-3				75
12	13-4				100
13	13-5				125
14	13-6				150
15	13-7				175
16	13-8				200

Notably, the burnishing speed and feed remained constant across all surfaces. Based on the findings from the initial phase of this research, the combination of this speed and feed yielded the optimal results for surface roughness, as well as high axial compressive residual stresses and microhardness

values. The selection of these optimal parameters is discussed in detail in the published Q1 paper titled: **Improving Surface Integrity by Optimizing Slide Diamond Burnishing Parameters After Hard Turning of 42CrMo4 Steel** [62].

Table 5. Burnishing parameters of the first-step and second-step SDB

Surface No.	Code	Preliminary SDB			Finishing SDB		
		v [m/min]	f [mm/rev]	F_{in} [N]	v [m/min]	f [mm/rev]	F_{fin} [N]
17	9-1	115 (750 rpm)	0.03	50	115 (750 rpm)	0.03	25
18	9-2						50
19	9-3						75
20	9-4						100
21	9-5						125
22	9-6						150
23	9-7						175
24	9-8						200
25	10-1			100			25
26	10-2						50
27	10-3						75
28	10-4						100
29	10-5						125
30	10-6						150
31	10-7						175
32	10-8						200
33	8-1			150			25
34	8-2						50
35	8-3						75
36	8-4						100
37	8-5						125
38	8-6						150
39	8-7						175
40	8-8						200

In order to assess the mean contact pressure exerted by the burnishing head for each burnishing force, Hertz theory was applied using the following equation [100]:

$$\bar{\sigma} = 0.410 \sqrt[3]{\frac{F_b E^2}{4R^2}} \quad (6)$$

Where

$\bar{\sigma}$: Mean contact pressure, [N/m²].

F_b : Burnishing force, [N].

E : Young's modulus of elasticity of the workpiece, [N/m²].

R : Radius of the burnishing head, [m].

Taking into account that the Young's modulus of elasticity of 42CrMo4 quenched and tempered steel is 200 GPa [101], results are depicted in Table 6.

Table 6. Mean contact pressures exerted by the burnishing head

F_b [N]	25	50	75	100	125	150	175	200
$\bar{\sigma}$ [MPa]	1120	1412	1616	1779	1916	2036	2143	2241

Samples underwent burnishing using an EU-400-01 universal lathe, as depicted in Figure 9, using a burnishing tool with a 3.5 mm radius tip made of PCD (polycrystalline diamond) manufactured at the Institute of Manufacturing Science, University of Miskolc. Based on findings from Nestler and Schubert's study [102], this radius value was chosen for its potential to enhance surface roughness in the SDB process. Furthermore, burnishing was carried out using SAE 15W-40 oil.

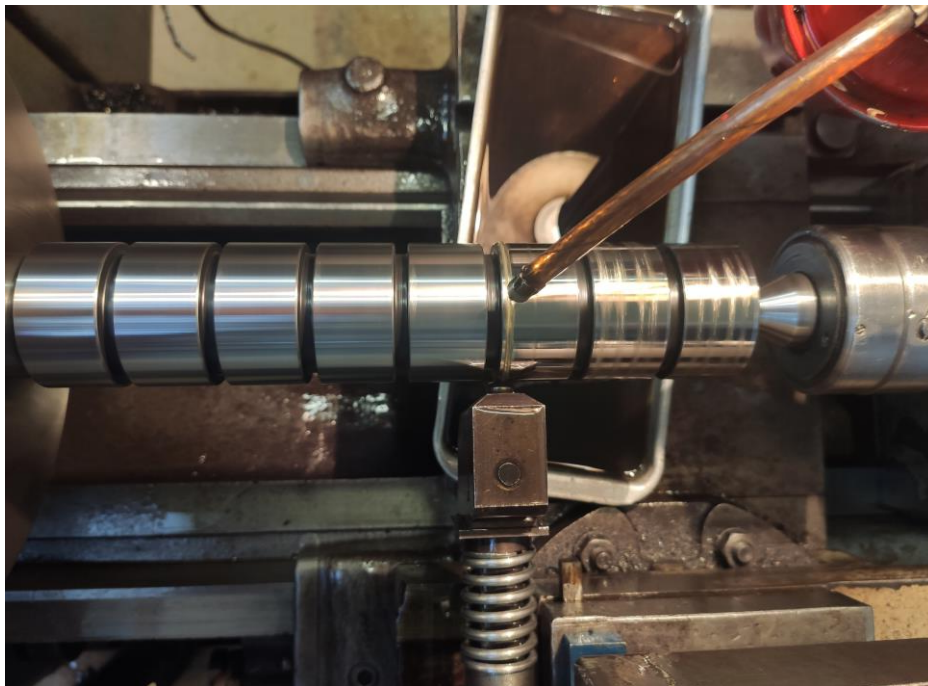


Figure 9. SDB process implementation

4.4. Measuring Residual Stresses

After turning, grinding, polishing, preliminary and finishing steps of SDB, residual stress components of the two main directions were measured, namely the axial (feed) and tangential (speed) directions, as depicted in Figure 10. The $\sin^2\psi$ method was used with a Stresstech - Xstress 3000 G3R type centerless diffractometer equipped with a Cr X-ray source. For measurements, the {211} of the ferrite phase reflections were measured. During the measurements, a collimator of 2 mm in diameter was utilized. The tilting number was 5 in both tilting directions (left and right), with maximum tilting angles of $\mp 45^\circ$. The exposure time was chosen to be 4 seconds. Background extraction was done using linear subtraction, and the material parameters were Young's modulus of 211 GPa and Poisson's ratio of 0.3. For each surface, three measurements were taken at equal angles of 120° at the perimeter, and the average was calculated. It is worth mentioning that stress measurements were taken after the burnishing process at varying intervals—sometimes after a few days, sometimes after weeks, or even months. This variability is due to the fact that no stress relaxation occurs after burnishing; otherwise, the method would be ineffective.

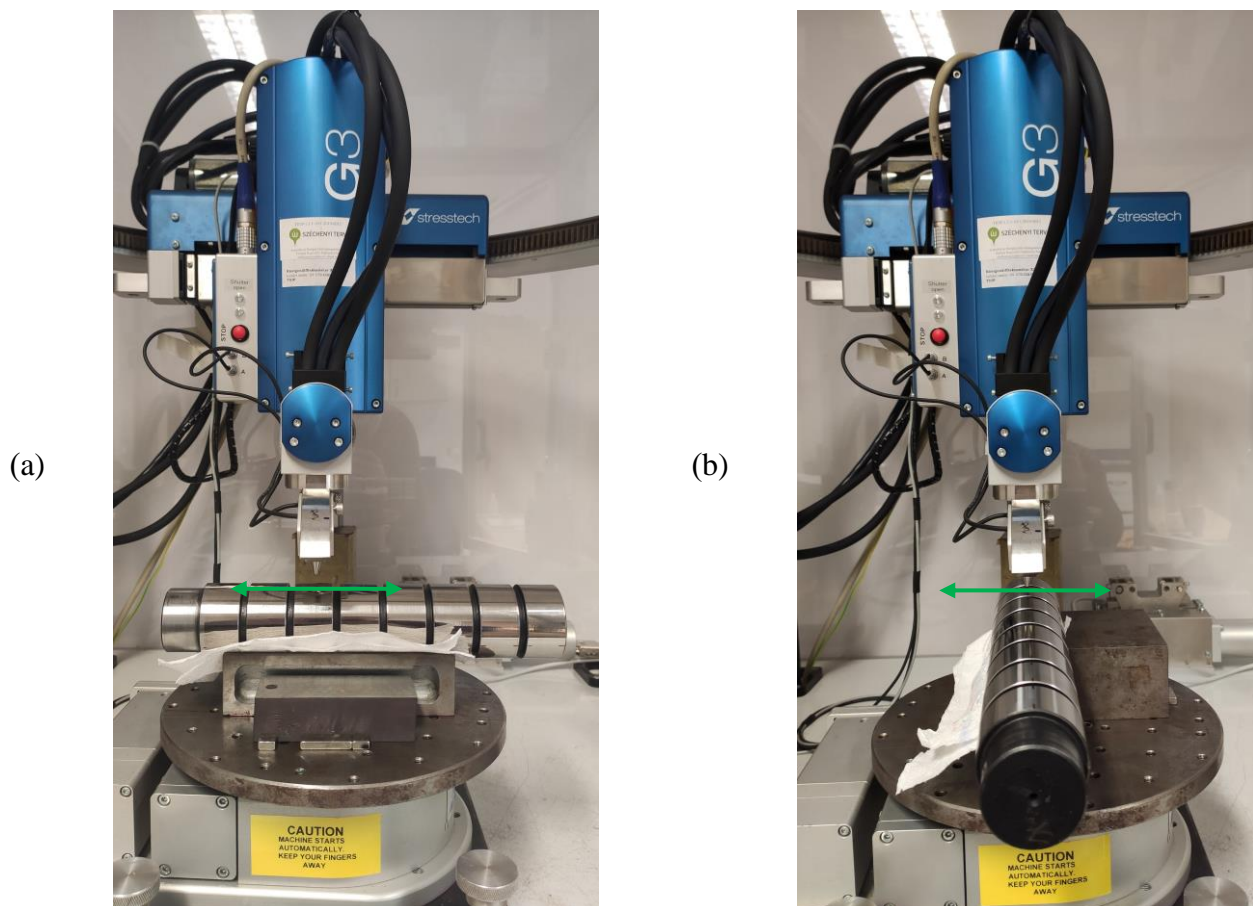


Figure 10. Measuring surface residual stresses in: (a) axial direction, (b) tangential direction

After analyzing the outcomes for surface residual stresses, surface roughness, and microhardness after the finishing step of burnishing, surfaces with the optimal results were selected for further

examination of their in-depth residual stresses. Besides, the in-depth residual stress distribution after turning, grinding, polishing, and the first step of burnishing was investigated. For that purpose, a QETCH 100 M electrolytic etcher from QATM was employed to remove the steel's layers, and the thickness of the etched layers was measured using the Mitutoyo ABSOLUTE depth gauge. Surface and in-depth stress measurements were carried out at the Institute of Physical Metallurgy, Metalforming and Nanotechnology at the University of Miskolc. Eventually, it is worth mentioning that for the whole measurements, the error range was less than ∓ 50 MPa.

4.5. Surface Roughness Measurements

The arithmetic mean surface roughness (R_a) of the burnished pieces was measured in the axial (feed) direction. In those measurements, the measurement length was 1.5 mm, the evaluation length was 1.25 mm, and the cut-off was 0.25 mm, chosen in accordance with ISO 21920-2:2021 for roughness measurements. Additionally, for the surfaces that underwent a two-step SDB and were burnished with 150 N in the first step, the kurtosis parameter (R_{ku}) was measured over lengths of 1.5 mm in both the axial and tangential directions. For the measurements of R_a and R_{ku} , three measurements—each of them was taken along a single line scan across the surface—were captured at equal angles of 120° around the perimeter, and the average value was calculated. In addition to the previous measurements, 3D surface topography was generated by scanning 1.5×1.5 mm areas for the purpose of visually assessing some selected surfaces. All of the aforementioned 2D and 3D measurements were conducted at the Institute of Manufacturing Science, University of Miskolc, using the confocal chromatic sensor on the AltiSurf 520 device, as shown in Figure 11.

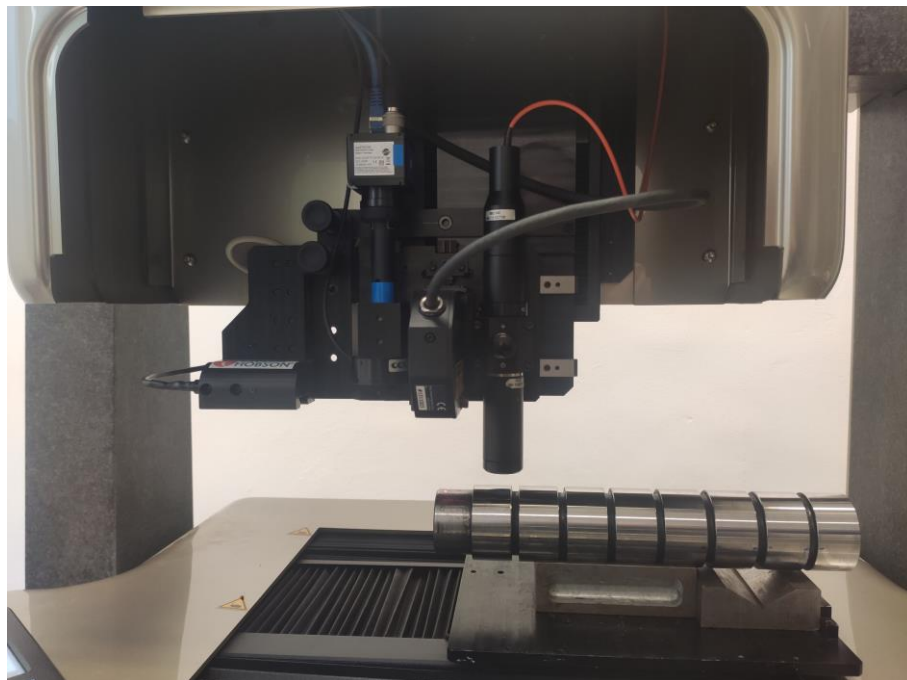


Figure 11. Measuring surface roughness, kurtosis, and 3D surface topography

4.6. Measuring Microhardness (HV 0.2)

After the finishing step of SDB, the microhardness of the entire surfaces was measured in the axial direction. This was conducted at the Institute of Physical Metallurgy, Metalforming and Nanotechnology at the University of Miskolc using the Wilson Instruments Tukon 2100 B device shown in Figure 12. Vickers microhardness was determined at three different points on the top of each surface using a 200-gram load, and the average value was then calculated.

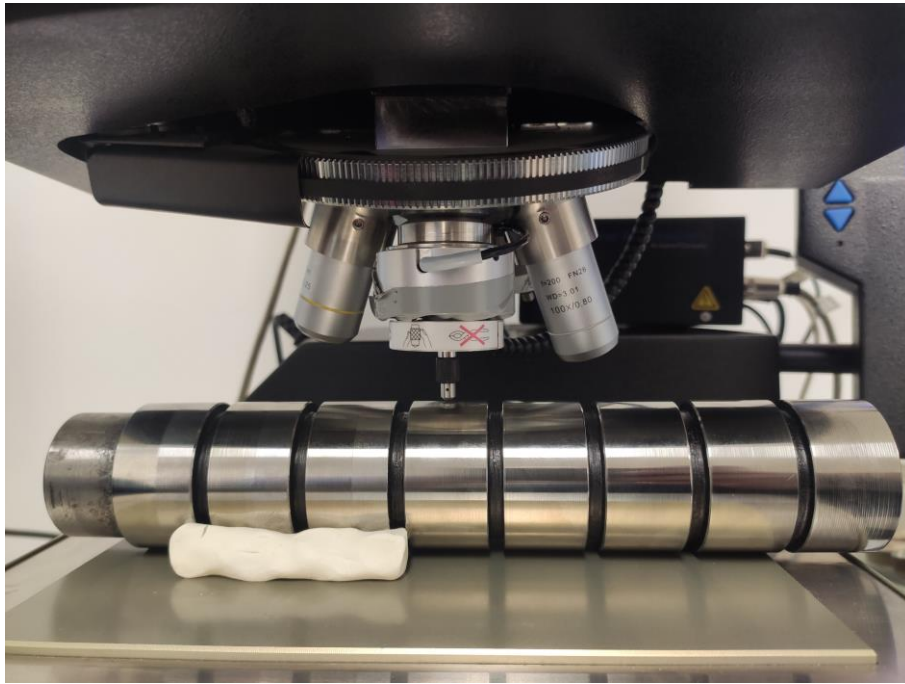


Figure 12. Measuring microhardness (HV 0.2)

4.7. SEM Investigations of Surface Morphology and Cross-Sectional Microstructure

After analyzing the outcomes for surface residual stresses, surface roughness, and microhardness after the finishing step of burnishing, surfaces with the optimal results were selected for further examination of their surface morphology and cross-sectional microstructure of the burnished layer using scanning electron microscopy (SEM). SEM micrographs were obtained at the Institute of Physical Metallurgy, Metalforming, and Nanotechnology at the University of Miskolc.

5. RESULTS AND DISCUSSION

5.1. Surface Residual Stresses

5.1.1. Surface Axial Residual Stress Component After the Finishing Step of SDB

As it was mentioned previously, axial residual stresses significantly contribute to improving the fatigue durability of rotating shafts and axles exposed to cyclic loading. The average values of surface axial residual stress component after turning, grinding, polishing, and the first step of SDB are illustrated in Figure 13. Compressive stresses were noted across all samples but varied in magnitude. Hard-turned surfaces registered an average stress of -130 MPa. Subsequent to that, the polished surfaces exhibited the least compressive stress at -169 MPa. Ground surfaces exhibited -509 MPa, and surfaces subjected to the first burnishing step presented the most substantial compressive stresses, exceeding -1100 MPa, depending on the applied force. Besides, it is relevant to mention that the average axial stress component on the surface that was burnished with a single-step SDB after turning by 200 N was -1228 MPa. These findings, along with the outcomes following the finishing SDB step, are presented in Table 10 in the appendix.

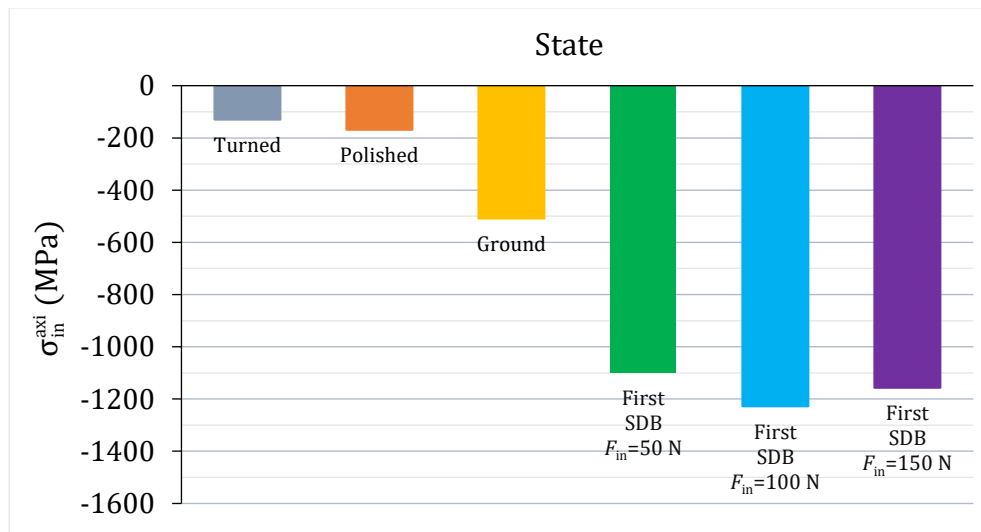


Figure 13. Surface axial residual stresses after turning, grinding, polishing, and first step of SDB

The average of surface axial residual stress components after the finishing step of the SDB process are depicted in Figure 14. A significant level of compressive residual stresses (CRS) on the ground and polished surfaces was induced. The dependence of the induced CRS magnitude on the finishing burnishing force was evident. With the five processes, a general trend was observed: An increase in the finishing burnishing force led to an increase in the generated CRS, with the exception of the polished surfaces burnished by forces ranging between 25 and 75 N.

Comparing the CRS values for surfaces that were ground-then-burnished and polished-then-burnished, it is observed that their outcomes tend to overlap after the burnishing step. This implies that, under certain forces (specifically between 25 and 75 N), the ground-then-burnished surfaces exhibit lower stress values. However, beyond this force range, the trend reverses, with the notable exception at a 175 N force, where the stress levels for both cases are roughly equivalent. In conclusion, applying a burnishing force greater than 75 N to a ground surface results in higher CRS compared to that achieved by polishing, then burnishing.

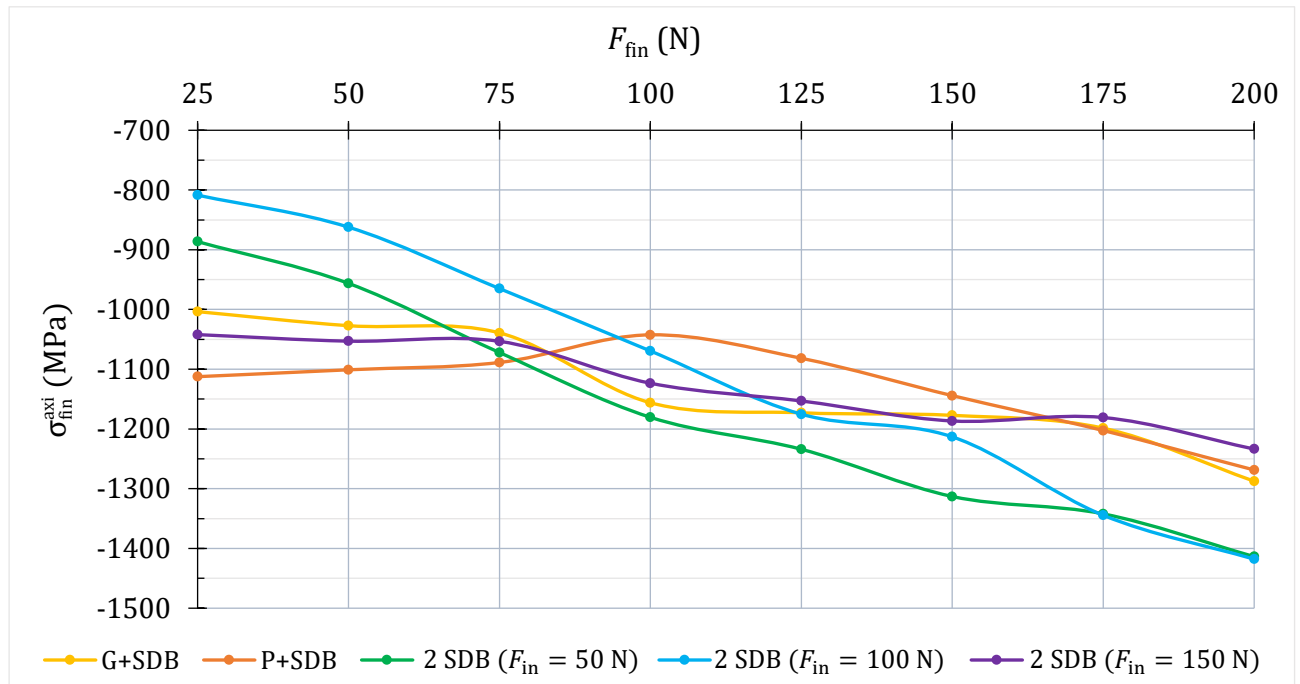


Figure 14. Surface axial residual stress component for the whole surfaces after the finishing step of SDB

The average results for both grinding, then burnishing, and polishing, then burnishing cases were very close, with a mean value of approximately -1130 MPa. However, the standard deviation for the ground-then-burnished surfaces was higher, at 99.3 MPa, compared to 73.3 MPa for the polished-then-burnished surfaces. This indicates a greater variability in response among the ground surfaces to the burnishing process compared to the polished surfaces. Evidently, the CRS for ground surfaces consistently increased with higher burnishing forces, a trend not observed with the polished surfaces.

On the other hand, with surfaces that underwent the two-step SDB process, the CRS was significantly influenced by the force of the first step of SDB. Generally, an increase in the second SDB force corresponded to higher CRS levels, but at varying rates depending on the force of the first SDB step. The behavior of surfaces burnished with 50 N and 100 N in the first step was similar, even showing identical stresses when subjected to the second-step burnishing forces of 175 N and 200 N. However, the stress values obtained after the second burnishing step with 75 to 200 N

applied to the surfaces that were burnished with 50 N in the first step surpassed those that were initially treated with 100 N and 150 N in the first step. Surfaces initially burnished with 150 N in the first step only outperformed the others when finishing forces of 25 and 50 N were applied due to the higher extent of plastic deformation exerted in the first step of burnishing, but for second-step forces between 75 and 100 N, they showed better results only in comparison to surfaces that were burnished with 100 N in the first step.

For detailed analysis, the range of the results, mean values, and standard deviation (STD) for the three groups of surfaces that underwent two-step SDB are shown in Table 7. The STD was assessed to determine the extent of CRS dependency on the first-step burnishing force during the second burnishing step. Notably, the surfaces subjected to the forces of 100 N and 50 N in the first burnishing step exhibited the highest STD values, respectively. This indicates that the preparatory work done by the first burnishing step on these two sets of surfaces made them more responsive to the second burnishing force, leading to a more consistent enhancement of the CRS as the force in the second step was increased.

Table 7. Surface axial residual stress mean and standard deviation (STD) values of the two-step burnished surfaces

F_{in} [N]	Range of σ_{fin}^{axi} [MPa]	Mean [MPa]	STD [MPa]
50	-886 to -1414	-1175	189
100	-809 to -1418	-1107	220
150	-1042 to -1234	-1128	73

In contrast, the surfaces burnished with 150 N in the first step exhibited the lowest standard deviation among the three groups, indicating a minimal variation in the CRS values, as seen in Figure 14. This suggests that employing the highest initial burnishing force of 150 N in the first step reduced the capacity of the surfaces to benefit from additional enhancements through the second-step burnishing forces in terms of CRS.

Comparing the results of the conventional approach of conducting SDB after grinding or polishing with the outcomes of the proposed two-step SDB method reveals that the optimal results, within the 25 to 75 N range of finishing burnishing force, were obtained when polishing, then burnishing, was applied. Within this same force range, the surfaces burnished with 100 N in the first step exhibited the lowest CRS outcomes. Conversely, for the finishing burnishing forces lying between 100 and 150 N, the least favourable outcomes occurred on the polished-then-burnished surfaces, while the best outcomes within this force range were observed on surfaces burnished in the first step with 50

N. For forces ranging from 175 to 200 N, the results split into two categories: the first category, achieving the highest CRS values, included surfaces burnished with 50 and 100 N in the first step, displaying very similar outcomes; the second category, showing the lowest stress values, encompassed the other three cases, with the lowest values recorded for surfaces at first burnished with 150 N.

To summarize, the CRS on the surface of a burnished workpiece is significantly determined by the finishing burnishing force applied, with a notable increase in stresses observed with higher forces. Yet, the effect is also contingent upon the surface's initial condition. For instance, in the finishing force range of 25 to 75 N, surfaces that underwent polishing before burnishing demonstrated the most significant improvement. Beyond this force spectrum, the optimal outcomes were on surfaces burnished with 50 N in the first step, then subjected to forces above 75 N, or to 175 N and beyond when burnished in the first step with 100 N. Overall, the maximum CRS values, reaching up to -1415 MPa, were achieved on surfaces that underwent a two-step burnishing process, initially at 50 or 100 N, followed by a second application of 200 N. In comparison, the highest CRS observed for the surface that was ground-then-burnished with 200 N was -1278 MPa.

5.1.1.1. Percentage of Axial Residual Stress Improvement of the Two-Step SDB Process

A critical aspect of evaluating the two-step SDB process is assessing the improvement in axial residual stress percentage ($\%I\sigma_{\text{axi}}$). This importance is rooted in the fact that burnishing operations on surfaces that have been turned, ground, or polished inevitably result in a substantial elevation of surface residual stresses, even converting any pre-existing tensile stresses into compressive ones. Consequently, a pivotal question arises: How does the finishing SDB process affect surfaces that have undergone previous burnishing? Therefore, careful examination of this percentage is essential to ascertain whether axial residual stresses on the turned and burnished surfaces are enhanced or not in the second step of burnishing and to understand how alterations in the first and second burnishing forces influence these stresses.

The percentage of the surface axial residual stress improvement was calculated using the following formula:

$$\%I\sigma_{\text{axi}} = \frac{\sigma_{\text{fin}}^{\text{axi}} - \sigma_{\text{in}}^{\text{axi}}}{\sigma_{\text{in}}^{\text{axi}}} \times 100\% \quad (7)$$

where:

$\%I\sigma_{\text{axi}}$: Percentage of axial surface residual stress improvement, [%].

$\sigma_{\text{in}}^{\text{axi}}$: Surface axial residual stress after the first SDB step (at $F_{\text{fin}} = 0.0$ N), [MPa].

$\sigma_{\text{fin}}^{\text{axi}}$: Surface axial residual stress after the second SDB step, [MPa].

In the appendix, Table 11 displays axial residual stress outcomes after the first burnishing step in the first row, followed by stress values and their percentage of improvement after the second burnishing step. Furthermore, the results of the $\%I\sigma_{axi}$ are illustrated in Figure 15. It is critical to recognize that negative values in the outcomes represent a decrease in residual stresses from their original levels, while positive values denote an increase of these stresses. Moreover, it is essential to highlight that results comparisons should be confined to surfaces within the same group and not across different categories, even if subjected to the same final burnishing force, owing to differing reference stress values (σ_{in}^{axi}).

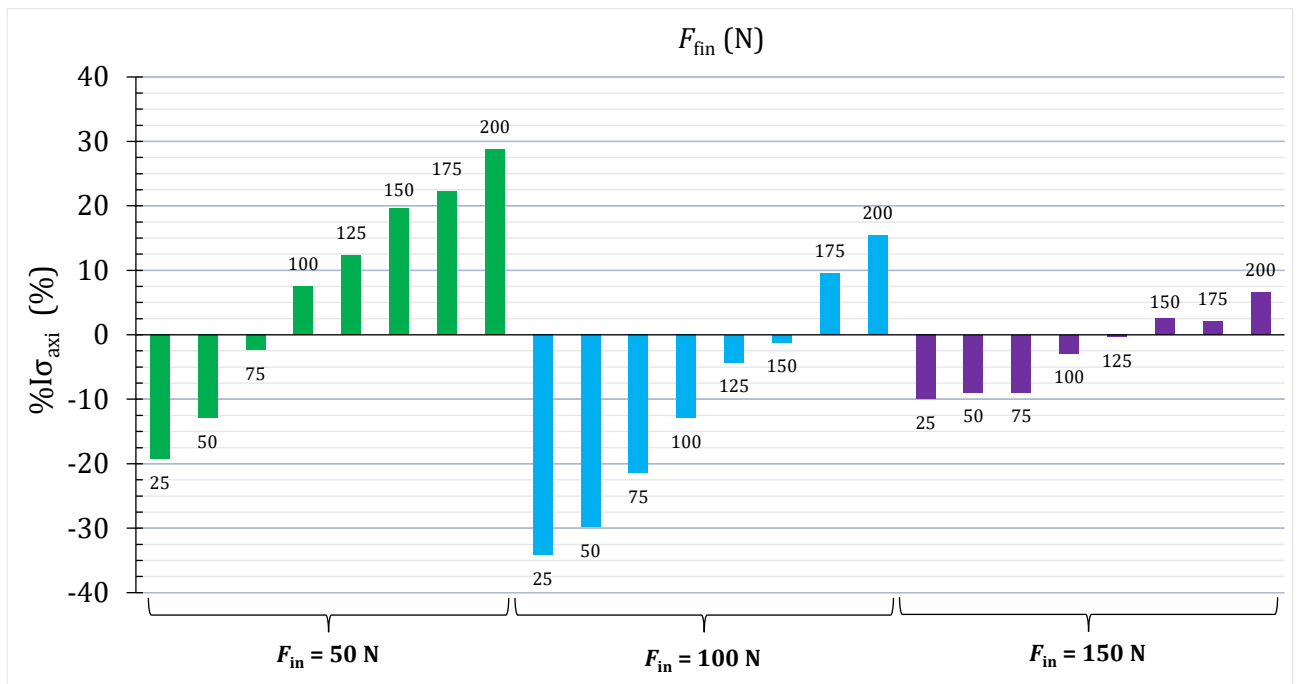


Figure 15. Improvement percentage in surface axial residual stresses for surfaces treated with two-step SDB

The chart analysis reveals distinct behaviors across the three sets of surfaces, each burnished with a different force in the first step. For the three groups, the general trend is that there is a noticeable improvement in axial stresses on certain surfaces, while others exhibit a reduction. Another general observation is that as the finishing burnishing force increases, the percentage of axial residual stress improvement tends to increase, and the onset of positive results happens after a specific burnishing force used in the second SDB step. Additionally, the trend implies that a more substantial final burnishing force enhances the increase of beneficial compressive stresses on the surface. The most significant enhancements are observed at the peak finishing force of 200 N.

The surfaces burnished with 50 N in the first step displayed a decrease in $\%I\sigma_{axi}$ at lower finishing forces of 25, 50, and 75 N, yielding reductions of 19.3%, 12.9%, and 2.4%, respectively. However, a shift occurred at a finishing force of 100 N, where improvement became positive at 7.5% and

continued to rise with increasing force. The greatest enhancement was observed at a finishing force of 200 N, achieving a notable 28.7% improvement.

The deterioration of residual stresses after the second burnishing step carried out on the previously burnished surfaces is attributed to stress relaxation. Following the first burnishing step, the surfaces experienced plastic deformation and compression to a specific extent and depth, influenced by the value of the force, which in this case was 50 N. This process resulted in an anisotropic topology within a certain depth of the material. Upon the subsequent burnishing step, since the force applied was not high enough to achieve further plastic deformation and compression of the material, the previously established anisotropic topology was disturbed and altered. As a result, the compressive stresses previously stored within the material were dissipated, attributed to stress relaxation from cyclic loading. Maximov et al. [64] and Varga and Ferencsik [81] observed a similar phenomenon when they explored the impact of multiple burnishing passes on surface residual stresses, noting changes with an increase in the number of passes. However, when the applied force exceeded 75 N in the second step of burnishing, the percentage of improvement in residual stresses turned positive, indicating that these higher forces were sufficient to impose additional plastic deformation and compressive stresses in the pre-burnished layers.

A similar pattern was observed in the group of surfaces burnished with 100 N in the first step. Within the range of second-step burnishing forces from 25 to 150 N, the percentage of improvement in residual stresses was negative. Notably, positive enhancements in residual stresses were only achieved with forces exceeding 150 N. Comparing with the previous group of surfaces burnished in the first step with 50 N, improvements in surface residual stresses were noted at increased finishing forces during the second burnishing step due to the higher initial burnishing force. This is attributed to the greater work hardening and plastic deformation induced by the higher first-step force, which in turn suggests a limitation in the effectiveness of the subsequent burnishing step.

Lastly, it is observed that for the third group, subjected to the highest burnishing force of 150 N in the first step, improvements in residual stresses were only realized with finishing burnishing forces of approximately 150 N and above. However, the percentage of improvement remained low, at 2.6%, 2.1%, and 6.6% for the finishing burnishing forces of 150 N, 175 N, and 200 N, respectively. The primary reason for this low percentage is the high burnishing force used in the first step, which limited the potential for enhancing compressive residual stresses within the range of finishing SDB forces applied.

In summary, based on the present findings within the specified range of the first and second SDB forces, to enhance axial residual stresses following the first step of the two-step SDB process, a second-step burnishing force greater than the first-step forces of 50 N and 100 N, and nearly equivalent to the 150 N is recommended. The subsequent analysis will determine the minimum second-step burnishing force necessary to begin improving compressive axial residual stresses for each set of surfaces.

Examining the data in Figure 15 reveals a pattern closely resembling a linear relationship, particularly evident in the first two sets of surfaces. To quantify this observation, Microsoft Excel was utilized to assume linearity and derive the equation for each line, with the specific equations presented in Table 8. The predicted R-square values were computed. This coefficient is critical as it quantifies the extent to which the statistical model aligns with the observed data, serving as a statistical indicator of the model's accuracy in fitting the dataset [103]. Furthermore, the table includes calculations of the finishing burnishing force values ($F_{fin-0.0}$) at which the percentage improvement in axial residual stress turns positive.

Table 8. Behavior equations of the results of percentage of surface axial residual stress improvement

F_{in} [N]	Equation	R^2 [%]	$F_{fin-0.0}$ [N]
50	$\%I\sigma_{axi} = 0.277F_{fin} - 24.2$ (8)	98	87
100	$\%I\sigma_{axi} = 0.292F_{fin} - 42.7$ (9)	99	146
150	$\%I\sigma_{axi} = 0.099F_{fin} - 13.6$ (10)	94	137

The high R^2 values indicate that the equations are a good representation of the results, demonstrating a significant correlation between the modeled data and the observed outcomes. According to the analysis, 74%, 46%, and -8.6% of the forces 50, 100, and 150 N needed to be added to them to reach 87, 146, and 137 N, respectively. The reason for this decreasing trend is the quality of surface produced after the first step of burnishing, depending on the value of force utilized in that step. This point will be examined in the section that discusses surface topography and morphology later.

5.1.2. Surface Tangential Residual Stress Component After the Finishing Step of SDB

Following the analysis of surface residual stress component in the axial (feed) direction in the previous subsection, this section will focus on discussing and examining the surface residual stress component in the tangential (speed) direction observed after completing the finishing step of the SDB process. It should be noted that while tangential stresses are generally less critical for fatigue life, they become significant when discussing the correlation between tangential stresses and surface topology later in the analysis.

Prior to the final SDB step, the average of tangential residual stress values after the various processes are depicted in Figure 16. Notably, stresses were found to be tensile after turning and polishing, in contrast to the compressive stresses observed after grinding and after the first SDB step. The sequence of highest tensile stress was observed following turning and then polishing. Among compressive stresses, the lowest CRS was recorded after grinding, followed by surfaces initially burnished with forces of 100 N, 150 N, and the lowest being those burnished with 50 N. Additionally, it is valuable to mention that the average tangential stress component on the surface that was burnished by a single-step SDB after turning using 200 N was -502 MPa.

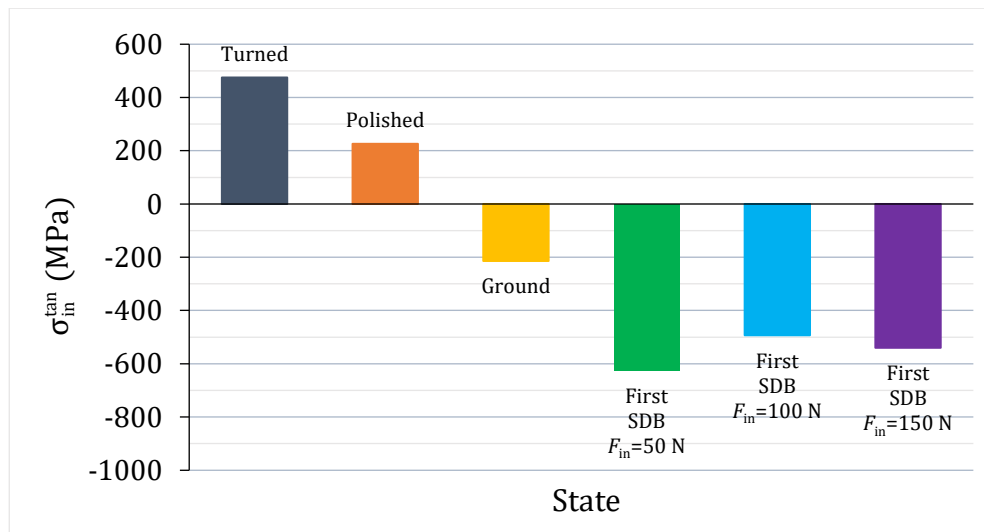


Figure 16. Surface tangential residual stress component after turning, grinding, polishing, and first step of SDB

Table 12 in the appendix details the tangential residual stress values following the SDB finishing step, indicating that all results fall within the compressive range. These findings are also illustrated in Figure 17. Before delving into the results, it is important to note that in this context, "increase" and "decrease" refer to stresses becoming more or less compressive, respectively. Additionally, a comparison between the initial state and subsequent burnishing force (0 and 25 N) in Table 12 reveals that the application of the lowest finishing force of 25 N generally led to an improvement (increase) in tangential stresses across all groups, with the exception of the surface initially

burnished with 50 N. Beyond this point, the predominant trend observed across all groups is a decrease in tangential stresses with higher finishing burnishing forces.

The figure reveals that tangential stresses after grinding, then burnishing, surpass those observed after polishing, then burnishing, except at the force of 75 N. This variation is primarily due to the distinct stress levels encountered after grinding compared to after polishing, where stresses were -214 MPa and 226 MPa, respectively. This makes the stresses more compressive by 440 MPa after grinding than after polishing. Therefore, concerning tangential residual stresses, employing grinding instead of polishing results in higher compressive residual stresses, provided that the grinding process was executed using parameters that were capable of generating compressive residual stresses.

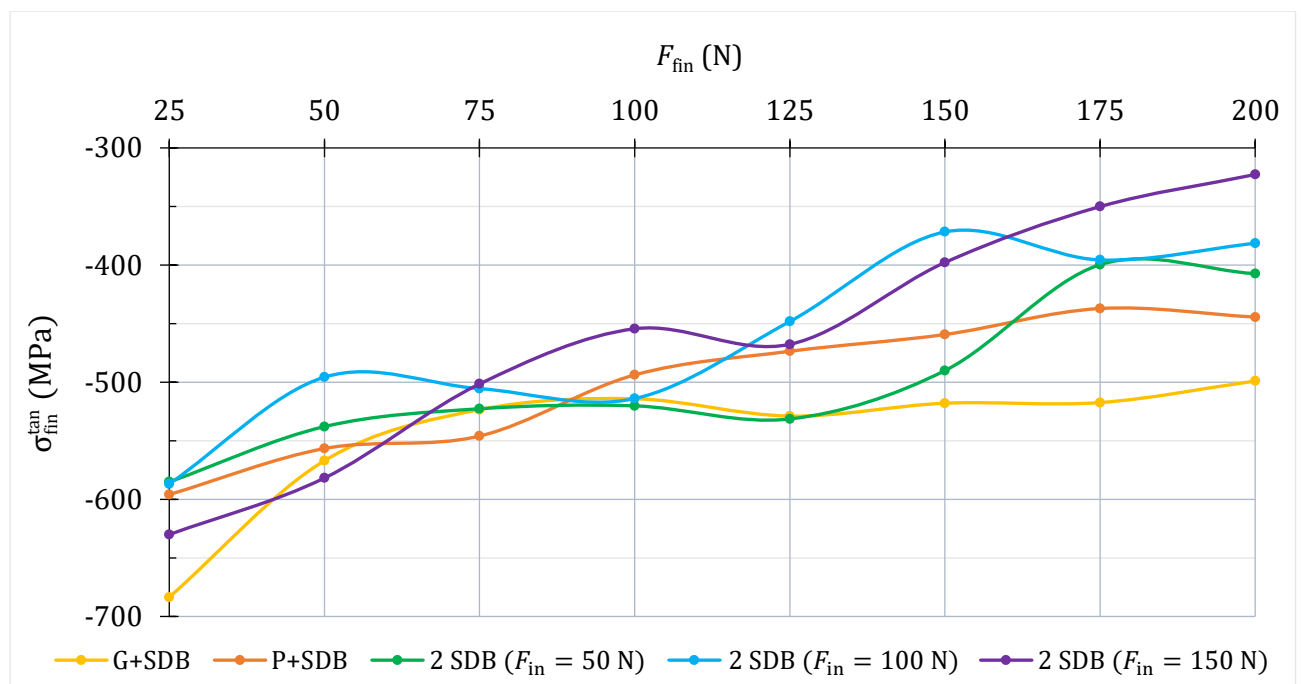


Figure 17. Surface tangential residual stress component for the whole surfaces after the finishing step of SDB

Comparing the results of the traditional processes (Grinding / Polishing + SDB) with the proposed two-step SDB, it is observed that tangential stresses resulting from grinding, then burnishing, were among the highest for certain burnishing forces. Specifically, grinding, then burnishing with a 25 N force and within the 150 to 200 N range produced the highest stresses. However, for the finishing forces between 75 and 125 N, stresses from grinding then burnishing and those from two-step SDB (initially using 50 N force) were nearly identical and emerged as the highest across all surfaces within that force range, with the exception of the 75 N burnishing force following polishing.

Upon comparing the results of polishing, then burnishing, with those from the two-step SDB approach, it was found that the conventional method yielded superior outcomes relative to the two-step SDB technique, especially when applying finishing burnishing forces of 75, 175, and 200 N.

Additionally, at forces like 25 and 50 N, this conventional approach yielded better results than two-step burnishing with initial forces of 50 and 100 N. However, with a first-step force of 150 N within this force range, the proposed method showed superior outcomes. Furthermore, using a 100 N finishing force, the tangential stress outputs on the polished surface were more favorable than those burnished with 150 N in the first step, but not as high as those treated in the first step with 50 and 100 N. Conversely, applying forces of 125 and 150 N in the conventional process led to more compressive outcomes than the proposed method on surfaces initially burnished with 100 and 150 N. Yet, within this force spectrum, the best results were achieved on surfaces that underwent two-step SDB, starting with a 50 N force. In conclusion, the superiority of either burnishing after polishing or implementing a two-step SDB process, particularly in terms of tangential residual stresses, depends on the initial burnishing force used in the two-step SDB process and the finishing burnishing force applied to either the polished or pre-burnished surfaces.

Following the analysis of tangential stress outcomes from surfaces treated with grinding, then burnishing, and polishing, then burnishing, and their subsequent comparison with the results from surfaces subjected to the two-step SDB, attention will now shift to comparing the results among surfaces that underwent the two-step SDB treatment. As illustrated in Figure 17, there is an overlap in the results. However, a closer look at the surfaces at first burnished with 50 N and 100 N reveals that, in most cases, the outcomes on surfaces at first treated with 50 N surpass those treated with 100 N. Nevertheless, their outcomes are remarkably similar when finishing forces of 25, 100, and 175 N were utilized.

Conversely, the outcomes for surfaces burnished with 150 N in the first step showcased a wider range compared to the first two groups. The highest tangential stress results were observed when employing the two lowest finishing forces of 25 N and 50 N. In contrast, the application of the highest finishing forces, 175 N and 200 N, yielded the lowest results. For the remaining forces, the outcomes were intermediate, falling between those of the other two groups, and even lower, as when the finishing force of 100 N was used. Therefore, a first-step burnishing force of 150 N followed by second-step forces of 25 or 50 N represents the most effective approach to maximizing compressive residual stresses in the tangential direction across surfaces subjected to two-step SDB.

Finally, Table 9 displays the range, mean values, and standard deviation of tangential stresses across the three groups. The group initially burnished with 50 N exhibited the highest mean value, attributed to its tangential stress values being more compressive on average compared to the other two groups. The groups initially burnished with 100 N and 150 N showed similar mean values. In terms of standard deviation, it was the lowest for the group initially burnished with 50 N, reflecting

a narrower range of values. Conversely, the group initially burnished with 150 N had the highest standard deviation, indicating a broader variability in its stress values.

Table 9. Mean and standard deviation values of the surface tangential residual stresses of the two-step burnished surfaces

F_{in} [N]	Range of σ_{fin}^{tan} [MPa]	Mean [MPa]	STD [MPa]
50	-400 to -585	-499	65
100	-372 to -587	-462	76
150	-323 to -630	-463	107

5.1.3. Relationship Between Surface Residual Stresses and Kurtosis Parameter (R_{ku})

Reducing surface roughness and generating compressive residual stresses on the surface are the primary objectives of the SDB process. It has been established that there is a positive correlation between the finishing burnishing force and axial compressive residual stresses, regardless of whether traditional or proposed methods are used. However, the relationship appears inversely in the tangential direction, presenting an unexpected outcome. Consequently, the critical question about this phenomenon arises: Why do tangential stresses decrease as the burnishing force increases?

The relationship between surface residual stresses and surface characteristics, such as smoothness and layer compactness, suggests that greater surface deterioration leads to more significant stress relaxation. Given that measuring the arithmetic mean surface roughness (R_a) in the tangential direction is meaningless, kurtosis surface roughness parameter (R_{ku}) was assessed to better understand this phenomenon.

To illustrate the difference between two surface profiles with different R_{ku} values, Figure 18 presents the surface profiles—from parallel measurements—of the same surface. One profile was measured in the axial direction, and the other in the tangential direction, each with a different average value of the kurtosis parameter.

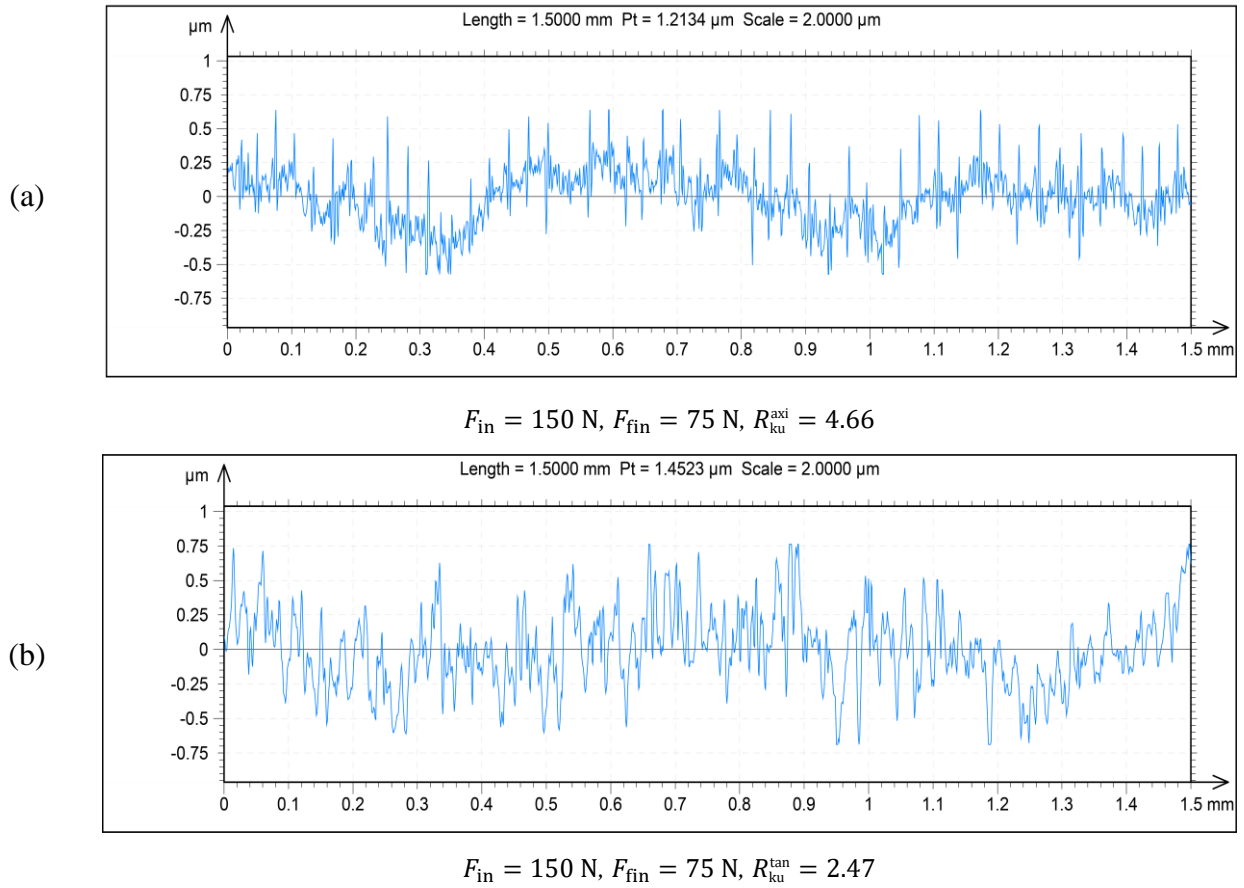


Figure 18. Axial and tangential roughness profile for the same surface with average R_{ku} values

Consequently, this parameter was evaluated for surfaces at first burnished with 150 N, both in the axial and tangential directions. The reason behind choosing this group of surfaces is the wide range of their tangential stress outcomes, as was depicted in Table 9. The findings of the kurtosis parameter and its relationship with the axial and tangential stresses are presented in Figure 19 for the axial direction and in Figure 20 for the tangential one.

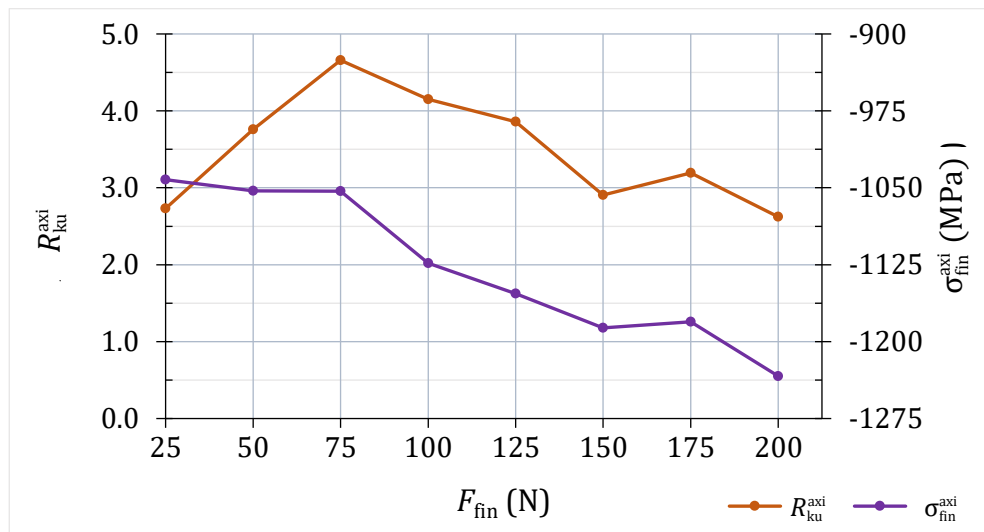


Figure 19. Relationship between surface residual stress component and average kurtosis parameter (R_{ku}) in the axial direction of surfaces burnished by 150 N in the first step

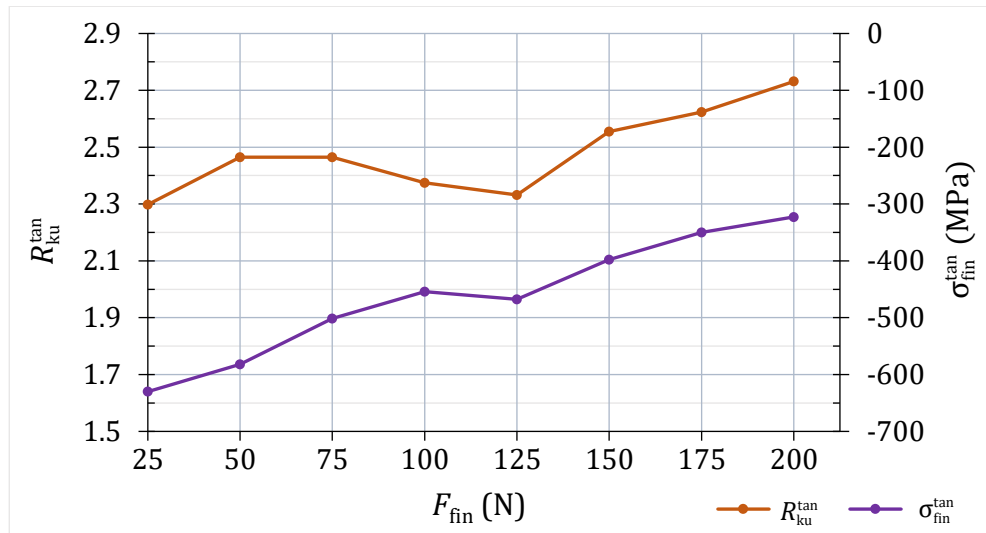


Figure 20. Relationship between surface residual stress component and average kurtosis parameter (R_{ku}) in the tangential direction of surfaces burnished by 150 N in the first step

The observed general trend in the axial direction is that as the finishing burnishing force increased, the values of R_{ku} decreased, indicating the creation of a surface profile with a lower number of high peaks and deep valleys, a reduction in surface sharpness, and a transition to a more compacted surface. This suggests that the peaks of the surface have become broader, offering a greater volume of material to resist deformation effects, such as deflection, due to compressive residual stress. Consequently, less stress relaxation can occur, and the residual stress values have increased, becoming more compressive in nature.

To clarify this idea, the concept is effectively illustrated in Figure 21. In Figure 21 (a), a stressed sheet and a bar are shown. Despite being under stress, these objects have their stresses retained without deflection due to their high thickness. However, when sliced, as shown Figure 21 (b), the stresses can no longer be retained. As a result, deflection occurs, leading to stress relaxation.

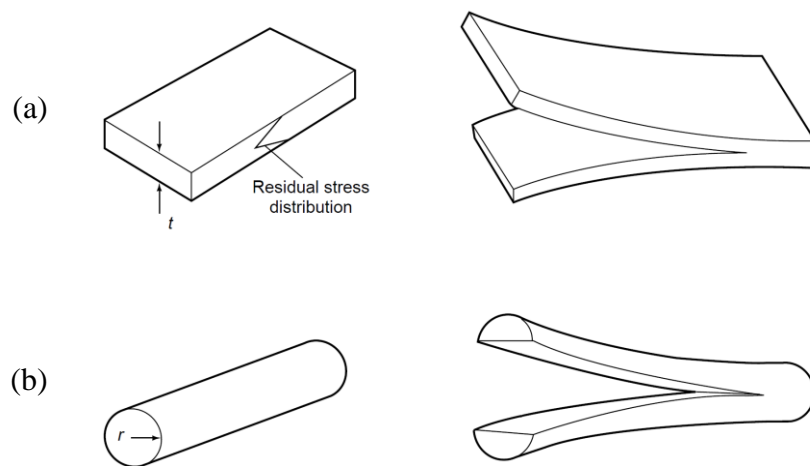


Figure 21. Dependence of stress retention and relaxation on thickness [104]

On the other hand, in the tangential direction, an increase in the finishing burnishing force led to a rise in the R_{ku} value, indicating an increase in the sharpness and number of high peaks (and deep valleys) on the surface, which means sharper surface peaks with reduced width were generated. Consequently, the thinner material within these peaks offered less resistance to deformation (deflection) caused by compressive residual stresses, facilitating stress relaxation, which ultimately resulted in lower surface residual stress values.

The deterioration of surface conditions in the tangential direction with increasing burnishing force can be attributed to the high relative speed between the burnishing head and the workpiece, reaching 115 m/min or 1916 mm/sec, which resulted in high shear strain rate. This high velocity did not allow sufficient time for the burnishing tool to effectively smooth and compress the surface. Consequently, rather than improving the surface, the rapid movement worsened the surface damage. As the burnishing force increased, the negative impact on the surface also intensified, leading to greater stress relaxation and a reduction in compressive residual stress values [62].

Whereas, in the axial direction, with the relative velocity being a mere 0.03 mm per revolution of the rotating bar—meaning low shear strain rate—the burnishing head had sufficient time to reduce surface roughness and exert compressive forces on the material's surface. Accordingly, as the burnishing force increased, the efficacy of burnishing also increased, leading to an enhancement in compressive residual stresses.

5.2. Residual Stress Depth Distributions

5.2.1. Axial Residual Stress Component Depth Distributions

The accurate measurement of residual stress component depth profiles in materials subjected to slide diamond burnishing is crucial for understanding and predicting their fatigue behavior. Hence, in this study, it was essential to investigate the depth stress profiles in detail following the various processes to facilitate a comparison of their outcomes. Figure 22 illustrates the distribution of axial residual stress across the surface and subsurface layers of the surfaces that were initially turned, ground, and polished. Also, in addition to the surfaces burnished once using 50, 100, 150, and 200 N, those treated with the traditional method of SDB following grinding and polishing, as well as those subjected to the proposed two-step SDB process finalizing with 200 N, were selected due to their display of the highest surface axial residual stresses, as noted in the previous section.

Initially, the surfaces underwent turning, resulting in the formation of a compressive residual stress zone. This zone extends approximately 110 μm in depth, with the highest stress level reaching about -600 MPa near the surface and about -100 MPa at the surface. Conversely, the grinding process mainly produced tensile residual stresses. However, just beneath the surface, a thin layer, approximately 5 μm deep, showed compressive stress, peaking at -509 MPa right at the surface. This compressive peak shifts to a tensile one of approximately 320 MPa at a depth of around 15 μm . Finally, the polishing of the turned surfaces modified the stress distribution. As a result, the compressive zone became a bit deeper than it was after turning, while simultaneously reducing the peak stress and increasing the surface compressive stresses.

After burnishing, the figure illustrates that the surface and subsurface residual stresses uniformly became compressive, exhibiting greater depth and magnitude, regardless of the stress distribution of the initial state. Additionally, it is observed that the residual stress profiles typically show a decrease in absolute value as depth increases (become less compressive). This decrease results from the way in which the material is impacted by the burnishing tool. Initially, high compressive stresses are experienced by the surface and near-surface layers due to the direct and intense impact of the burnishing tool, leading to plastic deformation in these top layers. As depth increases, the impact of the burnishing process is seen to diminish. This stress gradient is often attributed to the reduced influence of the mechanical work and strain hardening induced by the burnishing tool in the deeper layers.

What can also be noticed is that the region adjacent to the surface exhibits a pronounced steep gradient in residual stress. This layer is characterized by a rapid transition from a state of high compressive stress at the surface to significantly lower compressive stress at a shallow depth under

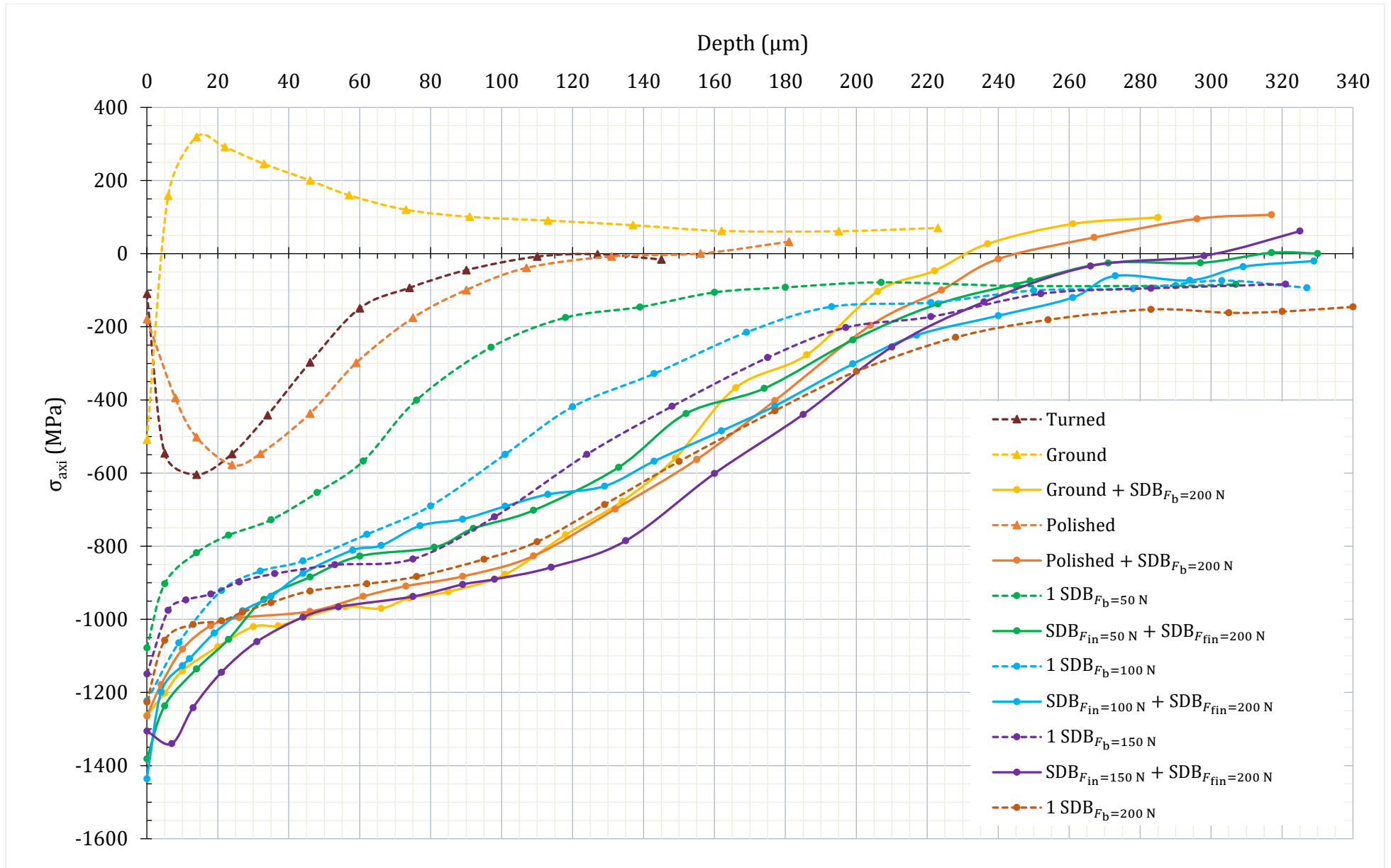


Figure 22. Axial residual stress component in-depth distributions after different processes

the surface, less than $\sim 10 \mu\text{m}$. The steepness of this gradient is indicative of an intense localized elastic deformation, largely confined to the near-surface region, as can be seen in Figure 23. Moreover, the gradient's steepness varies depending on the initial surface condition and the specific parameters of the SDB treatment, such as the applied force and whether a single or two-step approach was used.

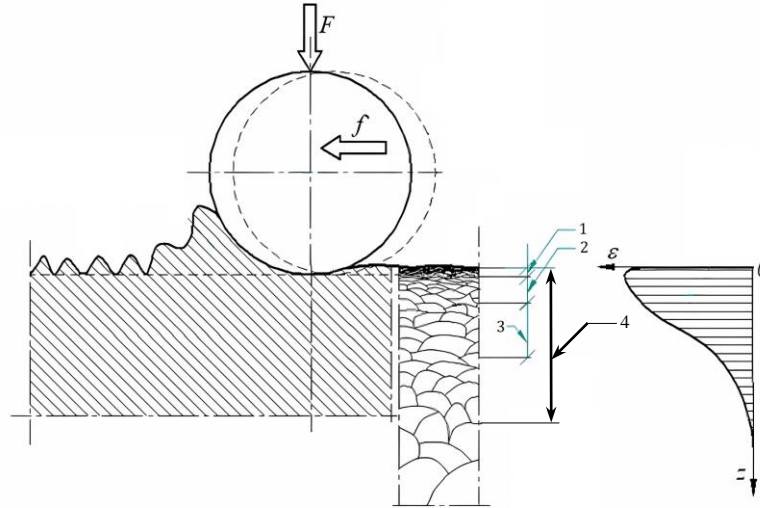


Figure 23. Schematic illustration of the burnishing process and the burnished layers [105]

1. Roughness zone, 2. Grain fragmentation zone, 3. Plastic deformation zone, 4. Elastic deformation zone

Another notable trend observed in the curves is the shift from the compressive to the tensile stress zones. Three distinct patterns emerge. The first involves surfaces that have been ground, then burnished, or polished, then burnished. For these, the transition from negative to positive stress occurs at a relatively shallow depth compared to other cases. Conversely, surfaces subjected to a two-step SDB process exhibit this shift at a deeper level. Meanwhile, surfaces treated with a single step of SDB display a consistent compressive stress profile extending to a greater depth, with no transition to tensile stress within the measured range. This suggests that the initial surface condition (whether turned, ground, polished, or burnished) significantly impacts the influence of the subsequent SDB process on the stress profile.

Now, a comparison in terms of the axial residual stress distribution will be held between the outcomes of the traditional and the proposed processes. The profiles of the ground-then-burnished and polished-then-burnished with 200 N surfaces demonstrate almost identical results, with only a slight difference. On the surface, a significant value of compressive residual stresses was achieved. It was higher than those resulted from the one-step SDB process and less than those achieved by the two-step process. When comparing to the outcomes of the one-step SDB process, particularly when applying the maximum force of 200 N, it is observed that the outcomes are generally similar up to a depth of about $180 \mu\text{m}$. However, at a shallower depth, specifically around $30 \mu\text{m}$, the ground-then-burnished surface exhibited higher performance.

When comparing to the outcomes of the two-step SDB process, it is evident that surfaces burnished after grinding or polishing exhibit different results. Generally, the surfaces of the samples that were ground, then burnished, or polished, then burnished showed lower compressive residual stresses than those treated with the two-step SDB. When examined in detail, the effectiveness of these methods varies based on depth and the initial burnishing force applied in the two-step process. Notably, the two-step SDB creates deeper compressed regions in the material (even beyond the depth of about 200 μm). However, it is clear that the surface burnished with 150 N in the first step and then 200 N in the second one demonstrated superior outcomes. This improvement is noticeable from the surface down to a depth of approximately 40 μm , and again beyond 100 μm . In conclusion, the proposed two-step SDB process potentially achieves higher compressive residual stress levels and higher compressed depth, compared to the conventional method of grinding or polishing followed by SDB. The effectiveness of this process largely depends on the first-step burnishing force used and the depth beneath the surface.

Lastly, the effect of the two-step SDB over the one-step SDB will be discussed, but firstly, the attributes of each process will be discussed. On the four surfaces subjected to the one-step SDB, the surface layer was found to have the lowest compressive stresses at the force of 50 N, while the highest compressive stresses were achieved by the forces of 100 and 200 N. It can be noted that the maximum compressive stress, suggested by the profile shapes, is reached at the surface for all forces, followed by a gradual decrease in stress magnitude with depth. Additionally, an increase in the burnishing force was observed to extend the compressive residual stress zone to greater magnitudes and depths. Each profile, after reaching a certain depth, tends to level off, signifying that the residual stress becomes relatively uniform as depth increases. The summit of this uniformity in residual stress is reached at varying depths, dependent on the level of force applied, with higher forces resulting in a deeper summit.

With regard to the depth profiles of the surfaces that underwent two-step SDB, a consistent trend is observed across all three profiles. As the depth increases from the surface, the compressive residual stresses decrease. Specifically, at the surface, the sample subjected to an initial force of 100 N exhibited the highest compressive residual stress, whereas the sample treated with 150 N showed the lowest.

To evaluate the effectiveness of the two-step SDB process versus the single-step SDB, the profiles of the two-step SDB will be compared with the one treated by a single 200 N burnishing force, as this force represents the finishing burnishing force in the two-step SDB. It is observed that, irrespective of the first-step burnishing force applied, samples subjected to the two-step SDB exhibit greater induced compressive residual stresses at the surface. These higher stresses,

depending on the value of the first-step burnishing force, extend to a certain depth, than those subjected to the single-step SDB. Additionally, the two-step SDB profiles tend to show a smoother transition from high compressive stress at the surface to lower stress levels at increased depths. In contrast, the one-step SDB profile drops more sharply from the peak stress to a plateau. This may suggest that the two-step process leads to a more gradual distribution of stress within the material.

Moreover, in the subsurface region (approximately 3 to 200 μm), the sample initially burnished with 150 N displayed the highest compressive residual stress, establishing it as the zone with the most significant compressive axial residual stress among all the samples in the study. At greater depths, the profiles of the two-step SDB converged, indicating that the effect of the additional step in the SDB process becomes less significant as depth increases, while the profile of the one-step SDB penetrated deeper into the material with a higher compressive stress level.

5.2.2. Results of Tangential Residual Stress Component Depth Distributions

After discussing the results of the residual stress component distribution in the axial direction, the main features of the tangential stress component distribution will be revealed here. Figure 24 displays how tangential residual stresses are distributed both on the surface and within the subsurface layers of the previously chosen samples. Initially, after the turning process, the distribution of tangential residual stress closely mirrors the axial one, with notable exceptions at the surface and the peak area of the compressive zone. On the surface, the axial stresses are compressive, but in the tangential direction, they begin as tensile. This tensile stress decreases and transitions into compressive stress at a depth of $\sim 3 \mu\text{m}$. The compressive stress then reaches its peak, which is lower than that in the axial direction, at about 25 μm depth, registering -521 MPa.

After grinding, the tangential stress pattern is almost the same as the axial one, but the stress on the surface is less, at -274 MPa. After polishing, the tangential residual stress is quite similar to the axial stress but differs at the surface, where it is tensile with a value of 202 MPa. This stress begins to change to compressive at a depth of 8 μm and reaches its highest compressive point at approximately 30 μm , showing a stress value of around -500 MPa.

Following the burnishing process, the figure demonstrates that both the surface and subsurface residual stresses evenly transitioned to a compressive condition. This change occurred with increased depth and intensity, independent of the original stress distribution in the initial state. It can be seen that the general trend beneath the surface is that compressive residual stresses initially increase (become more compressive) due to a combination of factors, such as the lateral flow of material caused by the burnishing process and the anisotropic nature of the material's response. This response leads to plastic deformation and strain hardening on the surface and subsurface layers,

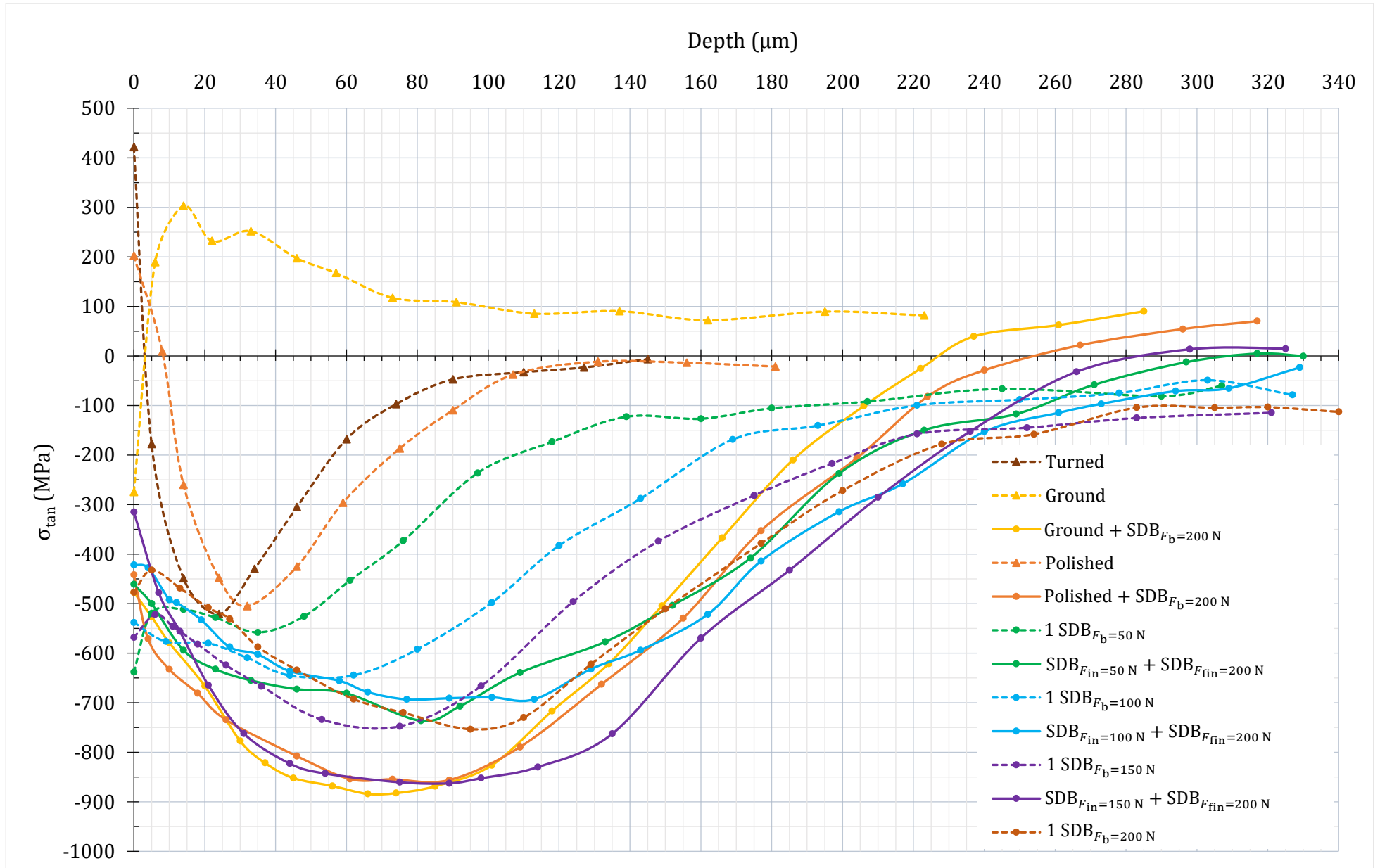


Figure 24. Tangential residual stress component in-depth distributions after different processes

which means an increase in the compressive residual stress distribution. Beyond the peak, these stresses tend to decrease as the effects of plastic deformation and strain hardening become less pronounced.

After SDB, the behavior of both ground-then-burnished and polished-then-burnished profiles appears similar. The stress patterns in each are nearly identical, overlapping from the surface to a depth of approximately 110 μm . Beyond this depth, the patterns diverge; polishing, then burnishing stress, becomes more compressively significant than those after grinding.

Comparing the stress distribution from burnishing the polished and ground surfaces at 200 N with that of a single 200 N burnishing pass after turning reveals that, while the surface compressive stress in all three samples is quite similar, burnishing after grinding or polishing results in a higher peak of compressive residual stress than when done after only turning. However, when grinding or polishing is followed by burnishing, the induced compressive stress is limited to a shallower depth before it transitions to tensile stress. In conclusion, the process of grinding or polishing after turning, followed by SDB, significantly enhances the ability of SDB to induce beneficial compressive stress within the material.

When comparing the residual stress distribution between ground-then-burnished and polished-then-burnished surfaces to those subjected to the two-step SDB, a similarity in surface stresses is observed. However, initiating the two-step SDB with a 150 N burnishing force yields slightly less compressive stress at the surface compared to other methods. Nevertheless, the stress profile at this first-step force exhibits a compressive stress peak closely aligned with those of the ground-then-burnished and polished-then-burnished samples, suggesting that a higher first-step force in the two-step SDB approach might match or even exceed the effectiveness of SDB after grinding or polishing, particularly given its deeper penetration into the material. Lastly, the two-step SDB profiles demonstrate a substantial induction of compressive stress deeper into the material, with a gradual transition from compressive to tensile regions, indicating a more profound impact in depth.

Before delving into a comparison between the one-step and two-step SDB processes, it is essential to understand the distinct trends exhibited by each group. Analyzing the single-step SDB first, the stress profiles suggest a noteworthy pattern regarding the surface-level residual stresses. Specifically, the profile of the 50 N force exhibited the highest compressive stress at the surface, while the 200 N application resulted in the lowest surface stress. The profiles for 100 N and 150 N forces fell within this range, demonstrating intermediate values of surface compressive stress. This observation leads to a general conclusion: an increase in the burnishing force tends to diminish the tangential residual stress on the surface. This decrease in stress is attributed to a relaxation effect,

potentially due to surface fatigue, which becomes more pronounced with higher levels of burnishing force, as previously discussed.

The profiles reveal another significant characteristic: a local reduction in compressive stresses just beneath the surface within a depth of less than 10 μm . This region encompasses the grain fragmentation and plastic deformation zones, identified as zones 2 and 3 in Figure 23, respectively. The observed stress diminution in this superficial layer is likely due to the stress relaxation phenomenon, which may include fatigue and microcracks formation, or it could be related to a reduction in dislocation density within these zones since this decrease in stress disappeared in the second step of burnishing, in which a higher force was used. Notably, the profile for the 100 N force was an exception since this stress relaxation effect is not evident. This discrepancy can be explained by the fact that the initial stress measurement under the surface for this profile was carried out at a depth of 9 μm . This detail confirms that the depth of the affected layer where stress relaxation is observable does not exceed 10 μm .

Finally, it is observable that with an increase in the burnishing force, there is generally an increase in the peak value of the induced compressive residual stress. However, when a force of 200 N was applied, it did not result in a higher maximum compressive stress compared to that achieved with 150 N. This suggests that there may be a threshold force level for the material, beyond which no further enhancement in the peak compressive stress value is observed. Nonetheless, with the application of the 200 N force, the depth at which the peak compressive stress occurred was deeper compared to the 150 N force. This trend was consistent across the profiles, indicating that the depth of peak residual stress increases with greater force application, which in turn suggests an expansion of the compressive residual stress area.

Regarding the samples that underwent the two-step SDB process, observations at the surface level indicate that the sample subjected to the lowest initial burnishing force exhibited the highest compressive stress in the tangential direction. This surface compressive stress is inversely related to the first-step burnishing force, i.e., the stress decreases as the force of the first SDB step increases. Beneath the surface, a comparison with the effects of a single SDB step reveals that the application of a second SDB step has the effect of unifying the stress profiles at shallower depths, particularly around 10 μm . Moreover, the residual stress distributions of the 50 N and 100 N first-step profiles show a remarkable similarity, with closely matched values. However, beyond the depth of approximately 20 μm , the sample initially burnished with 150 N exhibits a more pronounced peak in compressive stress. After the peaks, despite the different first-step forces, the convergence of profiles after the second burnishing step by 200 N indicates that the material may have reached a

state of saturation where additional force in the first step does not significantly change the residual stress distribution.

Now, since the 200 N represents the finishing burnishing force in the two-step SDB process, the profiles after the two-step SDB will be compared with the one representing the one-step SDB using 200 N to see how well the two-step SDB works compared to the one-step SDB. It is shown that the profile of the single burnishing step behaves, to a high extent, like those of the surfaces that underwent two-step burnishing with 50 N and 100 N initial forces. On the surface, the stress generated by the single-step and two-step SDB using 50 N first-step force was the highest and very close to each other. In the depth ranges between around 5 and 45 μm , the two-step SDB process generated higher compressive residual stresses regardless of the first-step burnishing force applied. The same thing happened in the depth ranges between around 130 and 230 μm when the first-step forces of 100 N and 150 N were initially used.

Furthermore, looking at the peaks of the stress profiles, the two-step SDB process, particularly with the 150 N first-step force, seems to achieve a higher compressive stress peak than the one-step process does. This suggests that using a high initial burnishing force can enhance the work-hardening effect. Lastly, after the peaks, the two-step SDB profiles converge, indicating a saturation level. Conversely, the one-step profile does not exhibit this convergence, which could mean that a single application of force does not fully saturate the material's capacity for work hardening.

5.3. Results of Surface Roughness

As previously mentioned, R_a surface roughness was measured in the axial direction. As an example, Figure 25 shows roughness profiles—from parallel measurements—for two surfaces with average R_a values, both were burnished with the same force in the first step, but with different forces in the second one.

Values of surface roughness before the finishing SDB step ($R_{a_{in}}$) are depicted in Figure 26. After burnishing, polishing, and grinding of the turned surfaces, it is obvious that the lowest surface roughness was for the surfaces that were initially burnished once by 100 and 150 N forces, followed by the polished surfaces, while the ground surfaces showed the highest roughness. In addition, the average surface roughness of the surface that was burnished with 200 N by a single-step SDB after turning is $0.068 \mu\text{m}$. These results, along with the results of the surface roughness after the finishing step of SDB applied to the ground, polished, and burnished surfaces, are shown in Table 13 in the appendix.

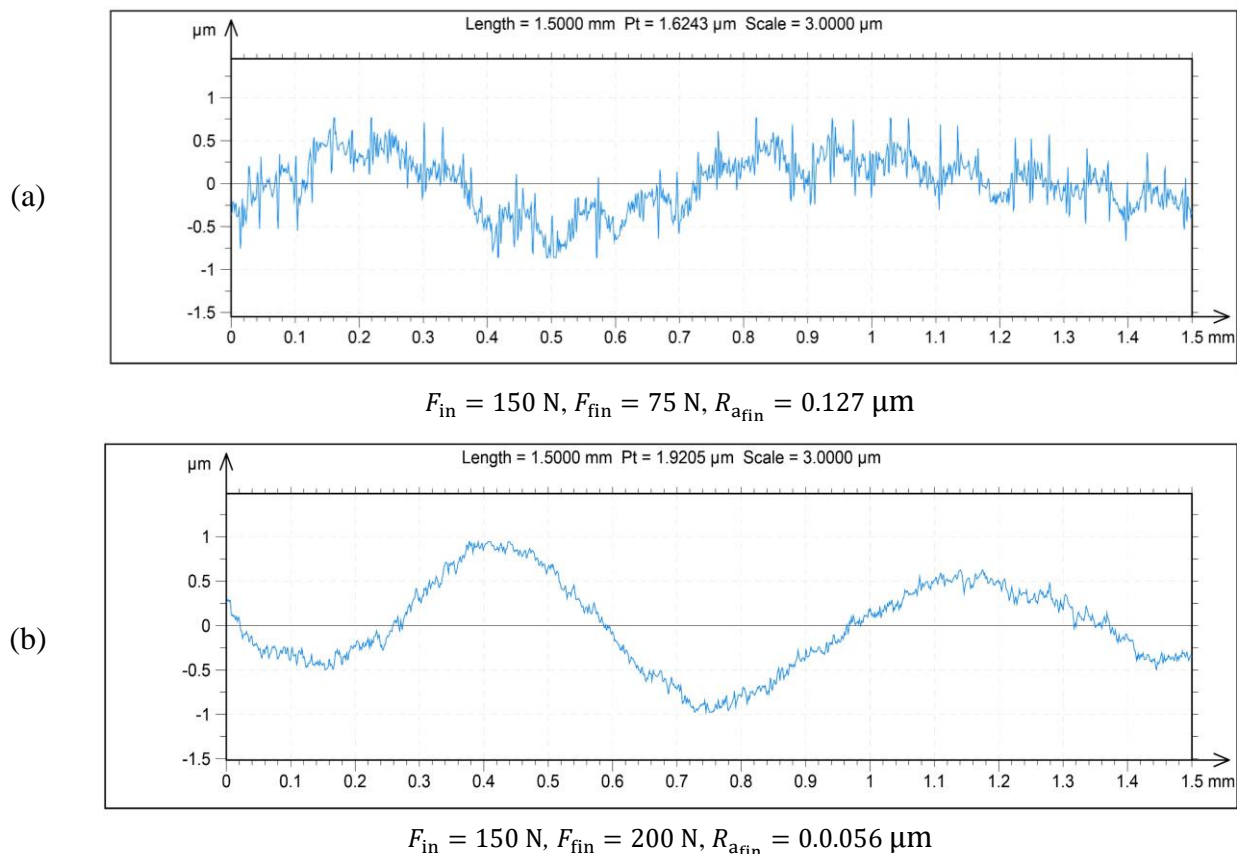


Figure 25. Surface roughness profile for two surfaces with average R_a values

Figure 27 illustrates the results following the finishing step of SDB. Initially, the results of the traditional process involving grinding or polishing, followed by SDB, will be discussed. Subsequently, these outcomes will be compared to those obtained from the two-step SDB process.

Before starting the comparison, it is important to note that the surface roughness was initially 0.454 μm after turning and then reduced to 0.248 μm and 0.133 μm after grinding and polishing, respectively. As a typical result of burnishing, the surface roughness of both ground and polished surfaces generally decreased following burnishing, with the exception of the polished surface burnished with 50 N. When examining the R_a values of surfaces that were previously ground versus those that were polished, the outcomes vary depending on the burnishing force applied. For instance, surfaces that were ground-then-burnished displayed lower R_a values with forces of 50 N and between 100 and 150 N, while polished-then-burnished surfaces showed lower R_a values with the other forces applied. Thus, the final surface roughness after the burnishing of ground and polished surfaces is influenced by the specific burnishing force used.

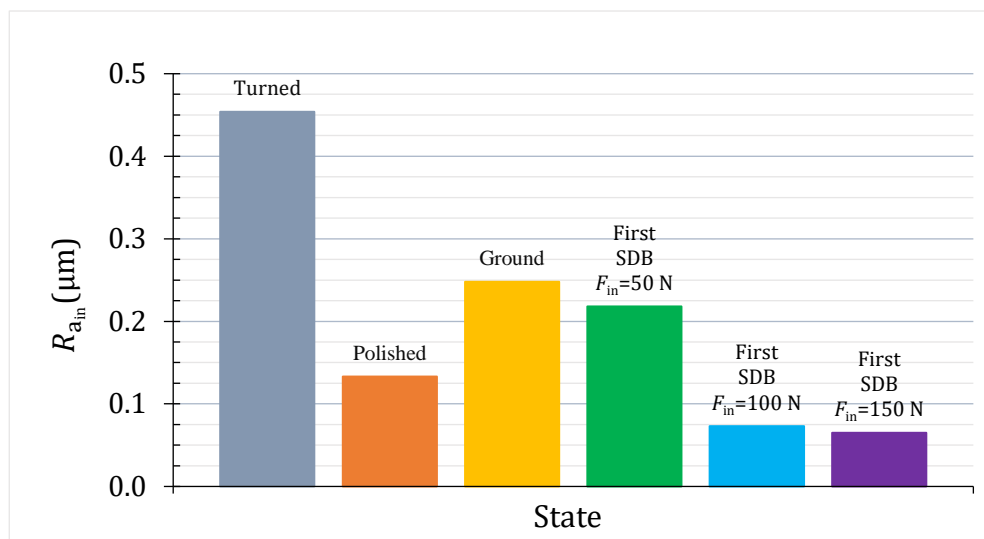


Figure 26. Surface roughness values after turning, grinding, polishing, and first step of SDB

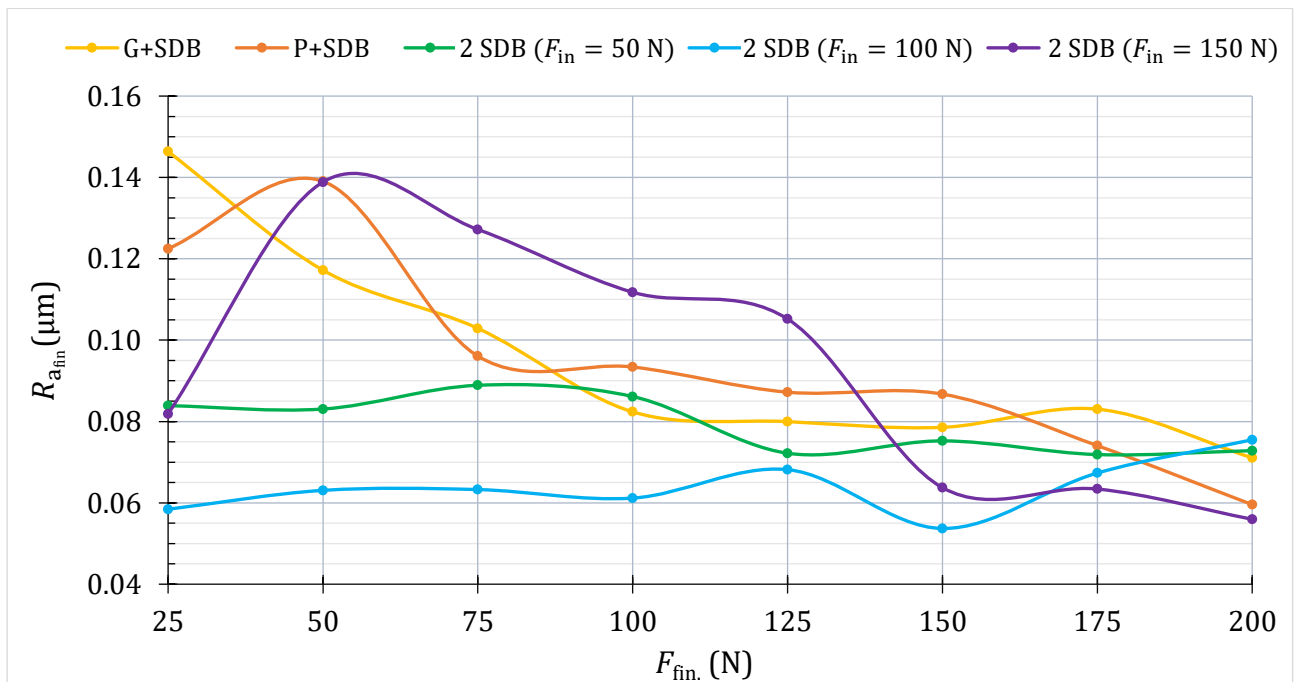


Figure 27. Surface roughness for the whole surfaces after the finishing step of SDB

When comparing the results of the two-step SDB process to those obtained by first grinding or polishing, then burnishing, it is evident that the surfaces subjected to the two-step SDB, particularly those treated with a force of 25 N in the second step, exhibit significantly lower surface roughness. This is notably true for the surface initially burnished with 100 N. However, the pattern shifts with the group of surfaces at first burnished with 150 N, where surfaces burnished in the second step with forces ranging from 50 to 125 N displayed the highest surface roughness across all 40 surfaces. Yet, this trend dramatically reverses when the second-step SDB forces between 150 and 200 N were applied.

For surfaces burnished with 50 and 100 N in the first step, it is clear that burnishing with any force in the second step generally results in better surface roughness compared to grinding or polishing followed by SDB. The main exception occurs when the surface at first burnished with 50 N is subsequently finished with 100 N second-step force; in this scenario, the surface that was ground-then-burnished exhibits slightly better roughness. Another exception arises with surfaces finished with a second-burnishing force of 200 N, where burnishing after polishing, followed by burnishing after grinding, showed superior results. Ultimately, regarding surface roughness, burnishing after grinding or polishing is not the optimal method; rather, starting with a first-step burnishing force of 100 N followed by a second burnishing step at 150 N proves to be the most effective strategy.

When evaluating the surface roughness outcomes among the three groups of surfaces that underwent the two-step SDB process, it is generally observed that the group initially burnished with 100 N achieved the best (lowest) surface roughness. Notably, six out of eight surfaces in this group displayed the lowest roughness values across all 24 surfaces, except for the last two surfaces treated with 175 N and 200 N in the second step in this group. The lowest R_a value recorded in this group was 0.054 μm , closely matching the roughness value of the surface initially burnished with 150 N in the first step and subsequently with 200 N in the second one. Additionally, this group exhibited relatively stable roughness results, ranging from 0.054 to 0.076 μm , with a low standard deviation of 0.0066 μm .

For the surfaces that were at first burnished with 50 N, their roughness outcomes are comparable to those initially burnished with 100 N, though generally higher, except for the last surface, which exhibits slightly better roughness. Specifically, the first surface finished with a 25 N force in the second step displays roughness similar to a corresponding surface that was burnished with a 150 N first-step force. Variability in this group's results is relatively low, with roughness values ranging from 0.072 to 0.089 μm and a standard deviation of 0.007 μm .

Lastly, examining the surfaces burnished with 150 N in the first step, the highest force used, reveals a distinct trend in surface roughness compared to the other two groups. Notably, the first surface, burnished with a second-step force of 25 N, generally exhibits the lowest roughness within its group, at 0.082 μm . However, increasing the second-step burnishing force to 50 N resulted in an increased roughness of 0.139 μm . Beyond this point, further increases in the burnishing force positively impacted the roughness, reaching a lowest roughness of 0.056 μm on the surface burnished with the maximum force of 200 N in the second step. This group also showed the greatest variability in results, with a standard deviation of 0.0316 μm , the highest among the groups.

In summary, applying a two-step SDB process, the lowest surface roughness is typically achieved by burnishing at first with 100 N, followed by a second pass using forces ranging from 25 to 150 N. Compared to this, initiating with 50 N and applying a second burnishing force between 25 and 175 N generally results in slightly higher roughness values, although they are sometimes comparable, except when using a second-step force of 200 N, where the roughness decreases. Conversely, starting with a 150 N force yields competitive roughness results when the second burnishing step is performed with forces between 150 and 200 N.

5.3.1. Percentage of Surface Roughness Improvement of the Two-Step SDB Process

In order to assess the efficacy of the two-step SDB process in terms of surface roughness, the improvement can be quantified using the dimensionless percentage of surface roughness improvement, calculated as follows:

$$\%IR_a = \frac{R_{a_{in}} - R_{a_{fin}}}{R_{a_{in}}} \times 100\% \quad (11)$$

where:

$\%IR_a$: Percentage of surface roughness improvement, [%].

$R_{a_{in}}$: Surface roughness after the first-step SDB (at $F_{fin} = 0.0$ N), [μm].

$R_{a_{fin}}$: Surface roughness after the second-step SDB, [μm].

It should be noted that the values of final surface roughness ($R_{a_{fin}}$) were subtracted from the initial values ($R_{a_{in}}$), not the opposite. This is because the burnishing process typically aims to reduce surface roughness, ideally resulting in $R_{a_{fin}}$ being less than $R_{a_{in}}$, which yields a positive $\%IR_a$, indicating an improvement. However, if the final surface roughness after burnishing is higher than the initial, $\%IR_a$ will be negative, signifying a degradation of surface roughness. According to the results of $\%IR_a$ listed in Table 14 and depicted in Figure 28, both improvements and deteriorations in surface roughness are observed, varying with the forces used in the first and second burnishing steps.

It should be noted that the initial burnishing step consistently enhances surface roughness compared to the state after turning. Accordingly, this chart details the further improvements in surface roughness achieved after the second burnishing step. Additionally, it is crucial to note that comparisons of results are only valid within the same group and not between different groups, even if they were burnished with the same second-step force. This is due to variations in the initial surface roughness ($R_{a_{in}}$) after the first burnishing step, which serve as different reference points. Additionally, negative results in the table mean that the surface roughness was downgraded after finally being burnished by that specific force, when compared to its value after the first step of SDB.

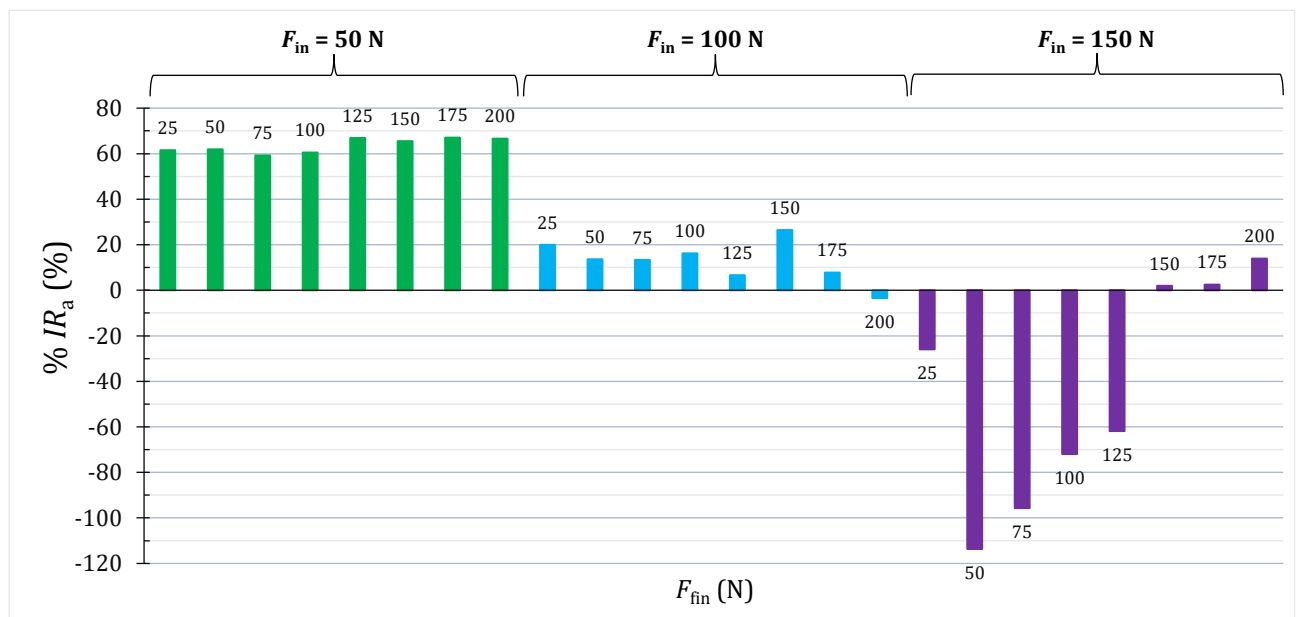


Figure 28. Results of the surface roughness improvement percentage in the two-step SDB process

For the surfaces that were initially burnished by 50 N, after the first burnishing step, their average surface roughness was $0.218 \mu\text{m}$. After the second step of SDB, % IR_a ranged between 59.2% and 67%. These percentages were the highest among the three groups. The high percentages of improvement are primarily due to the fact that the initial surface roughness of this group, after the first burnishing step, was higher compared to the other two groups. This higher initial roughness, characterized by more pronounced peaks and irregularities, enabled the burnishing process to more effectively reduce surface roughness. Finally, after the second burnishing step, the lowest percentages of improvement were for the surfaces burnished with 75 and 100 N, and the highest for the surfaces burnished between 125 and 200 N.

On the other hand, despite that the achieved surface roughness values of the surfaces burnished with a first-step force of 100 N are lower than those of surfaces burnished with 50 N, their percentages of surface roughness improvement are much lower, and the trend totally differs. This is because the

initial surface roughness of the group burnished with 100 N in the first step was 0.073 μm , significantly lower than the 0.218 μm observed for that burnished with 50 N in the first step.

In this group of surfaces, the impact of the final burnishing force varied, resulting in oscillating outcomes. The highest value of $\%IR_a$ was 26.4% for the surface subjected to 150 N in the second burnishing step, whilst the lowest was for the surface that was burnished by a second-step force of 200 N, with a value of -3.4%. The primary cause of this deterioration (increase) in surface roughness is that using too high forces can peel the surface and cause fatigue of the surface layer. Consequently, applying too much pressure to the surface of the burnished metal can worsen it and introduce defects [60], [63], and [64].

Eventually, for the group of surfaces burnished with the highest force of 150 N in the first step, the chart reveals a distinct trend in surface roughness results compared to others, highlighting the significant impact of the first-step burnishing force. The highest improvement in surface roughness was 14% for the surface burnished with 200 N in the second step, while the most substantial deterioration occurred on the surface finished with 50 N, showing a -114% change in roughness.

It is also evident that surface roughness deteriorated when surfaces were burnished with second-step forces ranging from 25 to 125 N. Within this range, the least degradation occurred with the lowest force of 25 N. However, a dramatic increase in surface roughness was observed when the subsequent force of 50 N was applied. Beyond this, from 75 to 200 N, a positive relationship was observed between the second-step burnishing force and the percentage of surface roughness improvement. This indicates that as the force increased, the improvement in surface roughness also increased, although $\%IR_a$ values remained negative when the second-step force was below approximately 150 N.

The primary reason for this pattern is that the first burnishing force of 150 N caused extensive plastic deformation, significantly refining the surface roughness from 0.454 μm after turning to 0.073 μm . However, when the second SDB step applied a force of 25 N, it scratched the surface, increasing its peaks and sharpness. Afterward, using a 50 N force further boosted the surface's sharpness due to its greater intensity. On the other hand, for the forces of 75, 100, and 125 N, the impact had a dual effect of enhancing the surface's sharpness and continuing the burnishing process. Within this range, the higher the force applied, the more significant the burnishing effect observed. Conversely, the higher forces of 150, 175, and 200 N were sufficient to significantly enhance the burnishing effect and reduce the surface roughness. This effect was previously shown in Figure 18.

In this group of surfaces, it is important to remember that the range of forces, where surface roughness deteriorated was from 25 to 125 N, all of which were lower than the first-step burnishing

force of 150 N. This suggests that when initially burnishing with 150 N, a force equal to or greater than 150 N is necessary in the second SDB step to improve surface roughness. Notably, this was not the case with the previous two groups, where a finishing force of just 25 N was sufficient to further reduce the surface roughness of the initially burnished surfaces.

The phenomenon observed is due to the fact that surfaces initially burnished with 150 N underwent extensive plastic deformation, reaching a work-hardening level where additional deformation in the second step of burnishing required higher forces. In contrast, surfaces from the other two groups were not as heavily deformed and could thus undergo further plastic deformation even with lower applied forces in the second step of burnishing. This is evident when comparing the microhardness of the first surface of each group after being burnished with 50 N, where microhardness values were 648, 753, and 879 HV 0.2 for surfaces initially burnished with 50, 100, and 150 N, respectively.

5.4. Results of Surface Microhardness

Since microhardness plays a crucial role in determining the fatigue life of the components subjected to cyclic loading, and to assess the effectiveness of the proposed process in doing two-step SDB over the traditional process of doing SDB once after grinding or polishing, it was measured on the surface of the samples after carrying out the finishing step of burnishing. Table 15, in the appendix, presents the average microhardness values obtained after the finishing step of SDB for various operations, as well as the microhardness measurements before the finishing SDB step (at $F_{fin} = 0.0$ N). Additionally, it is worth mentioning that the average microhardness value after turning was HV0.2 636. To evaluate the effectiveness of each process, all results are presented in Figure 29.

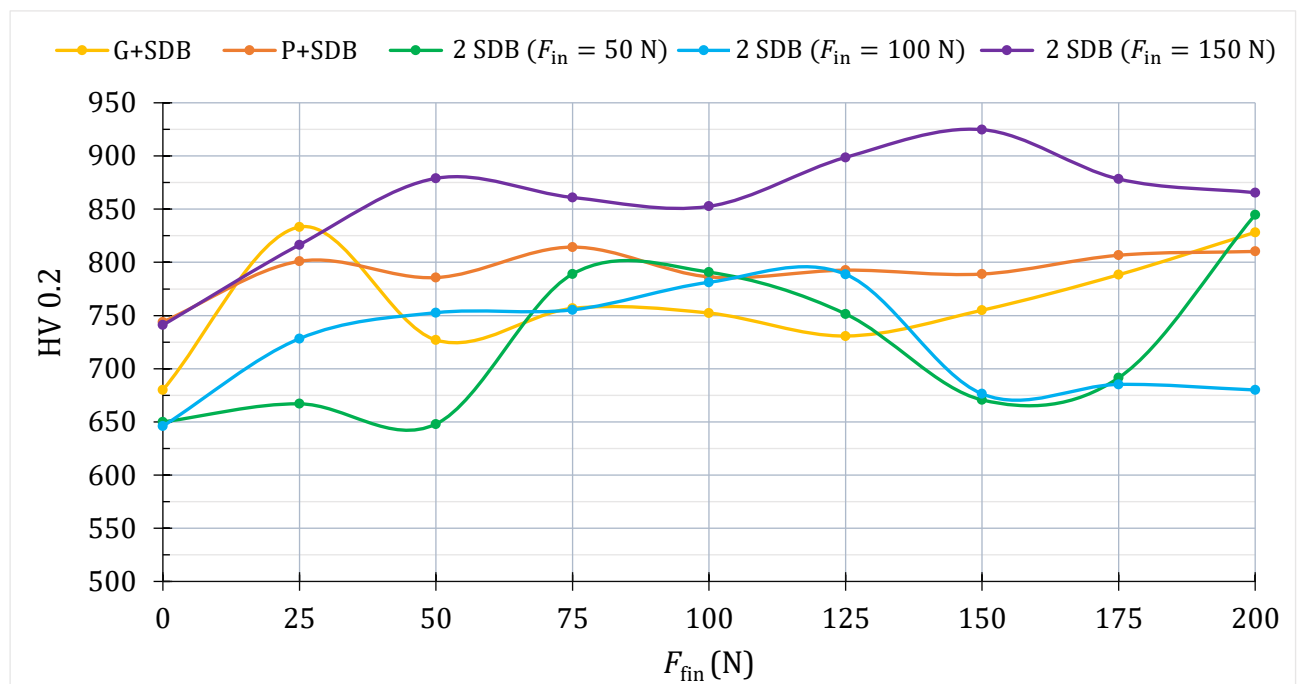


Figure 29. Surface microhardness for some surfaces after the finishing step of SDB

The graph leads to several key insights. First, it indicates that the microhardness following the SDB finishing step is enhanced irrespective of the approach taken, though the extent of this improvement is significantly influenced by the force applied in the SDB finishing step. Additionally, the microhardness profiles obtained from the two-step SDB method exhibit complex and less predictable patterns characterized by numerous peaks and troughs as the finishing burnishing force changes, particularly when initial burnishing forces of 50 N and 100 N are employed. In contrast, a more consistent trend emerges when a higher force of 150 N is used, approximately resulting in the highest microhardness values across all tested surfaces, including the ground-then-burnished, polished-then-burnished, and even the surface that was burnished with a single-step SDB after turning by 200 N, for which the average microhardness was 752.

Conversely, the microhardness profiles of the one-step SDB samples, processed either after grinding or after polishing, display trends indicating a more straightforward relationship between the finishing force and microhardness. This is especially evident in the polished-then-burnished samples, which consistently demonstrate higher microhardness values compared to the ground-then-burnished surfaces.

The clear correlation between the finishing burnishing force and the achieved microhardness in both single-step SDB, after grinding or polishing, and the two-step SDB, employing a 150 N first-step burnishing force, can be attributed to the surface's initial condition prior to the finishing SDB process. Specifically, after turning, the surface topography typically features pronounced peaks and valleys. However, grinding and polishing processes eliminated these peaks, resulting in a more uniform, semi-flat surface, particularly after polishing. This absence of peaks enhances the effectiveness of the burnishing process, leading to a uniformly hard surface behind the burnishing head. Consequently, the hardness tester's indenter could directly contact the uniformly burnished surface, facilitating accurate hardness measurement.

In the two-step SDB process, using lower first-step burnishing forces of 50 and 100 N after turning was inadequate to fully flatten surface peaks, resulting in uneven surface topology characterized by relatively high peaks and low valleys, particularly with the 50 N force, as will be shown later in Figure 31 (a) and (b). Additionally, after this first step of burnishing, the surface has been strain-hardened, but the hardness at the top of peaks differs from that at valleys. Consequently, the second burnishing step also produced a surface with uneven topology and hardness, making it difficult for the hardness tester's indenter to achieve uniform measurements.

In contrast, applying a 150 N force in the first burnishing step effectively smoothed the surface by flattening the peaks, creating a surface well-prepared for the second burnishing step. This preparation allowed for a surface with relatively low peaks and valleys and homogeneous hardness after the second step of burnishing, enhancing its suitability for microhardness measurement. In conclusion, these findings emphasize the importance of the initial surface features before applying the finishing burnishing step. These features will be visually investigated in the following section.

5.5. Analysis of Surface Topography and Morphology

5.5.1. 3D Surface Topography After Turning, After Grinding, and After Polishing

Depending on the results previously discussed, it was determined that, in general, surfaces ultimately burnished with a 200 N force exhibited superior surface integrity. Therefore, this section will delve into the visual characteristics of these surfaces.

The 3D topography after turning, grinding, and polishing is presented in Figure 30. After turning, as shown in Figure 30 (a), the surface exhibits a periodic, wavy pattern, indicating the repetitive tool path of the turning operation. Additionally, it is evident that the height differential between the peaks and valleys is significant, with the profile distinguished by pronounced sharp peaks.

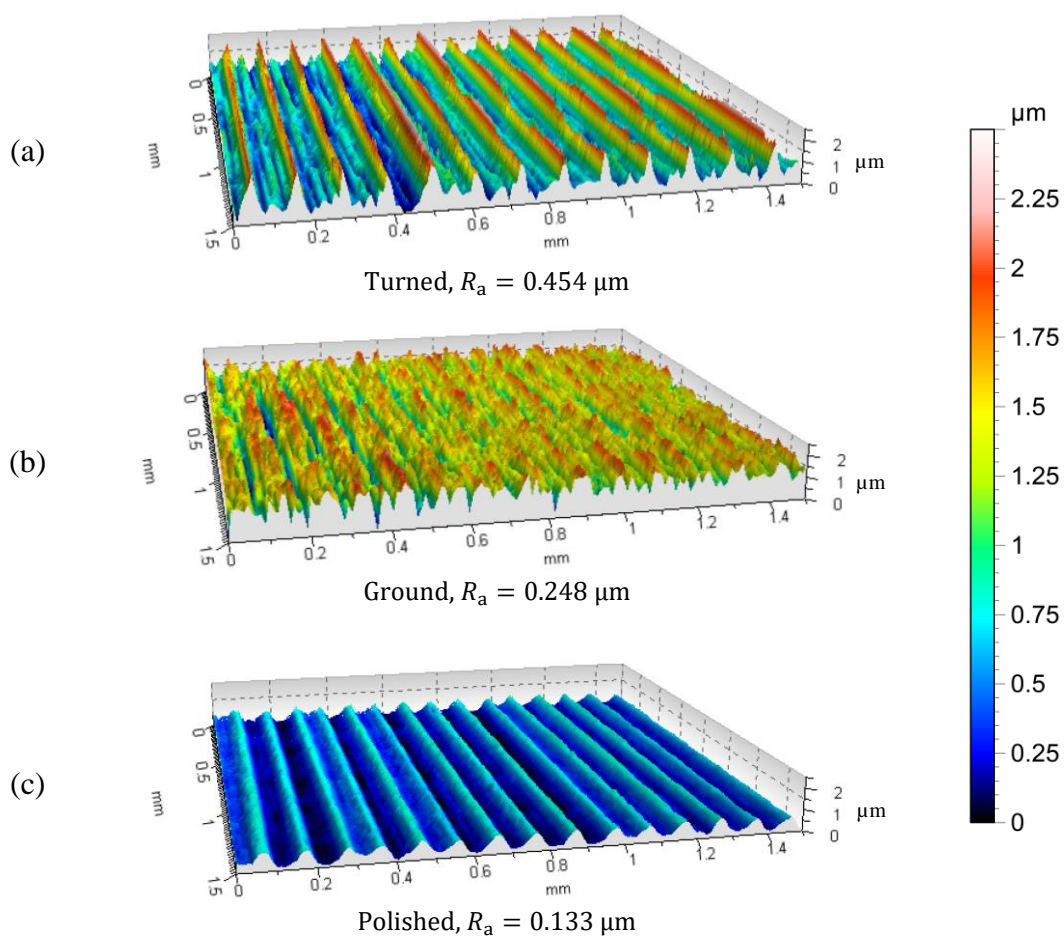


Figure 30. 3D surface topography and average R_a values after turning, after grinding, and after polishing

Following the grinding process, Figure 30 (b), the surface exhibits a more refined topology compared to the initial one resulting from the turning process. This is attributed to the grinding's abrasive mechanism, which effectively diminishes the protrusions of the peaks. Consequently, the height difference between the peaks and valleys on the ground surface is less compared to the turned surface. The average surface roughness measurement also decreased from $0.454 \mu\text{m}$ post-

turning to $0.248\ \mu\text{m}$ post-grinding, indicating a smoother finish with more suppressed and rounded peaks.

For the surface that underwent polishing after turning, Figure 30 (c) shows a very uniform pattern. Compared to the turned and turned-then-ground surfaces, it has rounded peaks and valleys due to the abrasive action of the process. The color gradient in the image suggests that there is less variation in height across the surface. The predominance of the blue color indicates that most of the surface is at the lower end of the micrometer scale, which means the polishing has effectively reduced surface irregularities and reduced the surface roughness, and this is reflected in the image by the lack of high peaks (red or orange colors) and the dominance of the smoother surface features (blue and green colors). In essence, compared to the turned and ground surfaces, it has an average surface roughness of $0.133\ \mu\text{m}$, exhibits the smoothest texture among the three, with the least variation in peak-to-valley height.

5.5.2. 3D Surface Topography After Turning and SDB

After performing one pass of SDB on the turned surface using 50, 100, 150, and 200 N, the resulting 3D surface topographies are shown in Figure 31. Applying a 50 N force during the SDB process, Figure 31. (a), resulted in the surface roughness being halved from the initial $0.454\ \mu\text{m}$ after turning to $0.218\ \mu\text{m}$, significantly smoothing out the asperities and resulting in a surface with a more regular pattern, softer valleys, and less pronounced peaks.

Doubling the burnishing force to 100 N, Figure 31 (b), has noticeably enhanced the surface quality, achieving exceptional smoothness with a roughness value of just $0.073\ \mu\text{m}$. This represents a dramatic decrease in surface irregularities, with a remarkable reduction from the initial roughness found on the turned surface. The burnishing has created a uniform topology, evident from the 3D topography, displaying a consistent pattern and minimal variation in peak-to-valley depth, as indicated by the dark to light blue scale colors. In conclusion, the increased force has effectively compressed the surface, producing a more pronounced flattening of the peaks and better filling of the valleys, thus refining the micro-topography.

The single pass of SDB with a force of 150 N, as depicted in Figure 31 (c), has produced a surface with outstanding smoothness, as indicated by the significantly reduced R_a value from $0.454\ \mu\text{m}$ to $0.065\ \mu\text{m}$. The topographical map reflects this enhancement, exhibiting minimal color variation, which suggests a very flat and even surface profile. The increased force has been particularly effective in creating a highly uniform surface, ironing out the defects from the turning process more effectively than the lower forces of 50 and 100 N. This has led to a surface with substantially flattened peaks and filled-in valleys, providing a more refined texture and a consistently

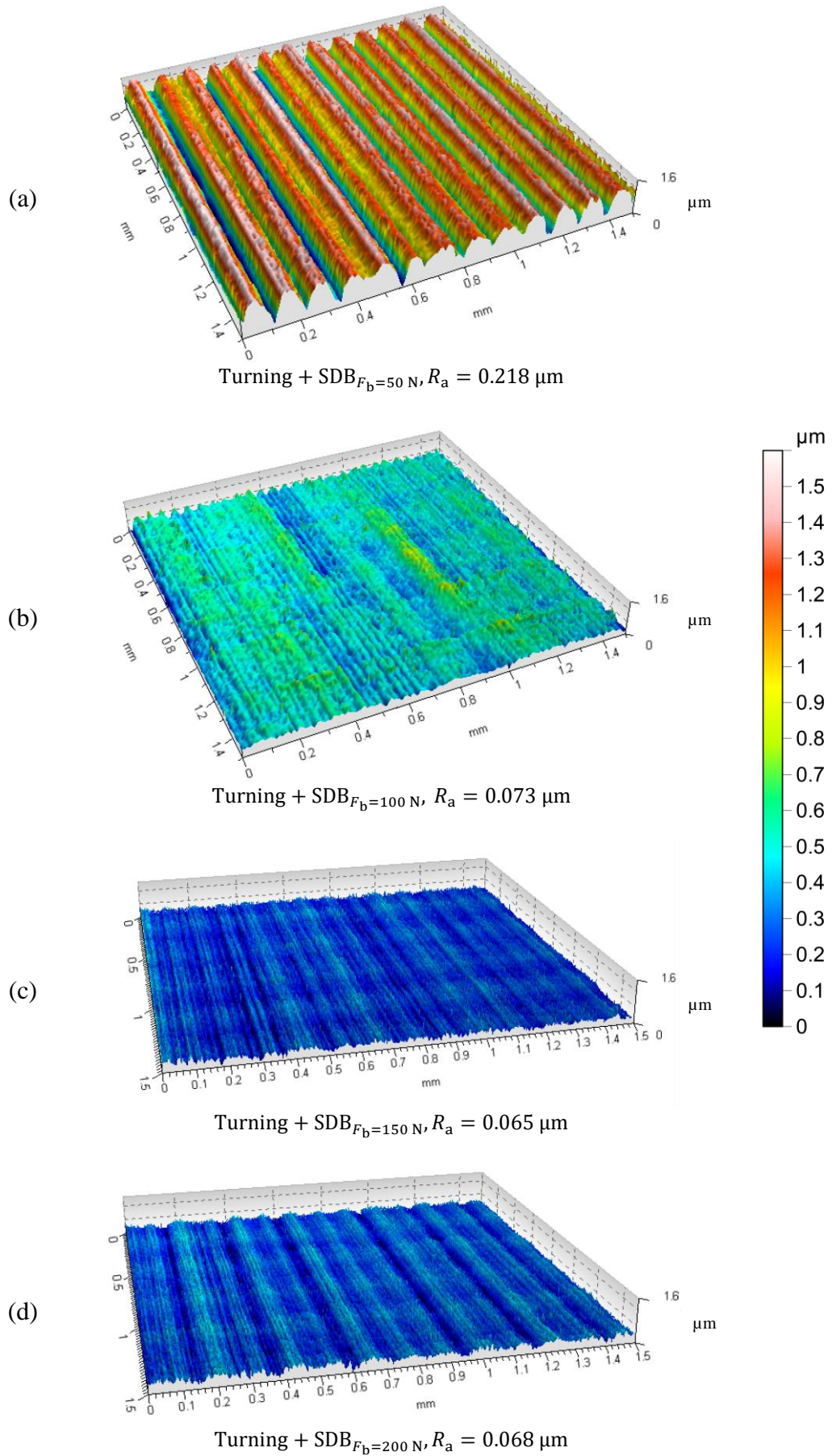


Figure 31. 3D surface topography and average R_a values after turning then SDB using:

(a) 50 N, (b) 100 N, (c) 150 N, and (d) 200 N

homogeneous appearance. Similarly, the same improved outcomes were also observed with the use of a 200 N force in burnishing, as Figure 31 (d) depicts. Visually, the surfaces treated with 150 N and 200 N forces appear quite similar, yet the latter displays a slightly higher roughness value.

From the previous discussion, it could be seen that the progressive increase in the burnishing force has sequentially improved the surface finish, with the 150 and 200 N applications yielding the most uniform and consistent surface, significantly transforming the original turned surface by compressing the material to achieve an even smoother and flatter finish.

Lastly, it is remarkable to note that, following the application of SDB using 100, 150, and 200 N forces, the surface topology exhibits the generation of new micro-peaks. These micro-peaks are primarily a result of the material being displaced and flowing in front of the burnishing tool under the substantial pressure exerted during SDB using these high forces [105], [108]. Therefore, forces higher than 50 N caused more pronounced plastic deformation, leading not only to the flattening of existing peaks but also to lateral material flow and swelling, resulting in new micro-peaks. However, the beneficial impact of applying greater force in the burnishing process, aimed at flattening and smoothing the surface, has its limits. When the force of 200 N was utilized, there was an observable increase in the outflow of material and the formation of material waves, exceeding what was seen with the force of 150 N. This excessive material displacement led to a slight increase in surface roughness for the surface burnished with 200 N compared to the one treated with 150 N.

5.5.3. 3D Surface Topography After Grinding and SDB, and After Polishing and SDB

Following the finishing SDB step using 200 N, Figure 32 displays the 3D surface topographies for surfaces treated with SDB after grinding and polishing, alongside for those subjected to the two-step SDB process. Average roughness values for those surfaces are also included in the figure.

The surface topology of the pre-ground surface after SDB, shown in Figure 32 (a), appears quite uniform, with noticeably smoother ridges than those seen after just grinding, which is typical of the SDB process's ability to even out the microscopic peaks and valleys. Additionally, the peaks on the burnished surface are suppressed and rounded, and the valleys are not as deep, showcasing the effective smoothing action of the diamond tool used in burnishing. This resulted in a surface with significantly reduced roughness and a smoother color transition when compared to the more pronounced ridges and varied color gradient of the ground surface.

Besides, the image depicted in Figure 32 (b) demonstrates that the surface, after being polished and treated with SDB, showcases a consistent pattern of gently sloping ridges and shallow valleys, indicative of the fine polishing followed by the smoothing effects of SDB. The resulting color gradient spans merely from dark to light blue, signifying minimal height variation and implying that

SDB has effectively smoothed out the peaks and valleys left from polishing. Compared to the pre-SDB image, the current surface exhibits less pronounced peaks and a more uniform surface, suggesting that SDB has further diminished surface roughness. Moreover, the generation of the micro-peaks after carrying out the burnishing process using 200 N is evident. This outflow effect is evidenced by the orientation of the newly formed peaks, which bend in alignment with the direction of movement of the burnishing head. Ultimately, the combined treatment of polishing and SDB has yielded a high-quality surface with a fine and uniform finish, enhancing the smoothness obtained from polishing alone and contributing to a high-quality surface with minimal height variations.

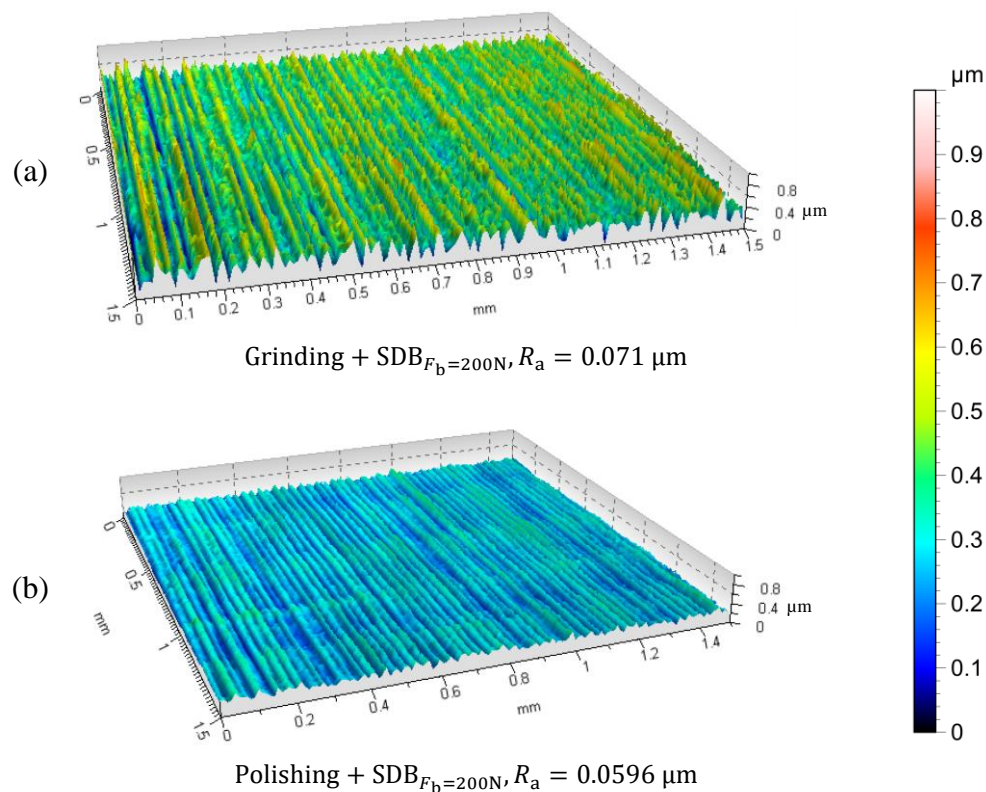


Figure 32. 3D Surface topography and average R_a values for different surfaces after grinding and SDB, and after polishing and SDB by 200 N

5.5.4. 3D Surface Topography After Two-Step SDB

The 3D surface topographies of the surfaces that had undergone two-step SDB after turning are shown in Figure 33 (a), (b), and (c), burnished in the first step with forces of 50, 100, and 150 N, and with 200 N in the second step, respectively. The observed impact of increasing the burnishing force on enhancing surface flattening and smoothing led to the anticipated outcome that surfaces undergoing a two-step SDB process would exhibit improved features after the second burnishing step, given that the force applied in the second step was greater than that in the first one. However, the primary consideration in this process was to understand the influence of the burnishing force of the first step on the end results.

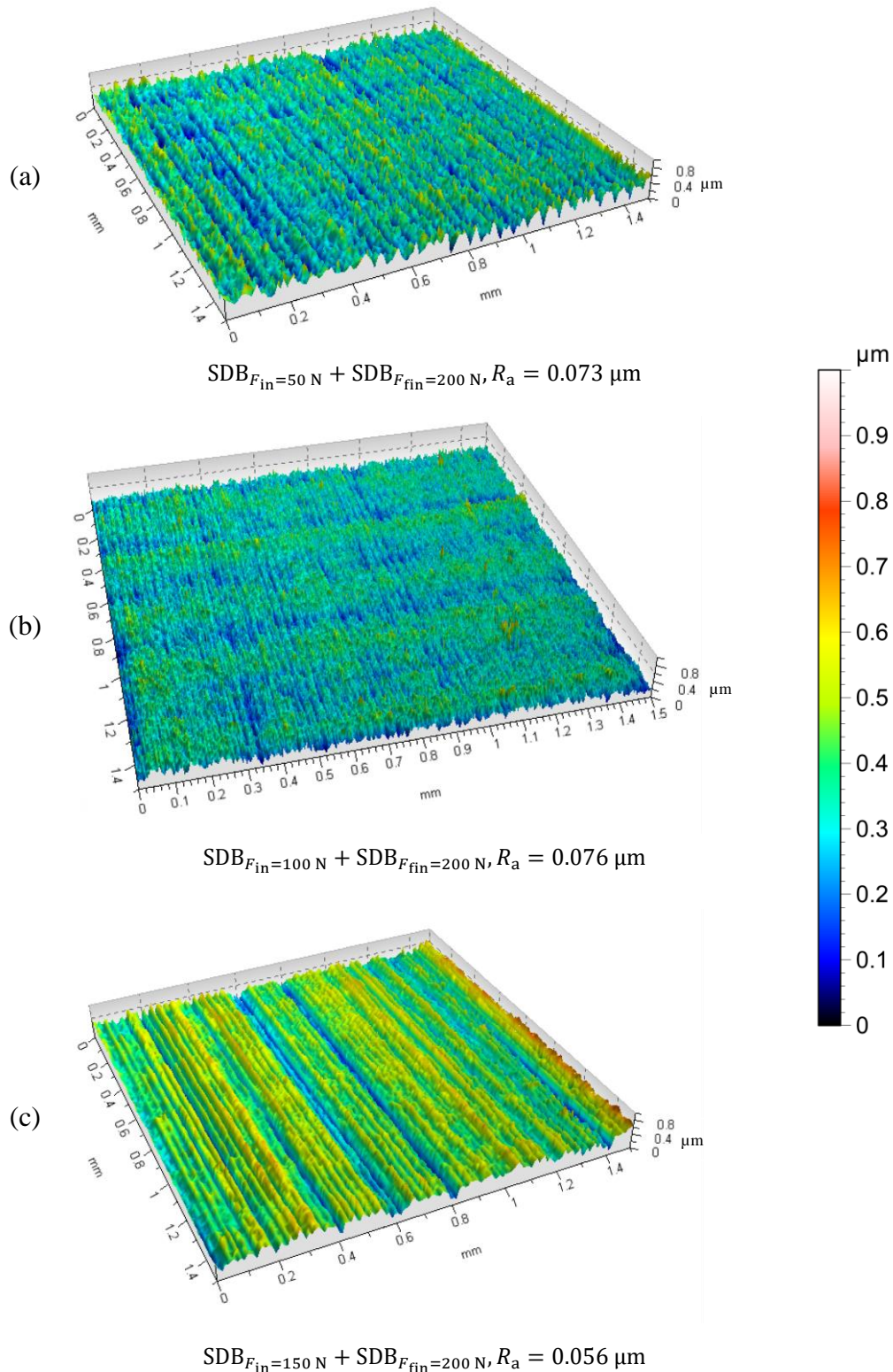


Figure 33. 3D Surface topography and average R_a values for different surfaces after two-step SDB using 200 N in the finishing step

Upon comparing the surface characteristics of the three samples subjected to the two-step SDB process, distinct differences emerge despite all being burnished with 200 N force in the second step. These variances are dependent on the initial burnishing force applied. Samples burnished with a higher force in the first step exhibited smoother and flatter surfaces. Specifically, the surface treated

with 150 N in the first step and with 200 N in the second step displayed the most significant improvement, surpassing the surface that was burnished a single time with 200 N.

In this proposed process, it is obvious that the application of a second burnishing pass with a higher force systematically refined the surface characteristics, improving uniformity and smoothness across the samples. It led to an even flatter surface profile, with a greater flattening of peaks and a more complete filling of valleys. Nevertheless, those improvements were highly dependent on the initial surface roughness characteristics, given that the smoothest surface before applying the second SDB step led to the most pronounced results, which highlights the vital importance of the initial surface state in achieving the final finish.

5.5.5. Surface Morphology After Grinding and SDB, and After Two-Step SDB

In addition to the 3D surface topography, another vital aspect of visual inspection post-SDB is examining the morphological features of the surfaces due to their significant impact on the mechanical part performance [84], [109]. SEM micrographs presenting the surface morphology for those treated with SDB following grinding and those subjected to the two-step SDB process using 200 N in the final stage are presented in Figure 34.

Figure 34 (a) depicts the morphology of the surface treated with grinding and SDB. It can be seen that despite the linear patterns from grinding, the surface appears relatively smooth, which is characteristic of the smoothing effects of SDB. One of the main features of the surface is the parallel lines or striations that run across the surface and are perpendicular to the axial feed direction. Some of those lines are burnished grooves that are left behind by the grinding process. Additionally, wave-like patterns or ripples are present, likely caused by the lateral flow of material during the burnishing process. In the areas between these patterns, the surface shows a smoothness that suggests SDB has successfully reduced the irregularities commonly associated with grinding.

Moreover, a remarkable characteristic of this surface is the presence of feed marks generated by the burnishing head due to the high force applied during the burnishing process, which are noticeable despite the steel's hardened state. These marks have an approximate spacing that aligns with the burnishing feed (0.03 mm/rev). Alongside these, various defects and imperfections, such as pits, scratches, protrusions, and microcracks, are detected, which, while typical to exist after grinding, are still evident and not entirely removed by the burnishing. In summary, despite the existence of some flaws and defects, the substantial force applied during burnishing has yielded a surface with significantly less roughness, improved uniformity, and greater overall smoothness.

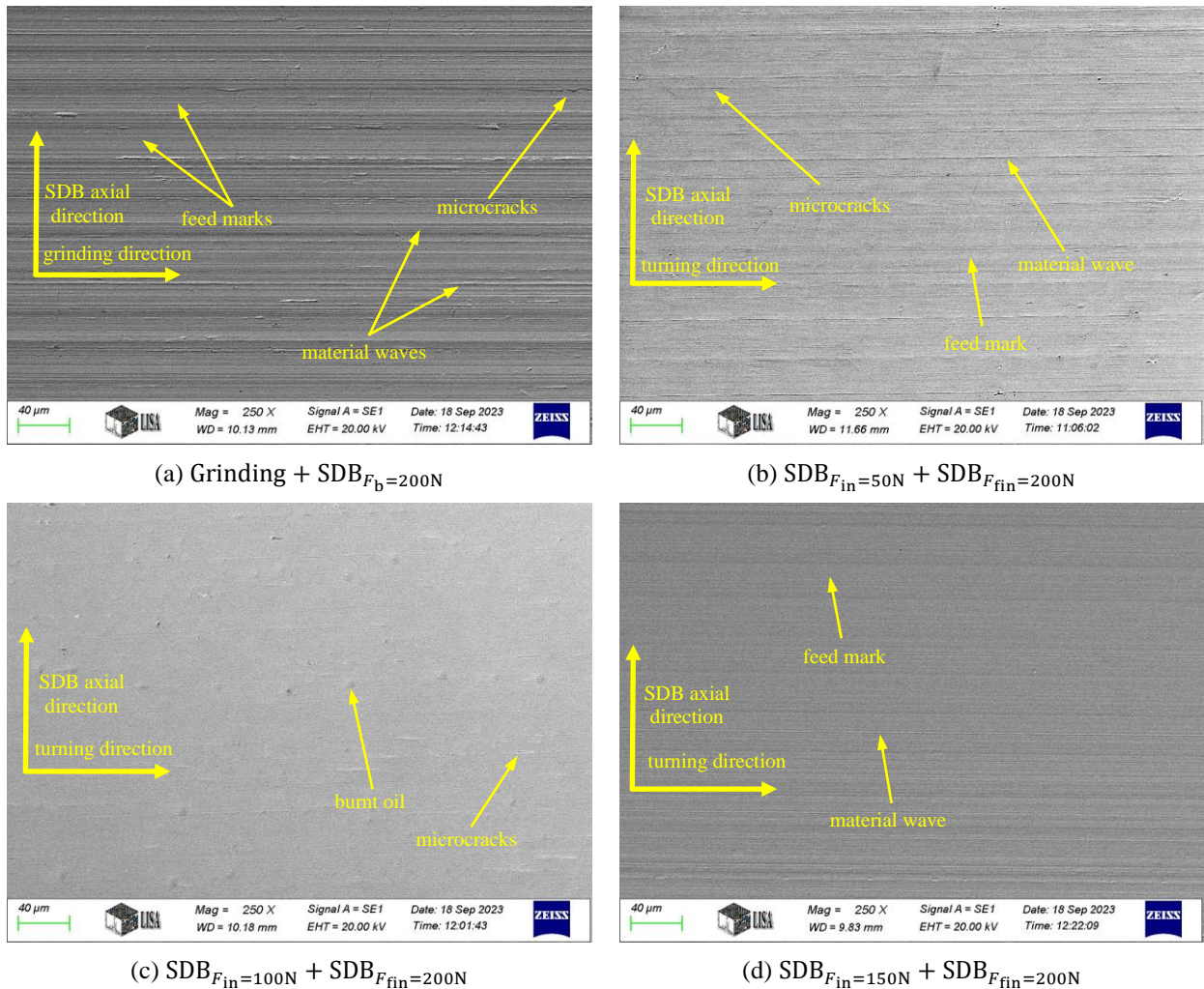


Figure 34. SEM images of surface morphology for surfaces after grinding and SDB, and two-step SDB by 200 N finishing force

The SEM image of the surface subjected to two-step SDB, with an initial pass by 50 N following turning and a final pass by 200 N, shown in Figure 34 (b), reveals several key features. The area seems uniformly smooth, implying an effective smoothing action from the SDB process, particularly in the second step with the higher force. The key characteristics include linear striation patterns or lines and a uniformly smooth texture between these patterns, highlighting the successful smoothing achieved by the SDB process, especially during the higher-force final step. Actually, some of those striations are in the form of material waves generated in the last burnishing step due to the high force. Another are in the form of micro-peaks created by the further flattening action of the large peaks left after the first step of burnishing post-turning. Additionally, the image reveals linear microcracks, which likely arose due to two factors. Firstly, in spite of the fact that the burnishing force in the second step was much higher than that in the first one, 200 N compared to 50N, it was unable to fully close the valleys that were left behind after the first burnishing step because those valleys were deep enough and hard to reach due to the work hardening caused by the first step of burnishing, which made the material flow in the second step uneven and difficult. The

second reason was the disturbed movement of the burnishing head on the rough, hard, and brittle surface created after the first step of burnishing.

Another clear feature was the alignment of feed marks or valleys perpendicular to the direction of the burnishing feed, which remain minimally visible even when a significant burnishing force was applied. This phenomenon could be attributed to the first burnishing step, in which a lesser force was employed to refine the surface post-turning and to create a work-hardened layer. This hardened surface hindered the burnishing head's ability to penetrate, and subsequently left behind feed marks.

The surface that underwent a two-step SDB process, starting with 100 N force and concluding with 200 N force, is depicted in Figure 34 (c). When compared to the surface at first burnished by 50 N, it is observable that the effect of using a higher initial burnishing force was of greater efficiency due to its increased ability in flattening the surface irregularities and ironing out the surface imperfections produced after turning. As shown, the result was a smoother surface with a more consistent and uniform topology and striation patterns that are likely finer and more refined due to the higher initial force. Also, the microcracks generated on this surface were much less pronounced. Moreover, no feed marks or valleys were formed due to the higher work hardening induced in the first step of burnishing. An exception to this surface's improved condition was the presence of burnt oil, as identified through elemental analysis.

Lastly, Figure 34 (d) shows the surface morphology of the material that has undergone a two-step SDB process, with the first step executed using 150 N following the turning process and the second step performed by 200 N. The surface exhibits a high degree of uniformity and smoothness, with an improved finish. In addition, the morphology of the surface is characterized by highly refined linear striations, indicative of a substantial initial flattening of surface irregularities. This striation-pattern consists of micro-peaks, material waves, and feed marks, which were all created in the first step of burnishing due to the high force. However, after the second step of burnishing, and cause of the higher force, those striations were further smoothed, creating a more homogenous appearance.

Moreover, what is strikingly apparent in this surface, compared to the previous surfaces, is the fewer and less pronounced imperfections such as pits and scratches, along with the absence of microcracks, which is considered a significant improvement in terms of enhancing the fatigue life. The main reason behind this is the well-prepared and improved surface after the first burnishing step. The high burnishing force in the first step was able to flatten the turned surface, suppressing its peaks and filling its valleys. Therefore, producing a better-prepared surface for the second pass and reducing the workload for the second 200 N pass.

In accordance with the previous discussion, in terms of the two-step SDB technique, the first burnishing force has a great influence on the final surface finish of the sample. Depending on its value, the lower force of the first step compared to the second one can smooth out the macroscopic peaks and valleys generated from the previous turning processes and serves to minimize imperfections like pits, scratches, and microcracks, allowing for a more consistent and refined surface morphology. This pre-smoothing effect would make the final 200 N pass more effective in achieving a high-quality finish, as it would have to work with fewer and less pronounced surface imperfections. Consequently, the final surface after the second step by 200 N would exhibit a finer topology with even fewer visible defects and a more homogeneous appearance.

When comparing the surface morphology achieved by grinding followed by SDB to that achieved through the two-step SDB process, it became evident that the latter process offers numerous benefits over the former traditional approach. It could be seen that the surfaces that experienced two-step SDB showed reduced surface defects like pits, material outflow (waves), scratches, and microcracks. Also, the two-step approach produced a more uniform surface topology. The reason behind those advantages is the gradual refinement applied through the proposed process, i.e., the first lower-force pass can deal with large-scale irregularities, while the subsequent higher-force pass focuses on the finer details, which can lead to a smoother surface with a more refined finish.

While the morphological image of the surface subjected to grinding, then SDB, revealed several material waves and striations, these defects were noticeably reduced after implementing the two-step SDB process. Indeed, the superiority of the two-step SDB process over grinding, then SDB, stems from the differences in how the burnishing process occurs in each approach. Actually, depending on the material hardness, there are two schemes for the SDB process. One is when the material is soft, and the other is for the hard, to very hard materials, as shown in Figure 35.

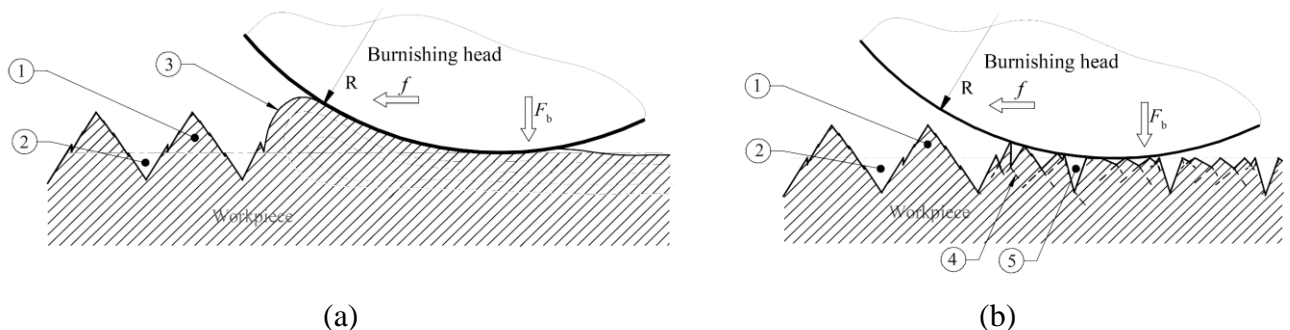


Figure 35. SDB process for: (a) soft materials; (b) hard materials; 1. surface peak, 2. surface valley, 3. material wave, 4. slip plane, 5. deep valley after burnishing [108]

In the case of SDB carried out after grinding, despite the fact that the material was initially hardened, due to the high force applied during the burnishing process, burnishing resulted in a

morphology displaying characteristics similar to those of soft materials treated with SDB, shown in part (a) of Figure 35.

According to Dzionk et al. [108], the burnishing of soft materials, like what happened with the ground surface, comprises successive stages. Initially, the burnishing tool applies significant pressure to the surface peaks, causing plastic deformation by sliding across the material's grain structures. This pressure flattens the rough peaks (1), leading to surface smoothing. Then, as pressure increases, the deformed material will be pushed into the adjacent voids, effectively raising the valleys (2) and lowering the peaks. During the final phase, the material that has been burnished fills in the gaps on the surface and advances along the area of contact towards the front part of the tool. In this case, when the burnishing head moves forward, exerting high pressure, the material will accumulate in front of the tool and moves with it. This movement will cause an outflow of the material in the form of a wave, represented by zone 3 in Figure 35. These waves might be dragged under the burnishing tool, leading to surface defects on the workpiece, thereby affecting the machined part's quality [105], [110].

Conversely, the application of the two-step SDB process significantly reduced, or even eliminated, material outflow and defects, particularly when the first-step burnishing forces of 100 and 150 N were employed. As was mentioned before, the application of SDB exerts work hardening on the burnished surface [54], [61], and [62], and this is the merit of the first step of SDB in this proposed process. Therefore, in the second step of burnishing, those hardened surfaces had followed the burnishing scheme of hard, to very hard materials, shown in part (b) of Figure 35.

In this case, when burnishing hard materials, the process significantly differs from that of softer materials due to the material's limited deformability. The plastic deformation encountered is predominantly confined to grain boundary slides. Pressing of the burnishing head on the peaks of surface irregularities results in slip deformation by slip planes, collapsing these peaks to form local plateaus and narrowing the valleys. This deformation does not lead to piled-up material or the wave formation phenomenon typically seen when burnishing soft materials [114].

5.6. Burnished Cross-Sectional Microstructure

In order to explore the impact of the burnishing technique on the microstructure and the influence of the first burnishing force in the case of two-step SDB, SEM micrographs in Figure 36 exhibit the cross-sectional microstructure of the burnished surfaces subjected to grinding, then SDB, and those treated by two-step SDB using the finishing burnishing force of 200 N. The images reveal pronounced plastic deformation of surface grains, with the top layer appearing significantly more compacted than the underlying material. The plastic deformation is manifested as inclined and elongated grains oriented in the direction of the burnishing tool's movement, a result of the pressure and friction exerted during the burnishing process.

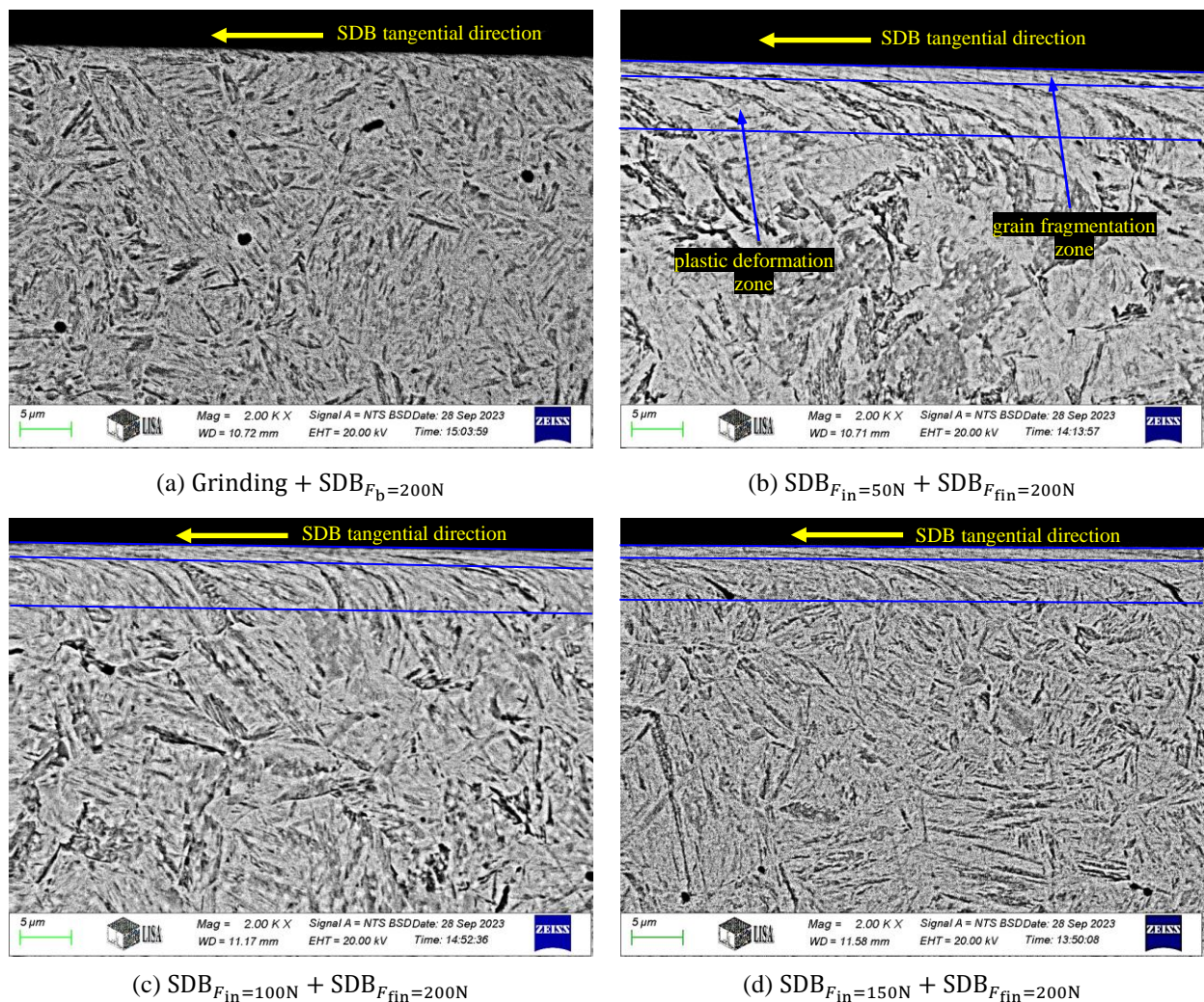


Figure 36. Cross-sectional microstructure SEM micrographs of surfaces subjected to grinding and SDB, and two-step SDB by 200 N

The four surfaces, while all finished with an equal burnishing force, exhibit notable differences. Specifically, the surface treated with grinding and burnishing, as depicted in Figure 36 (a), shows grains with less plastic deformation, less tilt, reduced compactness, and a lack of elongation in the burnishing direction compared to those subjected to the two-step SDB process shown in Figure 36

(b), (c), and (d). These marked differences in deformation and structural characteristics are primarily attributed to the additional burnishing step employed in the two-step SDB method, which induced a more substantial degree of plastic deformation on the surface layer. For this surface, the plastic deformation caused by the burnishing process penetrated to approximately 2 to 3 μm underneath the surface.

On the other hand, the grains subjected to the two-step SDB process tend to exhibit more uniform deformation and compaction due to the graduated force application. In addition, the grains in the surface layer are likely to appear more compressed and elongated along the direction of the burnishing tool's progression, indicating the extent of plastic deformation imparted by the sequenced two-step burnishing technique.

For the burnished layer, visual inspection indicates that the three surfaces show the same pattern. That layer consists of two main zones. The first zone, just beneath the surface, could be called the grain fragmentation zone, is characterized by fragmented and highly deformed grains dragged and elongated in the direction of the burnishing tool's movement. This layer has been directly affected by the burnishing process. It appears denser and more uniform due to the plastic deformation and material flow caused by the high pressure of the burnishing tool. Underneath this zone, there is a transitional zone, which could be called the plastic deformation zone, where the grains are less deformed, and the original microstructure of the material starts to become more evident. In this secondary zone, grains display a tilt and an orientation towards the surface, marking a gradual shift from the upper, intensively deformed zone to the core's material.

One remarkable feature of the grain fragmentation zone is its relationship with the first burnishing force. A higher force in the first burnishing step led to more compacted surface grains and a more refined surface texture, as the initial plastic deformation was more significant, making the second pass at 200 N more effective at producing a uniformly smooth surface.

Finally, one main difference between those three surfaces is the depth of the burnished layer, the fragmentation, and the plastic deformation zones. Utilizing the distance measurement tool of the SEM, the average depth of this layer was assessed by averaging three distinct measurements taken at various places on each surface. The findings revealed an inverse correlation between the first burnishing force and the layer's depth. Specifically, the average depths of the burnished layers were ~ 8.6 , ~ 7.2 , and ~ 6.4 μm for the surfaces burnished in the first step by the forces 50, 100, and 150 N, respectively.

The main reason behind this inverse relationship may refer to several reasons. Firstly, higher force in the first burnishing step causes greater work hardening of the surface layer. This increased

hardening can resist further plastic deformation, resulting in a shallower deformed layer during the second pass. Also, a higher force from the first step can push the material laterally across the surface, reducing the depth of the material that has been plastically deformed but creating a more compacted surface layer, which again reduces the depth of the subsequent deformation. Lastly, larger forces from the first step can also cause more intense grain refinement near the surface [75]. These finer grains are stronger and more resistant to deformation, which could reduce the depth of the affected layer when the second burnishing pass is applied.

In conclusion, through detailed analysis supported by 3D topographical data and SEM morphological and microstructural micrographs, it has been observed how the integrity of surfaces was substantially enhanced by the application of the SDB process, particularly when the approach of two-step SDB was used. A remarkable transformation in surface characteristics, which is not merely superficial but extends to underneath the surface level, has been revealed by the use of sequential application of the burnishing process, starting with 150 N and finishing with 200 N.

5.7. Comprehensive Explanation of the Results

From the previous results, it can be observed that although the initial surface roughness before applying the burnishing in the proposed process (turned surfaces) was higher than that before applying the conventional burnishing process (ground and polished surfaces), the two-step SDB achieved better results than the traditional processes. The results depended on the burnishing force used in the first and second steps of the burnishing process.

The reason behind these superior results is attributed to the mechanism by which the two-step slide diamond burnishing process occurs, compared to the burnishing after grinding or polishing. In the case of the single burnishing step performed on a ground or polished surface, part of the burnishing energy exerted by the burnishing head is primarily consumed by friction, which causes material outflow, therefore pushing the surface peaks forward and filling the valleys and so reducing surface roughness. The other part of the burnishing energy is consumed by inducing compressive residual stresses and increasing the microhardness. The same process also happens in the first step of the two-step SDB process.

In contrast, in the case of two-step slide diamond burnishing, when burnishing (in the second step) the strain-hardened, previously smoothed surface with a higher force than that used in the first step, less burnishing energy will be consumed by friction, and the further smoothing of the surface will occur via slip deformation along slip planes. Consequently, more energy will be available to induce additional compressive residual stresses and further increase the surface microhardness. This effect will be more pronounced when burnishing with a high force, like 150 N, in the first step, followed by a higher force, like 200 N, in the second step.

Additionally, when investigating the burnished cross-sectional microstructure of the surfaces related to the conventional and proposed processes, finally burnished with 200 N (Figure 36), and their in-depth tangential and axial residual stress components (Figure 37), a strong relationship can be observed. In the tangential direction, within the depth of less than 10 μm , which contains the visible plastic deformation of grains, it can be observed that the highest stress level is on the surface that was ground, then burnished, having the lowest rate of plastic deformation at the surface. Following this, the surfaces initially burnished with 50, 100, and 150 N, respectively, show decreasing stress levels. The reason for this is that within that depth, higher plastic deformation was caused by the high shear strain rate, such as that on the surface initially burnished with 150 N, which results in greater stress relaxation, leading to lower compressive stresses. As the deformation rate decreases, the material experiences less stress relaxation, resulting in a higher level of compressive residual stress in the tangential direction.

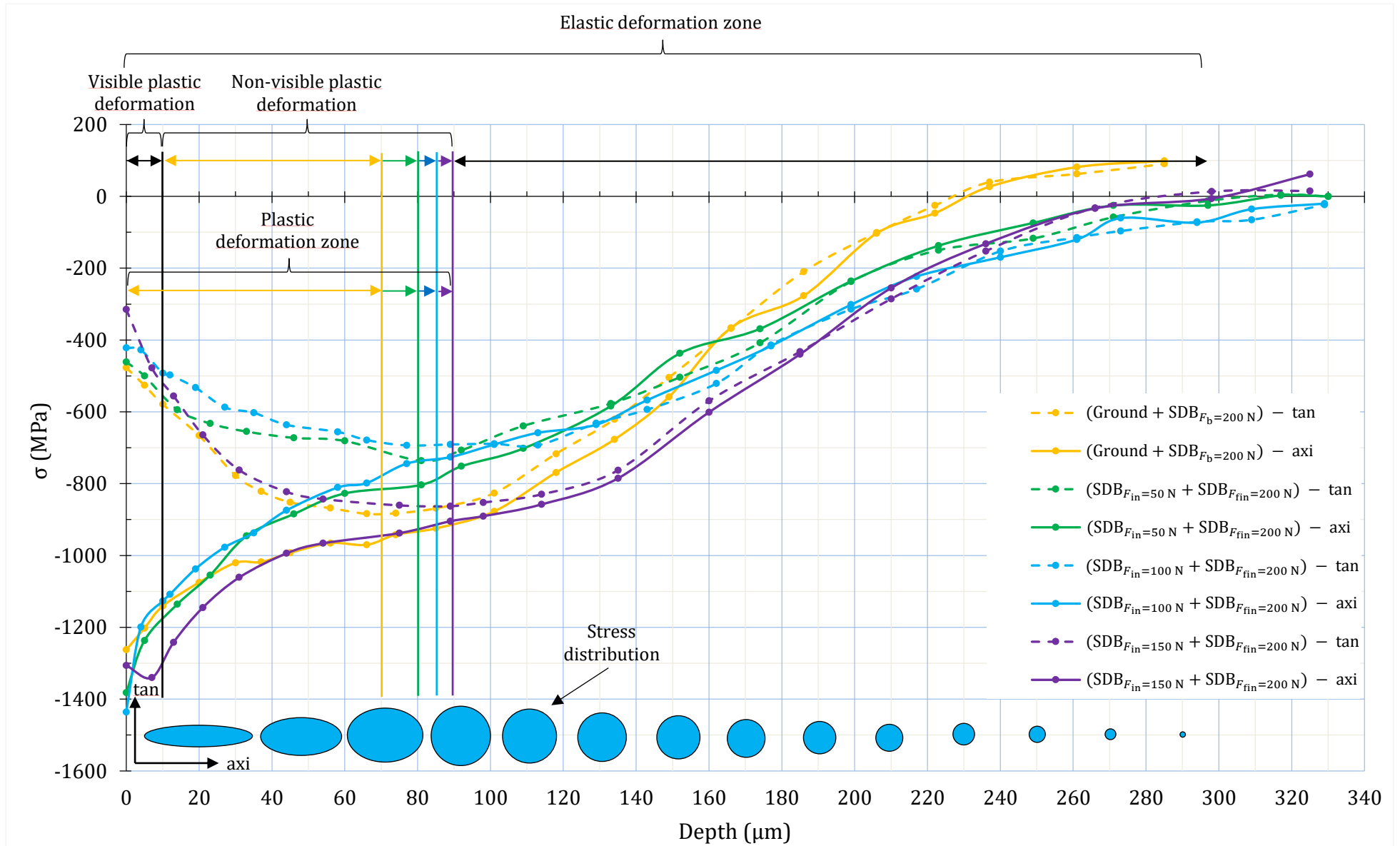


Figure 37. In-depth components of axial and tangential residual stresses and their respective zones after grinding, then SDB, and two-step SDB, using a finishing burnishing force of 200 N, and the representation of axial/tangential stress component distribution

However, in the axial direction, within the same depth of less than 10 μm , the opposite trend was observed. The surface that was ground, then burnished, had the lowest stress level, followed by the surfaces initially burnished with 50 N and 100 N, respectively. The root cause of this is the significantly lower shear strain rate in the axial direction compared to the tangential direction. As a result, the higher plastic deformation rate caused by the increasing first-step burnishing force, combined with the low shear strain rate, led to higher axial stresses. Nevertheless, it is evident that the surface initially burnished with 150 N was an exception due to the high fatigue caused by the high force, which resulted in stress relaxation. The same was observed by Nestler and Schubert [102].

It can also be noticed that for the axial stresses, there is a sudden decrease within that zone. This high gradient suggests very restricted plastic deformation, mostly limited to the area close to the surface. The ground-then-burnished surface shows the lowest gradient because it experienced the lowest rate of plastic deformation and, consequently, the lowest stress relaxation. As the rate of plastic deformation increased, as seen in the surfaces burnished with 50 N and 100 N in the first step, the rate of decrease in stresses also increased.

When it comes to the zone below the visible plastic deformation, contrary to what is suggested in the literature by Dzionk et al. [105]—in which they state that only elastic deformation occurs in the zone below the visible plastic deformation—it is proposed that plastic deformation (slip) also occurs in this region in the tangential direction. This can be explained by the variation of tangential and axial stress components until they reach a depth where they gain similar value.

In the plastic deformation zone of grains—which extends from the surface to the peak of the tangential stresses—there is slip in the tangential direction. Near the surface, the slip is notable due to the high shear strain rate, causing the visible plastic deformation of grains and, consequently, an intensive decrease of elastic lattice distortion in the tangential direction. Moving further in depth, the occurrence of slip decreases, and the elastic distortion increases. Slip remains present until the depth where the tangential and axial stress components equalize. This depth marks the end of the plastic deformation zone.

However, in the axial direction, no slip occurs near the surface due to the low shear strain rate. As a result, the elastic distortion of the lattice is not reduced. Upon moving further in depth, the elastic distortion continuously decreases. The in-depth residual stress distribution shown at the bottom of Figure 37 illustrates this interaction between the two stress components. Finally, at the end of the plastic deformation zone, no slip occurs, and the tangential and axial stress components equalize. Beyond this point, both stress components continue to decrease at the same rate until reaching the end of the elastic deformation zone.

6. SUMMARY AND CONCLUSION

This Ph.D. research examines the effectiveness of a two-step slide diamond burnishing (SDB) process compared to the traditional method of grinding or polishing, then burnishing. The study focuses on improving the surface integrity of 42CrMo4 hard-turned steel by minimizing initial surface roughness and avoiding the introduction of detrimental tensile stresses that are typically associated with grinding. Additionally, it explores the impact of sequential burnishing steps on the surface integrity components of the steel, aiming to demonstrate the advantages of the proposed method over conventional approaches.

Early in the study, experiments were conducted to determine how various burnishing parameters, specifically speed, feed, and force, affect the surface characteristics of hard-turned 42CrMo4 steel. The goal was to identify the optimal combination of these parameters to improve surface roughness in the first burnishing step. Once the optimum feed and speed were established within the tested range, these parameters and eight levels of burnishing force were applied in subsequent burnishing processes, both in the proposed and conventional methods.

To compare the outcomes of the proposed and conventional processes, five bars, each comprising eight surfaces, were hard-turned. Subsequently, one was ground and another polished. These ground and polished surfaces were then subjected to eight levels of burnishing force (25, 50, 75, ... 200 N). For the remaining three bars, one specific force of 50, 100, and 150 N was applied across all surfaces of each bar in the first burnishing step, followed by the same eight forces in the subsequent burnishing step. Following the second burnishing step, evaluations were conducted on surface axial and tangential residual stresses, surface roughness (R_a), and surface microhardness (HV 0.2) across all surfaces. Additionally, in-depth residual stress distribution, surface morphology, topography, and cross-sectional microstructure were analyzed for selected surfaces.

After analyzing the outcomes of the investigations, the following conclusions were drawn:

- Surface and in-depth residual stresses component:

1. The level of compressive residual stress induced on the surface of the burnished workpiece is influenced by both the initial treatment and the magnitude of the finishing burnishing force. While an increase in the finishing SDB force results in higher compressive residual stresses in the axial direction, it leads to reduced stresses in the tangential direction.
2. In the two-step SDB process, to significantly enhance surface axial residual stresses following the first burnishing step, the second burnishing force needs to be greater than the first one. Consequently, an initial burnishing force of 50 or 100 N followed by a second force of 200 N

proves to be the most effective combination, yielding higher compressive residual stresses in the axial direction than those achieved through burnishing after grinding or polishing at 200 N.

3. Surface tangential stresses are generally more compressive when burnishing follows grinding, compared to polishing, because initial stresses are compressive after grinding and tensile after polishing. Furthermore, the highest tangential residual stresses across all measured outcomes occurred when certain finishing burnishing forces were applied after grinding.
4. In the axial direction, an increase in the finishing burnishing force results in a decrease in the kurtosis parameter (R_{ku}) values. This decrease indicates a surface profile with broader and fewer high peaks and deeper valleys, leading to a reduction in surface sharpness and a transition to a more compacted and smoothed surface, which contributes to increased axial compressive residual stresses.
5. In the tangential direction, increasing the finishing burnishing force leads to an increase in the R_{ku} values, signifying a rise in the sharpness and quantity of high peaks and deep valleys. This profile alteration results in narrower peaks, which provide less resistance to deformation and lead to greater stress relaxation. Consequently, this results in reduced tangential compressive residual stresses as the burnishing force increases. As the finishing burnishing force increases, the tendency toward deteriorating the surface due to the high relative velocity between the burnishing head and the surface increases, too.
6. The surface treated with a two-step SDB process, burnished with 150 N in the first step and subsequently with 200 N in the second one, exhibited the deepest and most intense compressive residual stresses in both axial and tangential directions. This performance surpasses that of surfaces subjected to one-step SDB, or those burnished after grinding or polishing with 200 N.

- Surface roughness (R_a):

7. Applying suitable burnishing forces in both steps of the two-step SDB approach results in lower surface roughness compared to outcomes achieved by grinding or polishing, then burnishing. Specifically, using 100 N and 150 N in the first step, followed by 25 to 150 N and 175 to 200 N in the second step, respectively, optimizes surface smoothness.
8. Surfaces burnished initially with the highest first-step force of 150 N displayed a unique roughness pattern compared to those initially treated with 50 and 100 N, achieving the lowest roughness when treated with the highest second-step forces. This highlights that higher first-step forces necessitate equally high or higher subsequent second-step burnishing forces to improve or maintain surface quality due to the extensive plastic deformation induced by the high first-step force.

- Surface microhardness (HV 0.2):

9. The two-step SDB approach, particularly with a higher first-step burnishing force of 150 N, significantly enhances microhardness compared to the traditional single-step method after grinding or polishing.
10. While lower first-step forces (50 N and 100 N) in the two-step SDB create more complex and unpredictable microhardness profiles, indicating uneven surface topology, the higher first-step force of 150 N effectively prepares the surface for a more uniform and effective second burnishing step. In contrast, the conventional SDB method, especially after polishing, shows a straightforward and consistent increase in microhardness, highlighting the impact of initial surface smoothness on the effectiveness of the burnishing process in terms of microhardness.

- Surface topography, morphology, and cross-sectional microstructure

11. The 3D surface topography images clearly demonstrate the significance of the initial surface conditions prior to the final SDB step. In comparisons of outcomes from single-step burnishing, the surface that was polished before burnishing displayed the most uniform and consistent topography and the lowest surface roughness. This uniformity is due to the smooth and even surface achieved through polishing, which exhibits minimal height variation compared to those surfaces that were turned or ground.
12. The findings indicate that the surface characteristics from the two-step SDB approach, using 150 N in the first step and 200 N in the second one, are comparable to those achieved after polishing followed by a 200 N finishing burnishing force. Furthermore, the surface roughness resulting from the two-step SDB approach was even lower.
13. The morphology of the surface that was ground-then-burnished revealed the existence of striations, pits, microcracks, and feed marks. In contrast, the surfaces subjected to the two-step SDB process, particularly when subjected to high forces of 100 N and 150 N in the first step, showed more uniform smoothing and fewer imperfections, indicating a superior preparation in the first step that allowed for better final outcomes.
14. The traditional grinding followed by SDB showed less plastic deformation and compaction compared to the two-step SDB process, despite using the same finishing burnishing force of 200 N. The two-step process resulted in grains that were more uniformly deformed and compacted, showing pronounced elongation and orientation in the direction of the burnishing tool's movement.
15. In the two-step SDB process, a higher first-step burnishing force resulted in a more compacted surface grain structure and a more refined surface texture, making the second burnishing pass even more effective. Additionally, the depth of the burnished layer varied inversely with the first burnishing force used; higher initial forces led to shallower, yet more compacted

deformation zones due to greater work hardening, lateral material flow, and intensified grain refinement at the surface.

16. The previous conclusions imply the fact that the two-step SDB technique is more effective than the conventional approach of implementing burnishing after grinding or polishing in enhancing the surface integrity of the hard-turned 42CrMo4 steel, and could be employed as an alternative burnishing technique that saves time, money, and produces high quality surfaces.

- Overall conclusion

17. The two-step slide diamond burnishing process achieves superior surface quality compared to conventional methods, despite the higher initial surface roughness (prior to slide diamond burnishing). This is due to the optimized use of burnishing energy: less energy is consumed by friction in the second step, allowing more energy to further decrease surface roughness, induce more compressive residual stresses, and increase surface microhardness. This effect is particularly pronounced with higher forces, such as 150 N followed by 200 N, enhancing surface properties more effectively than the conventional process.
18. In two-step slide diamond burnishing and burnishing after grinding, plastic deformation of grains (slip) in the tangential direction extends beyond the visible plastic deformation zone until the tangential and axial stress components nearly equalize. Near the surface, high shear strain rates cause significant slip, leading to visible plastic deformation and reduced elastic lattice distortion. As depth increases, slip decreases, and elastic distortion increases, resulting in higher tangential stresses. At the end of the plastic deformation zone, slip ceases, and elastic lattice distortion equalizes for both tangential and axial directions.

7. CLAIMS

The following claims are valid for hard-turned 42CrMo4 steel with a hardness of 54 HRC and slide diamond burnishing using the optimum parameters of the examined values: a feed of 0.03 mm/rev and a speed of 115 m/min.

- Claim No. 1:

The proposed two-step slide diamond burnishing process performed with 150 N and then 200 N achieves the same level of compressive axial stress component on the surface, larger compressive axial and tangential stress components in depth, lower R_a surface roughness, higher HV 0.2 microhardness, and a flawless surface compared to single-step slide diamond burnishing with 200 N after grinding or polishing. The reason is that, in the second step of burnishing, less energy is consumed by friction compared to single-step slide diamond burnishing.

- Claim No. 2:

For the proposed two-step slide diamond burnishing process, increasing the second-step burnishing force in the 25–200 N range increases surface residual stresses and decreases the kurtosis parameter (R_{ku}) in the axial direction; however, it decreases surface residual stresses and increases R_{ku} in the tangential direction. The cause is attributed to the relative velocity between the workpiece surface and burnishing head, which is 1916 mm/s in the tangential direction and 0.03 mm per revolution in the axial direction. Under these very different velocities, the shear strain rates are completely different, and the material deforms differently. The high tangential velocity combined with an increase in burnishing force leads to increasing sharpness with more, narrow peaks, which deflect easily and retain minimal residual stresses. On the other hand, the low axial velocity combined with an increase in burnishing force leads to decreasing sharpness with less, wider peaks, which resist deflection and retain large residual stresses.

- Claim No. 3:

In the proposed two-step slide diamond burnishing process, axial surface residual stresses can be further improved in the second step compared to the first one when burnishing in the second step is done with at least ~87 N, ~146 N, and ~137 N when the first step is done with 50 N, 100 N, and 150 N, respectively.

- Claim No. 4:

The proposed two-step slide diamond burnishing process performed with 150 N and then 200 N results in larger compressive axial stress components from the depth of 0 to ~200 μm , larger in-depth compressive tangential stress components from ~10 μm to ~220 μm , lower R_a surface roughness, and higher HV 0.2 microhardness compared to one-step slide diamond burnishing

performed with 200 N. Moreover, two-step slide diamond burnishing performed with 50 N or 100 N and then 200 N achieves larger compressive axial stress components from the depth of 0 to ~30 μm compared to one-step slide diamond burnishing performed with 200 N. The reason is that, in the second step of burnishing, less energy is consumed by friction compared to single-step slide diamond burnishing.

- Claim No. 5:

In two-step slide diamond burnishing and burnishing after grinding, in the tangential direction, plastic deformation of grains (slip) does not only happen in the visible plastic deformation zone but until the tangential and axial stress components become almost equal. High shear strain rates near the surface in the tangential direction cause significant slip, leading to visible plastic deformation and reduced elastic lattice distortion. As depth increases, slip decreases, and the elastic distortion of the lattice increases, causing an increase in tangential stresses. Upon reaching the end of the plastic deformation zone, slip finishes and the elastic lattice distortion equalizes for the tangential direction and axial direction, in which no slip occurs due to low shear strain rates.

8. UTILIZATION OF THE CLAIMS

The findings from the study on the effects of two-step slide diamond burnishing (SDB) on 42CrMo4 hard-turned steel and its superiority over the outcomes of the conventional approach of implementing burnishing after grinding or polishing present a promising mean for significantly improving the mechanical properties of industrial components and reveal profound implications for the industry, particularly in sectors where the mechanical efficiency and durability of components are essential. These merits of the proposed approach make it an adequate option for adoption in the real industry.

Besides its superior outcomes in improving fatigue life, wear, and corrosion resistance over the traditional process, the feasibility of implementing two-step SDB in real industrial settings and its potential adoption and utilization across various sectors stem from the fact that this innovative technique can save space, time, money, and energy. By using the two-step SDB approach, it is possible to eliminate the need for subsequent finishing processes such as grinding and polishing after turning. This eliminates the requirement for separate grinding or polishing machines, allowing for the use of the same lathe directly after hard turning to conduct the burnishing.

Furthermore, performing burnishing directly on the lathe after hard turning proves more cost-effective than after grinding, due to the lower operational costs of using a lathe compared to the grinding machine, as noted by Kumar and Chauhan [115]. According to Tobola et al. [116], grinding costs account for an average of 40-70% of the total costs of precision products and may exceed many times the costs of machining, like turning.

In conclusion, the long-term benefits, such as extended component life and reduced failure rates, the process efficiency gained by potentially eliminating multiple post-processing steps, simplicity, energy savings, and cost and time effectiveness further underscore the need for the adoption of this method in the real industry. Moreover, this innovative method of using varied burnishing forces in the initial and subsequent steps opens the way for new scientific inquiries. These could include exploring the effects of altering the material and its hardness, parameters' ranges, initial roughness after turning, and the kurtosis parameter and its relationship with residual stresses.

9. PUBLICATIONS AND PRESENTATIONS

1. **Local Conference Presentation:** “Characterization of Residual Stresses Induced into Bearing Rings by Means of Turning in Soft State Using Different Turning Parameters”, *New Results in Materials Science*. Miskolc, 2021.
2. **J. Zaghal**, V. Mertinger, A. Filep, G. Varga, and M. Benke, “Characterization of residual stresses induced into bearing rings by means of soft turning using different turning parameters,” *J. Mach. Eng.*, vol. 21, no. 4, pp. 49–56, 2021, **Q2, Independent Citations: 1**, [10.36897/jme/144299](https://doi.org/10.36897/jme/144299)
3. **J. Zaghal**, V. Mertinger, Á. Filep, and M. Benke, “Characterization of residual stress state after turning of bearing rings”. *Doktorandusz Almanach*, vol. 1, pp. 313-318, 2022, **Independent Citations: 1**, http://epa.niif.hu/04600/04692/00001/pdf/EPA04692_doktorandusz_almanach_2022_313-318.pdf
4. **J. Zaghal**, V. Molnár, and M. Benke, “Improving surface integrity by optimizing slide diamond burnishing parameters after hard turning of 42CrMo4 steel,” *Int. J. Adv. Manuf. Technol.*, pp. 1–17, 2023, **Q1, Independent Citations: 3**, [10.1007/s00170-023-12008-6](https://doi.org/10.1007/s00170-023-12008-6)
5. **J. Zaghal** and M. Benke, “Determination of reliable area sizes for 3D roughness measurement,” *Cut. & Tools Technol. Syst.*, no. 98, pp. 3–12, 2023, **Independent Citations: 1**, <https://doi.org/10.20998/2078-7405.2023.98.01>

REFERENCES

- [1] U. Shirsat, B. Ahuja, and M. Dhuttargaon, “Effect of burnishing parameters on surface finish,” *J. Inst. Eng. Ser. C*, vol. 98, no. 4, pp. 431–436, 2017.
- [2] A. Saldaña-Robles, H. Plascencia-Mora, E. Aguilera-Gómez, A. Saldaña-Robles, A. Marquez-Herrera, and J. A. la Peña, “Influence of ball-burnishing on roughness, hardness and corrosion resistance of AISI 1045 steel,” *Surf. Coatings Technol.*, vol. 339, pp. 191–198, 2018.
- [3] R. Jerez-Mesa, Y. Landon, J. A. Travieso-Rodriguez, G. Dessenin, J. Lluma-Fuentes, and V. Wagner, “Topological surface integrity modification of AISI 1038 alloy after vibration-assisted ball burnishing,” *Surf. Coatings Technol.*, vol. 349, pp. 364–377, 2018.
- [4] M. Korzynski, “A model of smoothing slide ball-burnishing and an analysis of the parameter interaction,” *J. Mater. Process. Technol.*, vol. 209, no. 1, pp. 625–633, 2009.
- [5] C. Felhő and G. Varga, “2D FEM Investigation of Residual Stress in Diamond Burnishing,” *J. Manuf. Mater. Process.*, vol. 6, no. 5, p. 123, 2022.
- [6] V. Chomienne, F. Valiorgue, J. Rech, and C. Verdu, “Influence of ball burnishing on residual stress profile of a 15-5PH stainless steel,” *CIRP J. Manuf. Sci. Technol.*, vol. 13, pp. 90–96, 2016.
- [7] A. Rami, A. Kallel, S. Djemaa, T. Mabrouki, S. Sghaier, and H. Hamdi, “Numerical assessment of residual stresses induced by combining turning-burnishing (CoTuB) process of AISI 4140 steel using 3D simulation based on a mixed approach,” *Int. J. Adv. Manuf. Technol.*, vol. 97, no. 5, pp. 1897–1912, 2018.
- [8] F. C. Magalhães, C. E. H. Ventura, A. M. Abrão, B. Denkena, B. Breidenstein, and K. Meyer, “Prediction of surface residual stress and hardness induced by ball burnishing through neural networks,” *Int. J. Manuf. Res.*, vol. 14, no. 3, pp. 295–310, 2019.
- [9] M. Uddin, R. Santifoller, C. Hall, and T. Schlaefel, “Effect of Combined Grinding--Burnishing Process on Surface Integrity, Tribological, and Corrosion Performance of Laser-Clad Stellite 21 Alloys,” *Adv. Eng. Mater.*, vol. 25, no. 8, p. 2201332, 2023.
- [10] A. Skoczylas and M. Kłonica, “Selected Properties of the Surface Layer of C45 Steel Samples after Slide Burnishing,” *Materials (Basel)*, vol. 16, no. 19, p. 6513, 2023.
- [11] W. B. Săi and J. L. Lebrun, “Influence of finishing by burnishing on surface characteristics,” *J. Mater. Eng. Perform.*, vol. 12, pp. 37–40, 2003.

- [12] F.-J. Shiou and C.-C. Hsu, "Surface finishing of hardened and tempered stainless tool steel using sequential ball grinding, ball burnishing and ball polishing processes on a machining centre," *J. Mater. Process. Technol.*, vol. 205, no. 1–3, pp. 249–258, 2008.
- [13] S. Agarwal and P. V. Rao, "Experimental investigation of surface/subsurface damage formation and material removal mechanisms in SiC grinding," *Int. J. Mach. Tools Manuf.*, vol. 48, no. 6, pp. 698–710, 2008.
- [14] J. Zhang, W. Yu, E. Dong, Z. Zhang, J. Shi, and G. Gong, "Study on grinding and deformation fracture control of cold rolled titanium strip," *Metals (Basel)*, vol. 10, no. 3, p. 323, 2020.
- [15] D. Wenfeng, X. Jiuhua, C. Zhenzhen, S. Honghua, and F. Yucan, "Grindability and surface integrity of cast nickel-based superalloy in creep feed grinding with brazed CBN abrasive wheels," *Chinese J. Aeronaut.*, vol. 23, no. 4, pp. 501–510, 2010.
- [16] Y. Lyu, H. Yu, J. Wang, C. Chen, and L. Xiang, "Study on the grinding temperature of the grinding wheel with an abrasive phyllotactic pattern," *Int. J. Adv. Manuf. Technol.*, vol. 91, pp. 895–906, 2017.
- [17] Z. Wang, T. Yu, X. Wang, T. Zhang, J. Zhao, and P. H. Wen, "Grinding temperature field prediction by meshless finite block method with double infinite element," *Int. J. Mech. Sci.*, vol. 153, pp. 131–142, 2019.
- [18] H. Ling, C. Yang, S. Feng, and H. Lu, "Predictive model of grinding residual stress for linear guideway considering straightening history," *Int. J. Mech. Sci.*, vol. 176, p. 105536, 2020.
- [19] O. Fergani, Y. Shao, I. Lazoglu, and S. Y. Liang, "Temperature effects on grinding residual stress," *Procedia CIRP*, vol. 14, pp. 2–6, 2014.
- [20] A. Turnbull *et al.*, "Sensitivity of stress corrosion cracking of stainless steel to surface machining and grinding procedure," *Corros. Sci.*, vol. 53, no. 10, pp. 3398–3415, 2011.
- [21] S. Han, F. Valiorgue, M. Cici, H. Pascal, and J. Rech, "3D residual stress modelling in turning of AISI 4140 steel," *Prod. Eng.*, pp. 1–13, 2023.
- [22] M. Ulutan, O. N. Celik, H. Gasan, and U. Er, "Effect of different surface treatment methods on the friction and wear behavior of AISI 4140 steel," *J. Mater. Sci. Technol. Technol.*, vol. 26, no. 3, pp. 251–257, 2010, doi: 10.1016/S1005-0302(10)60042-4.
- [23] P. A. Ruiz-Trabolsi *et al.*, "A comparative analysis of the tribological behavior of hard layers obtained by three different hardened-surface processes on the surface of AISI 4140 steel,"

- Crystals*, vol. 12, no. 2, p. 298, 2022.
- [24] A. H. Meysami, R. Ghasemzadeh, S. H. Seyedein, and M. R. Aboutalebi, “An investigation on the microstructure and mechanical properties of direct-quenched and tempered AISI 4140 steel,” *Mater. & Des.*, vol. 31, no. 3, pp. 1570–1575, 2010.
- [25] R. Kluz, T. Trzepieciniski, M. Bucior, and K. Antosz, “Modelling of the Effect of Slide Burnishing on the Surface Roughness of 42CrMo4 Steel Shafts,” *Lect. Notes Mech. Eng.*, vol. 14, no. 5, pp. 415–424, 2021, doi: 10.1007/978-3-030-77719-7_41.
- [26] M. Korzynski, A. Pacana, and J. Cwanek, “Fatigue strength of chromium coated elements and possibility of its improvement with slide diamond burnishing,” *Surf. Coatings Technol.*, vol. 203, no. 12, pp. 1670–1676, 2009.
- [27] A. V Hankare, A. A. Sapkal, and A. A. Dounde, “Effect of diamond burnishing process on surface roughness of AISI 4140 alloy steel,” *J Adv Sci Technol*, vol. 13, no. 1, pp. 405–410, 2017.
- [28] M. Korzynski, J. Lubas, S. Swirad, and K. Dudek, “Surface layer characteristics due to slide diamond burnishing with a cylindrical-ended tool,” *J. Mater. Process. Technol.*, vol. 211, no. 1, pp. 84–94, 2011.
- [29] M. Korzynski, “Modeling and experimental validation of the force--surface roughness relation for smoothing burnishing with a spherical tool,” *Int. J. Mach. Tools Manuf.*, vol. 47, no. 12–13, pp. 1956–1964, 2007.
- [30] S. Świrad, “The surface texture analysis after sliding burnishing with cylindrical elements,” *Wear*, vol. 271, no. 3–4, pp. 576–581, 2011.
- [31] Q. Xu, Y. Liu, H. Lu, J. Liu, and G. Cai, “Surface integrity and corrosion resistance of 42CrMo4 high-strength steel strengthened by hard turning,” *Materials (Basel)*, vol. 14, no. 22, p. 6995, 2021.
- [32] Q. Xu, J. Zhao, and X. Ai, “Cutting performance of tools made of different materials in the machining of 42CrMo4 high-strength steel: a comparative study,” *Int. J. Adv. Manuf. Technol.*, vol. 93, no. 5, pp. 2061–2069, 2017.
- [33] J. T. Maximov, G. V Duncheva, A. P. Anchev, and M. D. Ichkova, “Slide burnishing—review and prospects,” *Int. J. Adv. Manuf. Technol.*, vol. 104, no. 1, pp. 785–801, 2019.
- [34] H. Chandler, *Heat treater’s guide: practices and procedures for irons and steels*. ASM international, 1994.

- [35] B. Sachin, S. Narendranath, and D. Chakradhar, "Enhancement of surface integrity by cryogenic diamond burnishing toward the improved functional performance of the components," *J. Brazilian Soc. Mech. Sci. Eng.*, vol. 41, pp. 1–13, 2019.
- [36] G. Liu, C. Huang, B. Zhao, W. Wang, and S. Sun, "Effect of machined surface integrity on fatigue performance of metal workpiece: A review," *Chinese J. Mech. Eng.*, vol. 34, no. 1, pp. 1–16, 2021.
- [37] M. D. Sangid, "The physics of fatigue crack initiation," *Int. J. Fatigue*, vol. 57, pp. 58–72, 2013.
- [38] J. Günther *et al.*, "On the effect of internal channels and surface roughness on the high-cycle fatigue performance of Ti-6Al-4V processed by SLM," *Mater. & Des.*, vol. 143, pp. 1–11, 2018.
- [39] J. Pegues, M. Roach, R. S. Williamson, and N. Shamsaei, "Surface roughness effects on the fatigue strength of additively manufactured Ti-6Al-4V," *Int. J. Fatigue*, vol. 116, pp. 543–552, 2018.
- [40] P. I. Christodoulou and A. T. Kermanidis, "A Combined Numerical--Analytical Study for Notched Fatigue Crack Initiation Assessment in TRIP Steel: A Local Strain and a Fracture Mechanics Approach," *Metals (Basel)*, vol. 13, no. 10, p. 1652, 2023.
- [41] D. Novovic, D. K. Aspinwall, R. C. Dewes, P. Bowen, and B. Griffiths, "The effect of surface and subsurface condition on the fatigue life of Ti--25V--15Cr--2Al--0.2 C% wt alloy," *CIRP Ann.*, vol. 65, no. 1, pp. 523–528, 2016.
- [42] J. Holmberg, J. Berglund, A. Wretland, and T. Beno, "Evaluation of surface integrity after high energy machining with EDM, laser beam machining and abrasive water jet machining of alloy 718," *Int. J. Adv. Manuf. Technol.*, vol. 100, pp. 1575–1591, 2019.
- [43] S. Świrad, D. Wydrzynski, P. Nieslony, and G. M. Królczyk, "Influence of hydrostatic burnishing strategy on the surface topography of martensitic steel," *Measurement*, vol. 138, pp. 590–601, 2019.
- [44] E. Maleki, G. H. Farrahi, K. Reza Kashyzadeh, O. Unal, M. Gugaliano, and S. Bagherifard, "Effects of conventional and severe shot peening on residual stress and fatigue strength of steel AISI 1060 and residual stress relaxation due to fatigue loading: experimental and numerical simulation," *Met. Mater. Int.*, vol. 27, no. 8, pp. 2575–2591, 2021.
- [45] A. Şahinoğlu and M. Rafeighi, "Investigation of vibration, sound intensity, machine current

- and surface roughness values of AISI 4140 during machining on the lathe,” *Arab. J. Sci. Eng.*, vol. 45, pp. 765–778, 2020.
- [46] M. Szutkowska, D. Toboła, L. Jaworska, and M. Rozmus, “New diamond composite tools and their impact on AISI 4140 alloy steel surface after slide burnishing,” *Mechanik*, vol. 92, no. 10, pp. 610–615, 2019.
- [47] B. Li, S. Zhang, R. Hu, and X. Zhang, “Dislocation density and grain size evolution in hard machining of H13 steel: Numerical and experimental investigation,” *J. Mater. Res. Technol.*, vol. 9, no. 3, pp. 4241–4254, 2020.
- [48] A. T. Abbas, S. Anwar, H. Hegab, F. Benyahia, H. Ali, and A. Elkaseer, “Comparative evaluation of surface quality, tool wear, and specific cutting energy for wiper and conventional carbide inserts in hard turning of AISI 4340 alloy steel,” *Materials (Basel)*, vol. 13, no. 22, p. 5233, 2020.
- [49] F. Kara, M. Karabatak, M. Ayyildiz, and E. Nas, “Effect of machinability, microstructure and hardness of deep cryogenic treatment in hard turning of AISI D2 steel with ceramic cutting,” *J. Mater. Res. Technol.*, vol. 9, no. 1, pp. 969–983, 2020.
- [50] N. Li, Y.-J. Chen, and D.-D. Kong, “Wear mechanism analysis and its effects on the cutting performance of PCBN inserts during turning of hardened 42CrMo,” *Int. J. Precis. Eng. Manuf.*, vol. 19, pp. 1355–1368, 2018.
- [51] V. Molnar, “Experimental Investigation of Tribology-Related Topography Parameters of Hard-Turned and Ground 16MnCr5 Surfaces,” *Lubricants*, vol. 11, no. 6, p. 263, 2023.
- [52] S. Saha, P. B. Zaman, M. I. H. Tusar, and N. R. Dhar, “Multi-objective genetic algorithm (MOGA) based optimization of high-pressure coolant assisted hard turning of 42CrMo4 steel,” *Int. J. Interact. Des. Manuf.*, vol. 16, no. 3, pp. 1253–1272, 2022.
- [53] E. D. Derakhshan and A. A. Akbari, “Experimental investigation on the effect of workpiece hardness and cutting speed on surface roughness in hard turning with CBN tools,” in *Proceedings of the world congress on engineering*, 2009, vol. 2, pp. 1–3.
- [54] Y.-W. Park, “Tool material dependence of hard turning on the surface quality,” *Int. J. Precis. Eng. Manuf.*, vol. 3, no. 1, pp. 76–82, 2002.
- [55] G. Duncheva, J. Maximov, A. Anchev, V. Dunchev, Y. Argirov, and S. Velkov, “Modeling and Optimization of Surface Integrity and Sliding Wear Resistance of Diamond-Burnished Holes in Austenitic Stainless Steel Cylinder Lines,” *Machines*, vol. 11, no. 9, p. 872, 2023.

- [56] J. J. Martell, C. R. Liu, and J. Shi, “Experimental investigation on variation of machined residual stresses by turning and grinding of hardened AISI 1053 steel,” *Int. J. Adv. Manuf. Technol.*, vol. 74, pp. 1381–1392, 2014.
- [57] V. Jafarpour and R. Moharrami, “Numerical Stress Analysis of Creep-Feed Grinding Through Finite Element Method in Inconel Alloy X-750,” *Mapta J. Mech. Ind. Eng.*, vol. 6, no. 01, pp. 1–9, 2022.
- [58] J. E. Hoffmann *et al.*, “Surface states by grinding thin strips of electrochemically deposited nanocrystalline nickel-iron,” *Mater. Test.*, vol. 64, no. 7, pp. 903–931, 2022.
- [59] A. Sorsa, M. Ruusunen, S. Santa-Aho, and M. Vippola, “Sub-Surface analysis of grinding burns with Barkhausen noise measurements,” *Materials (Basel)*, vol. 16, no. 1, p. 159, 2022.
- [60] S. K. Shihab, E. M. Mubarak, and R. H. Al-Kalali, “Influence and Optimization of Surface Roughness on Surface Integrity during Turning Using Grey Relational Analysis [J],” *J. Harbin Inst. Technol. (New Ser.)*, vol. 28, no. 2, pp. 38–46, 2021.
- [61] P. M. Duc, M. D. Dai, and L. H. Giang, “Modeling and optimizing the effects of insert angles on hard turning performance,” *Math. Probl. Eng.*, vol. 2021, pp. 1–18, 2021.
- [62] J. Zaghal, V. Molnár, and M. Benke, “Improving surface integrity by optimizing slide diamond burnishing parameters after hard turning of 42CrMo4 steel,” *Int. J. Adv. Manuf. Technol.*, pp. 1–17, 2023.
- [63] C. Felhő and G. Varga, “CAD and FEM modelling of theoretical roughness in diamond burnishing,” *Int. J. Precis. Eng. Manuf.*, vol. 23, no. 4, pp. 375–384, 2022.
- [64] J. T. Maximov, A. P. Anchev, G. V. Duncheva, N. Ganev, and K. F. Selimov, “Influence of the process parameters on the surface roughness, micro-hardness, and residual stresses in slide burnishing of high-strength aluminum alloys,” *J. Brazilian Soc. Mech. Sci. Eng.*, vol. 39, no. 8, pp. 3067–3078, 2017.
- [65] D. Wang, “Research on surface integrity and its influencing factors in the high-speed cutting of typical aluminum/titanium/nickel alloys: a review,” *Int. J. Adv. Manuf. Technol.*, pp. 1–28, 2023.
- [66] R. Çakıroğlu and M. Günay, “Effects of process parameters on fatigue behavior and surface integrity of tool steel produced by electrical discharge turning,” *Materwiss. Werksttech.*, vol. 54, no. 1, pp. 36–44, 2023.
- [67] A. Skoczylas, K. Zaleski, J. Matuszak, K. Ciecieląg, R. Zaleski, and M. Gorgol, “Influence

- of slide burnishing parameters on the surface layer properties of stainless steel and mean positron lifetime,” *Materials (Basel)*, vol. 15, no. 22, p. 8131, 2022.
- [68] V. P. Kuznetsova and A. V. Kosareva, “Increase of Wear and Heat Resistance of the AISI 304 Steel Surface Layer by Multi-Pass Nanostructuring Burnishing,” *J. Mater.*, vol. 1, no. 2, pp. 55–61, 2023.
- [69] L. Luca, S. Neagu-Ventzel, and I. Marinescu, “Effects of working parameters on surface finish in ball-burnishing of hardened steels,” *Precis. Eng.*, vol. 29, no. 2, pp. 253–256, 2005.
- [70] D. Borysenko, F. Welzel, B. Karpuschewski, J. Kundrák, and V. Voropai, “Simulation of the burnishing process on real surface structures,” *Precis. Eng.*, vol. 68, pp. 166–173, 2021.
- [71] F. Tesfom, I. Pásztor, and C. Felhő, “Flat diamond sliding burnishing surface roughness investigation,” *Multidiszcip. tudományok A Miskolci Egy. Közleménye*, vol. 12, no. 3, pp. 186–195, 2022.
- [72] H. Yamazaki, J. Zhu, and T. Tanaka, “Study on the Surface Enhancement of Thin-Walled Metallic Materials Using a Novel Double-Side Burnishing Tool,” *Int. J. Autom. Technol.*, vol. 17, no. 5, pp. 458–468, 2023.
- [73] H. Luo, J. Liu, L. Wang, and Q. Zhong, “Study of the mechanism of the burnishing process with cylindrical polycrystalline diamond tools,” *J. Mater. Process. Technol.*, vol. 180, no. 1–3, pp. 9–16, 2006.
- [74] J. Hua *et al.*, “Effect of feed rate, workpiece hardness and cutting edge on subsurface residual stress in the hard turning of bearing steel using chamfer + hone cutting edge geometry,” *Mater. Sci. Eng. A*, vol. 394, no. 1–2, pp. 238–248, 2005, doi: 10.1016/j.msea.2004.11.011.
- [75] J. T. Maximov, G. V. Duncheva, A. P. Anchev, N. Ganev, and V. P. Dunchev, “Effect of cyclic hardening on fatigue performance of slide burnished components made of low-alloy medium carbon steel,” *Fatigue & Fract. Eng. Mater. & Struct.*, vol. 42, no. 6, pp. 1414–1425, 2019.
- [76] G. V. Duncheva, J. T. Maximov, A. P. Anchev, V. P. Dunchev, and Y. B. Argirov, “Multi-objective optimization of the internal diamond burnishing process,” *Mater. Manuf. Process.*, vol. 37, no. 4, pp. 428–436, 2022.
- [77] A. D. Krawitz, *Introduction to diffraction in materials science and engineering*. 2001.
- [78] J. T. Maximov, A. P. Anchev, V. P. Dunchev, N. Ganev, G. V. Duncheva, and K. F. Selimov, “Effect of slide burnishing basic parameters on fatigue performance of 2024-T3 high-

- strength aluminium alloy,” *Fatigue & Fract. Eng. Mater. & Struct.*, vol. 40, no. 11, pp. 1893–1904, 2017.
- [79] J. T. Maximov, A. P. Anchev, G. V. Duncheva, N. Ganev, K. F. Selimov, and V. P. Dunchev, “Impact of slide diamond burnishing additional parameters on fatigue behaviour of 2024-T3 Al alloy,” *Fatigue Fract. Eng. Mater. Struct.*, vol. 42, no. 1, pp. 363–373, 2019.
- [80] J. T. Maximov, G. V. Duncheva, A. P. Anchev, V. P. Dunchev, and M. D. Ichkova, “Improvement in fatigue strength of 41Cr4 steel through slide diamond burnishing,” *J. Brazilian Soc. Mech. Sci. Eng.*, vol. 42, no. 4, pp. 1–20, 2020.
- [81] G. Varga and V. Ferencsik, “Investigation of the influence of different burnishing parameters on shape correctness and residual stresses,” in *IOP Conference Series: Materials Science and Engineering*, 2018, vol. 448, no. 1, p. 12016.
- [82] M. Okada *et al.*, “Development and characterization of diamond tip burnishing with a rotary tool,” *J. Mater. Process. Technol.*, vol. 244, pp. 106–115, 2017.
- [83] K. Konefal, M. Korzynski, Z. Byczkowska, and K. Korzynska, “Improved corrosion resistance of stainless steel X6CrNiMoTi17-12-2 by slide diamond burnishing,” *J. Mater. Process. Technol.*, vol. 213, no. 11, pp. 1997–2004, 2013.
- [84] S. C. Cagan, C. I. Pruncu, and B. B. Buldum, “An investigation into ball burnishing process of magnesium alloy on CNC lathe using different environments,” *J. Magnes. Alloy.*, vol. 8, no. 4, pp. 1061–1070, 2020.
- [85] N. Duboust *et al.*, “An optical method for measuring surface roughness of machined carbon fibre-reinforced plastic composites,” *J. Compos. Mater.*, vol. 51, no. 3, pp. 289–302, 2017.
- [86] R. Horváth, Á. Drégelyi-Kiss, and G. Mátyási, “The examination of surface roughness parameters in the fine turning of hypereutectic aluminium alloys,” *Sci. Bull. Politeh. Bucharest Ser. D*, vol. 77, no. 2, pp. 205–216, 2015.
- [87] L. R. da Silva, D. A. Couto, F. V. dos Santo, F. J. Duarte, R. S. Mazzaro, and G. V. Veloso, “Evaluation of machined surface of the hardened AISI 4340 steel through roughness and residual stress parameters in turning and grinding,” *Int. J. Adv. Manuf. Technol.*, vol. 107, pp. 791–803, 2020.
- [88] E. C. T. Ba, M. R. Dumont, P. S. Martins, R. M. Drumond, M. P. da Cruz, and V. F. Vieira, “Investigation of the effects of skewness R_{sk} and kurtosis R_{ku} on tribological behavior in a pin-on-disc test of surfaces machined by conventional milling and turning processes,” *Mater.*

- Res.*, vol. 24, p. e20200435, 2021.
- [89] E. S. Gadelmawla, M. M. Koura, T. M. A. Maksoud, I. M. Elewa, and H. H. Soliman, “Roughness parameters,” *J. Mater. Process. Technol.*, vol. 123, no. 1, pp. 133–145, 2002.
- [90] K. Líska, J. Kodácsy, and J. Líska, “Investigation of the microgeometry after hard turning and diamond burnishing,” in *Advanced Materials Research*, 2012, vol. 472, pp. 902–907.
- [91] W. Bouzid, O. Tsoumarev, and K. Sai, “An investigation of surface roughness of burnished AISI 1042 steel,” *Int. J. Adv. Manuf. Technol.*, vol. 24, pp. 120–125, 2004.
- [92] D. TOBOŁA, W. Brostow, K. Czechowski, P. Rusek, and I. Wronska, “Structure and properties of burnished and nitrided AISI D2 tool steel,” *Mater. Sci.*, vol. 21, no. 4, pp. 511–516, 2015.
- [93] W. Brostow, K. Czechowski, W. Polowski, P. Rusek, D. Toboła, and I. Wronska, “Slide diamond burnishing of tool steels with adhesive coatings and diffusion layers,” *Mater. Res. Innov.*, vol. 17, no. 4, pp. 269–277, 2013.
- [94] J. Huuki and S. V. A. Laakso, “Surface improvement of shafts by the diamond burnishing and ultrasonic burnishing techniques,” *Int. J. Mach. Mach. Mater.*, vol. 19, no. 3, pp. 246–259, 2017.
- [95] G. D. Revankar, R. Shetty, S. S. Rao, and V. N. Gaitonde, “Wear resistance enhancement of titanium alloy (Ti–6Al–4V) by ball burnishing process,” *J. Mater. Res. Technol.*, vol. 6, no. 1, pp. 13–32, 2017.
- [96] G. V. Duncheva, J. T. Maximov, A. P. Anchev, V. P. Dunchev, and Y. B. Argirov, “Improvement in wear resistance performance of CuAl₁₈Fe₃ single-phase aluminum bronze via slide diamond burnishing,” *J. Mater. Eng. Perform.*, vol. 31, no. 3, pp. 2466–2478, 2022.
- [97] O. Taamallah, H. Hamadache, N. Mokas, A. Amirat, and B. Hamadi, “Investigation of the Effects of Slide Diamond Burnishing Process on the Mechanical Performance of GCr15 Steel,” *J. Fail. Anal. Prev.*, pp. 1–13, 2023.
- [98] D. Toboła, W. Brostow, K. Czechowski, and P. Rusek, “Improvement of wear resistance of some cold working tool steels,” *Wear*, vol. 382, pp. 29–39, 2017.
- [99] J. Łabanowski and A. Ossowska, “Influence of burnishing on stress corrosion cracking susceptibility of duplex steel,” *work*, vol. 5, no. 6, p. 7, 2006.
- [100] V. K. Gorana, V. K. Jain, and G. K. Lal, “Forces prediction during material deformation in

- abrasive flow machining,” *Wear*, vol. 260, no. 1–2, pp. 128–139, 2006.
- [101] R. G. Budynas, J. K. Nisbett, and others, *Shigley’s mechanical engineering design*, vol. 9. McGraw-Hill New York, 2011.
- [102] A. Nestler and A. Schubert, “Effect of machining parameters on surface properties in slide diamond burnishing of aluminium matrix composites,” *Mater. Today Proc.*, vol. 2, pp. S156–S161, 2015.
- [103] B. Sachin, C. M. Rao, G. M. Naik, and N. P. Puneet, “Influence of slide burnishing process on the surface characteristics of precipitation hardenable steel,” *SN Appl. Sci.*, vol. 3, pp. 1–13, 2021.
- [104] G. E. Totten, *Handbook of residual stress and deformation of steel*. ASM international, 2002.
- [105] S. Dzionk, W. Przybylski, and B. Ścibiorski, “The possibilities of improving the fatigue durability of the ship propeller shaft by burnishing process,” *Machines*, vol. 8, no. 4, p. 63, 2020.
- [106] A. A. Ibrahim, “An investigation into ball burnishing process of carbon steel on a lathe,” in *Proceedings of Al-Azhar Engineering Tenth International Conference, Cairo, Egypt*, 2008, vol. 2426.
- [107] T. C. Dyl, A. Charchalis, G. Stradomski, and D. Rydz, “Impact of processing parameters on surface roughness and strain hardening of two-phase stainless steel,” *J. KONES*, vol. 26, 2019.
- [108] S. Dzionk, B. Scibiorski, and W. Przybylski, “Surface texture analysis of hardened shafts after ceramic ball burnishing,” *Materials (Basel)*, vol. 12, no. 2, p. 204, 2019.
- [109] D. Carou, E. M. Rubio, C. H. Lauro, and J. P. Davim, “Experimental investigation on surface finish during intermittent turning of UNS M11917 magnesium alloy under dry and near dry machining conditions,” *Measurement*, vol. 56, pp. 136–154, 2014.
- [110] L. Hiegemann, C. Weddeling, and A. E. Tekkaya, “Analytical contact pressure model for predicting roughness of ball burnished surfaces,” *J. Mater. Process. Technol.*, vol. 232, pp. 63–77, 2016.
- [111] J. Maximov, G. Duncheva, A. Anchev, V. Dunchev, Y. Argirov, and M. Nikolova, “Effects of Heat Treatment and Diamond Burnishing on Fatigue Behaviour and Corrosion Resistance of AISI 304 Austenitic Stainless Steel,” *Appl. Sci.*, vol. 13, no. 4, p. 2570, 2023.

- [112] D. A. de Oliveira, P. P. Brito, F. de Castro Magalhães, P. C. Azzi, J. D. Ardisson, and A. M. Abrao, “Influence of low plasticity burnishing on the formation of strain induced martensite in the surface layer,” *J. Mater. Res. Technol.*, vol. 27, pp. 4573–4594, 2023.
- [113] W. Grzesik and K. Żak, “Producing high quality hardened parts using sequential hard turning and ball burnishing operations,” *Precis. Eng.*, vol. 37, no. 4, pp. 849–855, 2013.
- [114] B. Ścibiorski and S. Dzionk, “The roughness of the hardened steel surface created by the rolling-burnishing process,” *Solid State Phenom.*, vol. 220, pp. 881–886, 2015.
- [115] P. Kumar, S. R. Chauhan, and A. Aggarwal, “Hard turning and machine tool: a review,” *Int. J. Manuf. Technol. Manag.*, vol. 29, no. 3–4, pp. 252–270, 2015.
- [116] D. Tobola, K. Czechowski, J. Laszkiewicz-Lukasik, and S. Cygan, “Secondary Operations: Burnishing of PM Tool Steels Using Diamond Composite Material,” in *European Congress and Exhibition on Powder Metallurgy. European PM Conference Proceedings*, 2015, p. 1.

APPENDIX

Table 10. Surface residual stresses in the axial direction after the finishing step of SDB

F_{fin} [N]	σ_{fin}^{axi} [MPa]				
	Ground + SDB	Polished + SDB	Two-Step SDB		
			$F_{in} = 50$ N	$F_{in} = 100$ N	$F_{in} = 150$ N
0	-509	-169	-1098	-1228	-1157
25	-1004	-1112	-886	-809	-1042
50	-1027	-1101	-956	-862	-1053
75	-1039	-1089	-1072	-965	-1053
100	-1156	-1042	-1181	-1069	-1123
125	-1173	-1082	-1234	-1175	-1153
150	-1177	-1144	-1313	-1213	-1187
175	-1199	-1203	-1342	-1344	-1181
200	-1287	-1269	-1414	-1418	-1234

Table 11. Results of the percentage of surface axial residual stress improvement of the two-step burnished surfaces

F_{fin} [N]	$F_{in} = 50$ N		$F_{in} = 100$ N		$F_{in} = 150$ N	
	σ_{fin}^{axi} [MPa]	% $I\sigma_{axi}$ [%]	σ_{fin}^{axi} [MPa]	% $I\sigma_{axi}$ [%]	σ_{fin}^{axi} [MPa]	% $I\sigma_{axi}$ [%]
0	-1098	0	-1228	0	-1157	0
25	-886	-19.3	-809	-34.2	-1042	-9.9
50	-956	-12.9	-862	-29.8	-1053	-9.0
75	-1072	-2.4	-965	-21.4	-1053	-9.0
100	-1181	7.5	-1069	-12.9	-1123	-2.9
125	-1234	12.4	-1175	-4.3	-1153	-0.3
150	-1313	19.6	-1213	-1.2	-1187	2.6
175	-1342	22.2	-1344	9.5	-1181	2.1
200	-1414	28.7	-1418	15.5	-1234	6.6

Table 12. Surface residual stresses in the tangential direction after the finishing step of SDB

$F_{fin.}$ [N]	σ_{fin}^{tan} [MPa]				
	Ground + SDB	Polished + SDB	Two-Step SDB		
			$F_{in} = 50$ N	$F_{in} = 100$ N	$F_{in} = 150$ N
0	-214	226	-626	-493	-543
25	-684	-596	-585	-587	-630
50	-567	-557	-538	-496	-582
75	-523	-588	-523	-506	-502
100	-514	-494	-520	-514	-454
125	-529	-474	-531	-448	-468
150	-518	-459	-490	-372	-398
175	-517	-437	-400	-396	-350
200	-499	-444	-407	-381	-323

Table 13.Surface roughness values after the finishing step of SDB

F_{fin} [N]	$R_{a_{fin}}$ [μm]				
	Ground + SDB	Polished + SDB	Two-Step SDB		
			$F_{in} = 50 \text{ N}$	$F_{in} = 100 \text{ N}$	$F_{in} = 150 \text{ N}$
0	0.248	0.133	0.218	0.073	0.065
25	0.146	0.1225	0.084	0.058	0.082
50	0.117	0.139	0.083	0.063	0.139
75	0.103	0.0961	0.089	0.063	0.127
100	0.082	0.0934	0.086	0.061	0.112
125	0.08	0.0872	0.072	0.068	0.105
150	0.079	0.0867	0.075	0.054	0.064
175	0.083	0.0741	0.072	0.067	0.063
200	0.071	0.0596	0.073	0.076	0.056

Table 14. Percentage of surface roughness improvement Results after the second step of SDB

F_{fin} [N]	$F_{in} = 50 \text{ N}$		$F_{in} = 100 \text{ N}$		$F_{in} = 150 \text{ N}$	
	$R_{a_{fin}}$ [μm]	% IR_a [%]	$R_{a_{fin}}$ [μm]	% IR_a [%]	$R_{a_{fin}}$ [μm]	% IR_a [%]
0	0.218	0	0.073	0	0.065	0
25	0.084	61.5	0.058	20.0	0.082	-25.9
50	0.083	61.9	0.063	13.6	0.139	-113.6
75	0.089	59.2	0.063	13.3	0.127	-95.7
100	0.086	60.5	0.061	16.2	0.112	-71.9
125	0.072	66.9	0.068	6.6	0.105	-61.8
150	0.075	65.5	0.054	26.4	0.064	1.9
175	0.072	67.0	0.067	7.8	0.063	2.5
200	0.073	66.6	0.076	-3.4	0.056	13.9

Table 15. Surface microhardness values (HV 0.2) after the finishing SDB

F_{fin} [N]	HV 0.2				
	Ground + SDB	Polished + SDB	Two-Step SDB		
			$F_{in} = 50 \text{ N}$	$F_{in} = 100 \text{ N}$	$F_{in} = 150 \text{ N}$
0	680	744	650	646	741
25	833	801	667	728	817
50	727	786	648	753	879
75	757	814	789	755	861
100	752	786	791	781	853
125	731	793	752	789	899
150	755	789	671	676	925
175	788	807	692	685	878
200	828	810	845	680	866